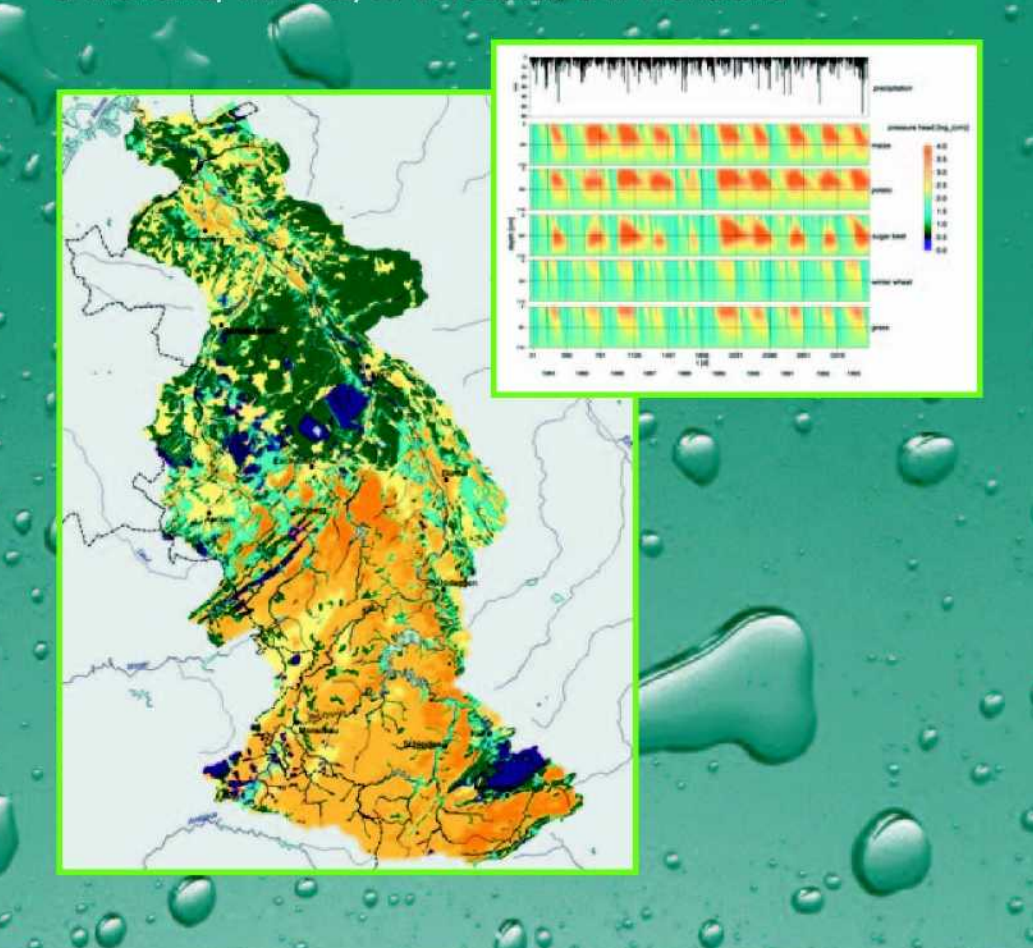


MOSYRUR

Water balance analysis in the Rur basin

H. Bogena, M. Herbst, J.-F. Hake, R. Kunkel

C. Montzka, Th. Pütz, H. Vereecken & F. Wendland



Umwelt Environment



Forschungszentrum Jülich GmbH Programmgruppe Systemforschung und Technologische Entwicklung Institut für Chemie und Dynamik der Geosphäre IV: Agrosphäre

MOSYRUR

Water balance analysis in the Rur basin

Heye Bogena, Michael Herbst, Jürgen-Friedrich Hake, Ralf Kunkel, Carsten Montzka, Thomas Pütz, Harry Vereecken, Frank Wendland

Schriften des Forschungszentrums Jülich Reihe Umwelt/Environment

Band/Volume 52

ISSN 1433-5530 ISBN 3-89336-385-8

Bibliographic information published by Die Deutsche Bibliothek. Die Deutsche Bibliothek lists this publication in the Deutsche Nationalbibliografie; detailed bibliographic data are available in the Internet http://dnb.ddb.de>.

Publisher and Forschungszentrum Jülich GmbH

Distributor: Zentralbibliothek

52425 Jülich

Phone +49 (0) 2461 61-5368 · Fax +49 (0) 2461 61-6103

e-mail: zb-publikation@fz-juelich.de Internet: http://www.fz-juelich.de/zb

Cover Design: Grafische Betriebe, Forschungszentrum Jülich GmbH

Grafische Betriebe, Forschungszentrum Jülich GmbH Printer:

Copyright: Forschungszentrum Jülich 2005

Schriften des Forschungszentrums Jülich Reihe Umwelt/Environment Band/Volume 52

ISSN 1433-5530 ISBN 3-89336-385-8

Neither this book nor any part of it may be reproduced or transmitted in any form or by any means, electronic or mechanical, including photocopying, microfilming, and recording, or by any information storage and retrieval system, without permission in writing from the publisher.

Table of Contents

1	Inti	oduction	5
	1.1	Challenges for the management of water resources	7
	1.2	Project goals	8
	1.3	Areas of investigation	9
2	Des	scription of the models	11
	2.1	The TRACE Model	13
		2.1.1 Geometry	13
		2.1.2 Numerical solution	14
		2.1.3 Boundary conditions	14
		2.1.4 Soil hydraulic properties	15
		2.1.5 The plant module SUCROS	16
	2.2	The GROWA Model	20
		2.2.1 Plane unpaved sites with deep water tables	20
		2.2.2 High relief terrains	22
		2.2.3 Groundwater-affected sites	23
		2.2.4 Urban regions	25
		2.2.5 Deriving the groundwater recharge	27
		2.2.6 Determining the BFI values from gauge data	27
		2.2.7 Identification of runoff-effective site conditions	29
		2.2.8 Attribution of area-differentiated BFI values	31
3	Dat	ta preparation and regionalization	35
	3.1	Microscale	37
		3.1.1 Material and Methods	37
		3.1.2 Results	40
	3.2	Macroscale	45
		3.2.1 Climatic data bases	46
		3.2.2 Landcover data	51
		3.2.3 Soil data	55
		3.2.4 Hydrogeological data base	66
		3.2.5 Topographic data	71
		3.2.6 Discharge data	74

4	Мо	del results	77
	4.1	Microscale	79
	4.2	Macroscale	81
		4.2.1 Actual evapotranspiration	83
		4.2.2 Total runoff	86
		4.2.3 Groundwater recharge	88
		4.2.4 Direct runoff	91
		4.2.5 Predominating runoff components	94
5	Мо	del Validation	97
	5.1	Microscale	99
		5.1.1 Measurements and model input	99
		5.1.2 Lysimeter experiment	101
		5.1.3 Field experiment	105
	5.2	Macroscale	106
		5.2.1 Total runoff	110
		5.2.2 Groundwater recharge and direct runoff	111
	5.3	Analysis of scale effects	114
		5.3.1 Procedure	114
		5.3.2 Results	115
6	Dis	aggregation of nutrient balances	121
	6.1	Introduction and Objectives	123
	6.2	Database	123
	6.3	Image Processing	124
		6.3.1 Preprocessing	124
		6.3.2 Classification	126
		6.3.3 Accuracy assessment and classification results	131
		6.3.4 Disaggregation	135
	6.4	Conclusion	138
7	Sui	mmary	141
Q	Raf	arancas	147

Introduction

1.1 Challenges for the management of water resources

Dependent on the regional hydrogeological conditions water resources management practices in the Rur basin differ greatly. The upland region is characterized by solid rock strata of low permeability. Therefore the groundwater aquifers are limited and runoff generation occurs mainly through direct runoff. Consequently the water resources in this part of the Rur basin are managed by reservoirs. In all, there are ten reservoirs in the catchment area of the Rur, which are used for drinking water supply, energy generation and flood control. In the adjacent flatland region to the north there are abundant loose rock aquifers, with high groundwater recharge rates. Accordingly, these aquifers are subject to an intensive groundwater withdrawal for drinking and service water purposes. For example, major amounts of service water are extracted in the Heinsberg region and along the River Rur between Düren and Jülich. Additionally, sumping wells for keeping open-cast lignite mines dry are also maintained (e.g. the open-cast pit Inden).

Quantitatively, a clear resources surplus is available in total in the Rur catchment area despite numerous water uses and the sumping measures. The local availability of water for industrial and ecological purposes, however, is problematic. Groundwater-dependent biotopes and agricultural areas are locally affected by groundwater lowering due to extraction for drinking water supply. The sumping measures for keeping the open-pit mines dry have an extensive effect. For example, they have led to translocations of underground catchment boundaries and thus to a translocation of protective zones.

Qualitatively, the groundwater and the surface waters are affected by diffuse inputs of agricultural activities (e.g. plant nutrients, pesticides) and point source emissions from landfills and abandoned contaminated sites. In addition, the groundwater is linearly polluted due to leaky draining channels. In order to avoid cost-intensive purification measures, this has led, for example, to groundwater extractions from deeper, still unpolluted groundwater storeys in the region of the Rur block. However, due to the open-cast lignite mines, the groundwater quality of the deeper aquifers itself has been affected in some areas due to groundwater acidification induced by pyrite oxidation and because of a rise of strongly mineralized deep-circulating waters.

The above problems have been recognized by the water management authorities. In the different subareas of the river basin, local measures are therefore

implemented in order to minimize the anthropogenic influence. Nearly all water utilities with nitrate problems, for example, have entered into cooperations with agriculture. The stock of aquatic biotopes along the receiving waters is maintained e.g. by water-holding measures. Integrated sustainable water management concepts, however, only exist rudimentarily and for small subregions in most cases.

1.2 Project goals

The research project "Development of an integrative model system for the sustainable water management in the catchment of the River Rur (MO-SYRUR)" was initiated by the Institute of Chemistry and Dynamics of the Geosphere, Department Agrosphere (ICG-IV) and the Program Group Systems Analysis and Technology Evaluation (STE) of the Research Centre Jülich.

The aim of the research project planned by ICG-IV and STE is to develop an implementation-oriented integrated modelling system to facilitate a sustainable management of the water resources in the Rur basin. This is to be accomplished on the basis of a quantitative and qualitative analysis of the status of water resources and of the current water uses in the Rur basin.

An essential objective of the project is the water balance modelling on different scale levels to evaluate measures for the quantitative management of water resources under the conditions prevailing in the Rur basin. This includes process-oriented studies and modelling in small representative test areas and also methods for the large-area GIS-based water balance estimations in the river basin.

ICG-IV and STE have already gathered a long-standing experience on these topics. A particular scientific challenge in this context is the development of upscaling and downscaling methods for the models for parameterizing and characterizing the water balance and transport of substances in landscape units and geological structures. Additionally, modern technologies of remote sensing and digital image processing can be applied in order to achieve high resolution landcover information as a basis for the hydrological modelling.

This report summarizes the results of the research activities of the first project phase (2002-2004), which has been focused on the analysis of the quantitative status of the water resources in Rur basin and the water balance at different scales.

1.3 Areas of investigation

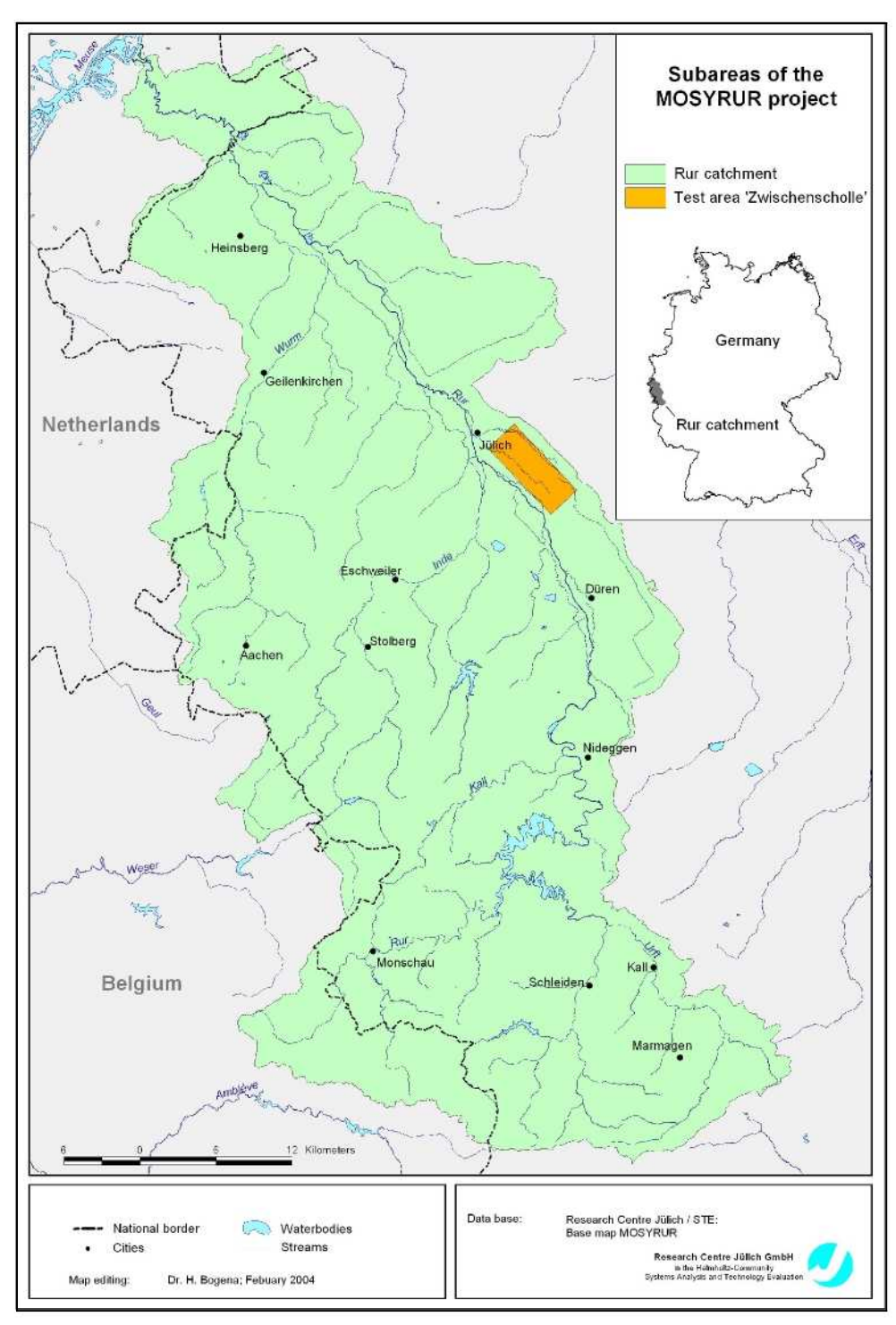
The areas of investigation have been chosen according to the existing instruments and modelling systems developed and applied at FZJ, i.e. at ICG-IV and STE, for modelling water fluxes in soil and groundwater systems at different scale levels. Map 1 shows the investigated subareas of the MOSYRUR project.

The entire catchment area of the River Rur with a total area of 2354 km² represents the macroscale. It is situated in the Lower Rhine Embayment, which is a geological subsidence structure located in North Rhine-Westphalia (Germany). About 157 km² (6.7 %) of the Rur basin is in Belgium and about 108 km² (4.6 %) on Dutch territory. A detailed description of the Rur catchment concerning land use as well as climatological, pedological and geological characteristics is given in Chapter 3.2.

The studies relating to the entire catchment area are performed at STE. For this purpose, modelling instruments developed at STE for application in macroscale water catchment areas (between approx. 1,000 km² and more than 100,000 km²) will be used, with which water resources, area drainage and the transport of diffuse pollutants (e.g. excess fertilizers from agricultural land use) can be modelled and analysed. The modelling instruments were successfully used in past years in various national and international research projects (e.g. in the project *REGLUD* funded in the framework of the BMBF research priority "river basin management" and the EU project *EUROCAT*).

A subarea of the middle Rur, the test area 'Zwischenscholle', which is about 20 km² in size, was selected as the microscale test region (see Map 1). For this subarea, the percolation to the groundwater and the water transport in the aquifer was modelled three-dimensionally and with a high time resolution using the TRACE model (Herbst et al., 2003).

These models will be set up in parallel for the entire region and for subregions. By means of a comparison of the input data and the model results obtained for the entire catchment area with those of individual subregions it will be possible, as part of the project, to specify conclusions concerning the validity of the large-area models and the accuracy of the simulation results for the subregions.



Map 1: The investigated subareas in the MOSYRUR project.

Description of the models

2.1 The TRACE Model

TRACE (Vereecken et al. 1994) is a massive-parallel computer code developed to solve water flow in large scale soil-groundwater systems. It is based on the 3DFEMWATER code (Yeh, 1987). The model has mainly been used to generate stochastic flow fields in order to test stochastic theories of solute transport (Neuendorf 1986, Döring 1997, Schwarze et al. 2001, Englert 2003). In the framework of the PEGASE project, the model was applied to agricultural soils with groundwater influence. Therefore changes to the numerical solution, the upper boundary conditions and handling of soil hydraulic properties were necessary to properly compute the unsaturated-saturated flow of water in cropped soils. To calculate plant growth the plant module SUCROS (Spitters et al. 1988) was integrated in the TRACE model. This model allows to calculate the LAI and rooting depth of agricultural crops, which are needed for the calculation of the actual evapotranspiration. The core of TRACE is the following modified version of the Richards' equation:

$$F_{h} \cdot \frac{\partial h(\overrightarrow{s})}{\partial t} = \frac{\partial}{\partial \overrightarrow{s}} (\overrightarrow{K}(\overrightarrow{s}, h) \cdot \frac{\partial (h(\overrightarrow{s}) + z)}{\partial \overrightarrow{s}}) + S(\overrightarrow{s}, t) \quad with \quad F_{h} = \frac{\partial \theta}{\partial h} + S_{h}$$
(1)

2.1.1 Geometry

The equation given in the introduction is solved using Galerkin-type finite elements. The flow domain is represented by isoparameteric hexahedrons. Every element consists of eight corner nodes and six sides. The element can be distorted (see Fig. 7 right hand side) but the nodes of every side have to be located on the same plane.

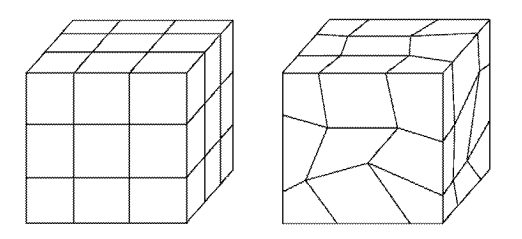


Fig. 1: Two examples of geometry.

In order to comply with specific requirements of GIS (e.g. regular grid) and to provide rapid access to node indices the number of nodes in one direction of space is kept constant, e.g. *nx* and *ny* elements in x and y-direction respectively.

2.1.2 Numerical solution

In order to improve the numerical solution for unsaturated conditions, several modifications were carried out. TRACE calculates the 3-dimensional unsaturated/saturated water flow in porous media with a modified Picard-iteration scheme (Celia et al. 1990) which is applied in combination with a preconditioned conjugate gradient method in order to solve the modified version of the Richards' equation numerically. It was necessary to improve the mass balance in the unsaturated zone. Thus the approach of Celia et al. was implemented in combination with a mass lumping approach and a modified convergence criterion according to Huang et al. (1996). Furthermore a convergence dependent dynamic relaxation time factor was introduced to improve numerical stability and computation speed.

2.1.3 Boundary conditions

A special type of boundary condition relevant for the regional scale application is the 'global Dirichlet boundary condition'. This boundary condition can only be applied to the vertical sides of the flow domain. For every vertical node column of the vertical sides the groundwater level G_L [L] must be given. For this vertical column of nodes all unsaturated nodes are set at a no-flow boundary (Cauchy, with q_c =0, see Tab. 1).

Tab. 1: Available boundary conditions in TRACE

Boundary condition	Definition
Total flux (Cauchy)	$q_c = -K \cdot \nabla H$
Flux (Neumann)	$q_n = -K \cdot \nabla h$
Head (Dirichlet)	given h
Seepage face (lysimeter)	q=0 for $h<0$ or Dirichlet with $h=0$

For the saturated nodes hydrostatic equilibrium is assumed and pressure head h is calculated from G_L -z, where z is the local z-coordinate. Total head H [L] is

equal to h + z. Another special type of boundary condition was implemented for the atmospheric boundary. This boundary condition is described by a variable type boundary. Depending on atmospheric conditions either a Dirichlet or Cauchy boundary conditions is prevailing. The change between both types is based on two pre-set pressure heads h_{min} [L] and h_{con} [L] need to be given. The former is set when soil becomes to dry to sustain the potential evaporation and the latter one is used to describe the process of ponding. During infiltration a flow boundary condition (Cauchy) is applied until h_{con} is reached. Then TRACE switches to a Dirichlet boundary condition and the pressure head at the soil surface is set to h_{con} (e.g. 1 cm). The infiltration excess is removed at the next timestep. A similar concept is applied for the reduction of evaporation. A flux boundary is applied until h_{min} is reached (e.g. 10^{-4} cm). At this point TRACE switches to a fixed head boundary condition set to h_{min} .

2.1.4 Soil hydraulic properties

Two approaches were implemented, which describe the soil water retention and the unsaturated hydraulic conductivity. The first one is the very commonly used approach of Mualem/Van Genuchten (Van Genuchten 1980):

$$\theta(h) = \theta_r + \frac{\theta_s - \theta_r}{\left(1 + \left(\alpha |h|\right)^n\right)^n} \quad and \quad K(h) = K_s \frac{\left(1 - \left(\alpha |h|\right)^{mn}\right)^2}{\left(1 + \left(\alpha |h|\right)^n\right)^{2.5m}} \tag{2}$$

where θ denotes the water content [L³ L³], h is the pressure head [L], θ_r is the residual water content [L³ L³], θ_s is the water content at saturation [L³ L³], α is the inverse of the bubbling pressure [L¹], K_s [L T¹] is the saturated hydraulic conductivity and m and n are dimensionless shape parameters. The following equation yields $\partial\theta/\partial h$, which is necessary to calculate the specific water capacity:

$$C(h) = \frac{(\theta_s - \theta_r)mn\alpha^n h^{n-1}}{\left(1 + (\alpha|h|)^n\right)^{m+1}}$$
(3)

For the second approach the parameter m of the retention function of Van Genuchten is set equal to 1. Thus the closed analytical expression of the Mualem/van Genuchten approach for the K(h) function is lost. Instead the unsaturated hydraulic conductivity function of Gardner (1958) was applied:

$$\theta(h) = \theta_r + \frac{\theta_s - \theta_r}{1 + (\alpha |h|)^n} \quad and \quad K(h) = \frac{K_s}{1 + (b|h|)^c}$$
 (4)

Here two new parameters b (cm $^{-1}$) and c (-) are introduced. The derivative of θ against h is given by:

$$C(h) = \frac{(\theta_s - \theta_r)n\alpha^n h^{n-1}}{\left(1 + (\alpha|h|)^n\right)^2}$$
 (5)

2.1.5 The plant module SUCROS

In order to take plant related processes into account the SUCROS module (Spitters 1988), implemented in WAVE was adapted to TRACE. During the implementation several modifications and extensions were necessary to link SUCROS and TRACE, mainly because TRACE is a 3-d model applicable to regional scale problems while WAVE was designed for local scale 1-d problems. In the following the basic concepts of SUCROS are explained in connection to the modifications during the implementation in TRACE.

In contrast to most of the plant modules in soil water models SUCROS calculates the leaf area index (LAI). In SUCROS the green leaf area index (LAI $_{green}$) is calculated from the biomass development, which is a function of the plant specific CO $_2$ assimilation and photosynthetic active radiation. Details on the basic principles of crop growth simulation can be found in the SUCROS manual (Spitters et al. 1988).

The main purpose of a plant module is to describe root extraction of water from the soil by plants, the process of interception loss at the canopy and to estimate the amount of potential evaporation from the soil surface. The first step is to calculate the potential evapotranspiration for the reference grass cover ET_{pot} [L T^{-1}], e.g. with the approach of Penman/Monteith. In order to describe the seasonal deviation of the potential evapotranspiration of crops to the one of the grass reference the approach of Doorenbos and Pruitt (1977) is applied (see also Fig. 2):

$$ET_{crop} = ET_{pot}K_C \tag{6}$$

where Et_{crop} [L T^{-1}] is the plant specific potential evapotranspiration and K_c [-] is the crop conversion factor. The leaf area index LAI [L² L⁻²] is used to separate potential evaporation and transpiration.

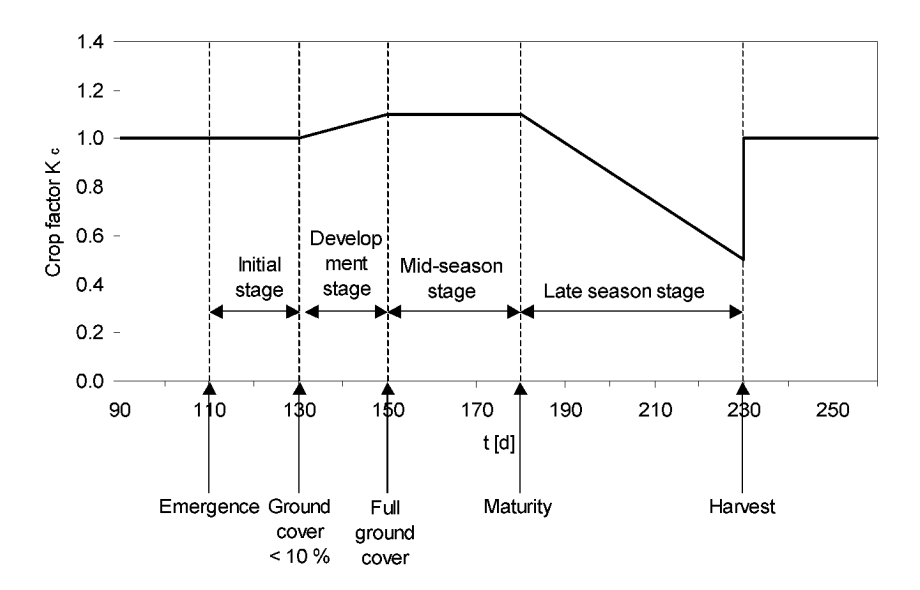


Fig. 2: Time course of the crop K_C factor for TRACE according to Doorenbos & Pruitt (1977) approach.

The basic assumption is that the amount of potential transpiration T_p [L T^{-1}] increases with increasing soil cover by leafs and the potential evaporation E_p [L T^{-1}] is reduced accordingly:

$$E_p = ET_{crop}e^{-0.6LAI} \quad and \quad T_P = ET_{crop} - E_p - E_i$$
 (7)

where E_i is the amount evaporation from the interception storage. For the estimation of the actual evapotranspiration T_a [L T^{-1}] the actual pressure head h [L] averaged for the volume under consideration is taken into account. The dimensionless reduction factor α [-] of Feddes (1978) is used:

$$T_{a} = T_{P}\alpha(h) \tag{8}$$

In order to describe the relation between h and α the four threshold pressure heads h₁, h_{2h} and h₃ [L] need to be given. First the threshold value h₂ [L] depending on the transpiration demand is computed:

$$h_{2} = \begin{cases} h_{2l} & T_{P} < 0.1\\ h_{2h} + \frac{0.5 - T_{P}}{0.4} (h_{2l} - h_{2h}) & for & 0.1 \le T_{P} < 0.5\\ h_{2h} & T_{P} \ge 0.5 \end{cases}$$
(9)

where the threshold values of T_p are given in mm d^{-1} . Then the reduction factor is calculated according to:

$$\alpha(h) = \begin{cases} \frac{h_0 - h}{h_0 - h_1} & h_0 \le h \le h_1 \\ 1 & \text{for } h_1 \le h \le h_2 \\ \frac{h_2 - h}{h_3} & h_2 \le h \le h_3 \end{cases}$$
 (10)

Root extraction in the element e S_e [T^{-1}] is calculated from the actual transpiration T_a [L T^{-1}], the corresponding surface area A_T [L^2], the normalized root density ω_e [-] and the volume of the element V_e [L^3].

$$S_e = \frac{T_a A_T \omega_e}{V_e} \quad with \quad \sum_{i=1}^n \omega_{e,i} = 1$$
 (11)

where n is the number of elements with roots below the corresponding surface. To calculate the normalized root density, the root density [-] for relative depths [-] must be specified as input. The relative rooting depth ranges between the soil surface and the actual rooting depth (=1). After averaging the z-coordinates of the element and with the given root depth the root density g_e [-] can be interpolated. Knowing the root density of the n corresponding elements allows to calculate the normalized root density of the element:

$$\omega_e = \frac{g_e}{\sum_{i=1}^n g_{e,i}} \tag{12}$$

The estimation of the interception loss is based on the concept of an overflowing bucket (Rutter, 1971). Basic assumption is, that the Precipitation N_0 [L T^{-1}] is separated into a fraction stored on the leafs N_i [L T^{-1}] and the fraction reaching the soil surface N_p [L T^{-1}]:

$$N_0 = N_p + N_i \tag{13}$$

The overflowing bucket is filled with precipitation until the maximum is reached and the fraction above the maximum is taken as the fraction reaching the soil surface. This maximum is calculated from the LAI [-]:

$$S_i = 0.2LAI \tag{14}$$

where S_i is the interception capacity [L], equivalent to the maximum volume of interception. Water is taken out of the interception storage by evaporation:

$$E_{i} = (ET_{crop} - E_{p}) \frac{C_{i}}{S_{i}}$$

$$\tag{15}$$

where E_i [L] is the amount of evaporation from intercept for the particular time step, and C_i [L] is the interception storage for that time step. Then the amount of interception can be estimated from:

$$N_{i} = \begin{cases} 0 & N_{0} = 0 \\ S_{i} - C_{i} & for & S_{i} - C_{i} < N_{0} \\ N_{0} & S_{i} - C_{i} > N_{0} \end{cases}$$
 (16)

Alternatively the empirical approach of Hoyningen-Huene (1983) for interception can be applied to time steps equal to or larger than one day:

$$N_i = -0.42 + 0.245N_0 + 0.2LAI + 0.0271N_0LAI - 0.0111N_0^2 - 0.0109LAI^2$$
 (18)

In order to account for water stress on dry matter growth rate per unit area R_m [M L⁻² T⁻¹], the dry matter growth rate per unit area R_m [M L⁻² T⁻¹] calculated from the radiation conditions is scaled with the ratio between actual and potential transpiration:

$$R_m = R_g \frac{T_a}{T_p} \tag{19}$$

A special module for perennial vegetation like forest was developed. Here the basic assumption is, that the same seasonal behaviour of the plant appears every year. The key parameters LAI, rooting depth and the K_c value must be

given as a function of the day of the year. A linear interpolation is applied for times between the given parameter values.

2.2 The GROWA Model

The raster based GROWA model consists of several modules for determining the long-term annual averages of the main water balance components (actual evapotranspiration, total discharge, direct runoff and groundwater recharge). The basis for calculating the total runoff level is the water balance equation, according to which the annual total runoff level on a long-term average is given by the difference between the mean annual precipitation and the mean annual actual evapotranspiration. In contrast to precipitation being measured directly at gauging stations, the actual evapotranspiration must be determined by modelling approaches.

2.2.1 Plane unpaved sites with deep water tables

The method of Renger & Wessolek (1996) allows a calculation of the annual actual evapotranspiration (ETa_{RW}) for plane unpaved sites with deep water tables (Eq. 20).

$$ETa_{RW} = a \cdot P_{wi} + b \cdot P_{su} + c \cdot \log(W_{pl}) + d \cdot ET_o + e$$
(20)

ETa_{RW}: Actual evapotranspiration according to Renger & Wessolek [mm/a]

a,b,c,d,e : Land use specific coefficients [-]

 P_{wi} , P_{su} : Winter and summer precipitation [mm/a] W_{pl} : Plant available soil water content [mm] ET_o: Potential evapotranspiration [mm/a]

The landcover enters in Eq. 20 via the land use-specific coefficients of regression a...e, which are listed in Tab. 2. For arable land, grassland and coniferous forest the regression constants according to Renger & Wessolek (1996) are used. For deciduous forest constants according to Renger & Strebel (1980) are used. It has to be noted that in this case, instead of the half-year levels of precipitation, only the mean annual precipitation is considered and that the plant available volume of soil water is not taken into account. In order to determine the mean actual evapotranspiration of vegetation-free areas, a simple approach of Proksch (1990) is applied. This method was derived from

lysimeter results for different soils (DVWK, 1996) and takes only the annual level of precipitation into account.

Tab. 2: Land use-specific regression coefficients for the calculation of actual evapotranspiration according to ¹Renger & Wessolek (1996), ²Renger & Strebel (1980) und ³Proksch (1990).

Land cover	а	b	С	d _{Haude}	е
Arable land ¹	0,08	0,39	153	0,12	-109
Pastures ¹	0,10	0,48	286	0,10	-330
Coniferous forest ¹	0,29	0,33	166	0,19	-127
Deciduous forest ²	0,047	0,047	0	0,02	430,1
Vegetation-free areas ³	0,074	0,074	0	0	59,2

The annual sum of the potential evapotranspiration, ET_O, relates to the method of Haude (1954), see Eq. 4. However, the FAO (Food and Agriculture Organization) recommends the grass reference evapotranspiration as an internationally uniform standard (Allen et al., 1994). The grass reference evapotranspiration is based on the Penman-Monteith relation (ATV-DVWK, 2002) and was determined nationwide by Wendling (1995) on the part of the German Meteorological Services (DWD). In the case that the grass reference evapotranspiration according to Wendling (1995) is used, the regression constant d must be modified as follows (Kunkel & Wendland, 1998):

$$d_{Wendling} = 0.926 \cdot d_{Haude} \tag{21}$$

The empirical actual evapotranspiration calculation method of Renger & Wessolek (1996) is based on the physical approach of Rijtema (1968). in order to cover the small-scale variability of soils and vegetation, it takes a large number of site factors into account. However, this method is restricted to plane unpaved sites with deep water tables, where the mean soil percolation rate corresponds to the mean groundwater recharge. Hennings (2000) specifies a maximum slope gradient of 3.5 % as the application limit for this method. In addition, climatologically restrictions have to be considered. For agricultural areas, the annual precipitation should not exceed 800 mm and for forests a value of 1300 mm should not be exceeded. If these conditions are not fulfilled, the calculation approach according to Renger & Wessolek (1996) cannot be directly used.

In order to ensure a universal application, Kunkel & Wendland (1998, 2002) extended the methodology of the Renger-Wessolek. The modifications include the consideration of topography, groundwater influence and pavement. In addition, it was ensured that the calculated actual evapotranspiration level, on the one hand, does not become higher than the maximum evapotranspiration and, on the other hand, is not lower than the precipitation level for those sites having deep water tables.

2.2.2 High relief terrains

In high relief terrains, the actual evapotranspiration level is additionally affected by the relief factors slope and aspect. This influence can be taken into account in the form of a correction factor f_h :

$$ETa_{relief} = f_h(\alpha, \varphi) \cdot ETr_{RW}$$
 (22)

ETa_{relief}: Actual evapotranspiration in high relief terrains [mm/a]

A relevant investigation in upland regions was performed by Golf (1981), whose results were generalized by Kunkel and Wendland (1998):

$$f_h(\alpha, \varphi) = \varphi \left[1.605 \cdot 10^{-2} \cdot \sin(\alpha - 90) - 2.5 \cdot 10^{-4} \right] + 1$$
 (23)

 α : aspect [°] φ : slope [°]

In Fig. 3 the dependence of the correction factor on aspect and slope is shown in the form of a graph. It can be clearly seen that the evapotranspiration on southerly exposed slopes predominates that on northern slopes. Thus, for example, a 16 % higher evapotranspiration level is found for southerly exposed slopes with a slope gradient of 10° than in plane ground. For northerly exposed slopes with a slope gradient of 10°, in contrast, an evapotranspiration level is found which only corresponds to 84 % of the value for plane conditions. These differences increase with rising slope gradient. Due to the additive correlation between precipitation and actual evapotranspiration in the calculation of the total runoff level, this may lead to a considerable modification of the runoff levels under certain conditions.

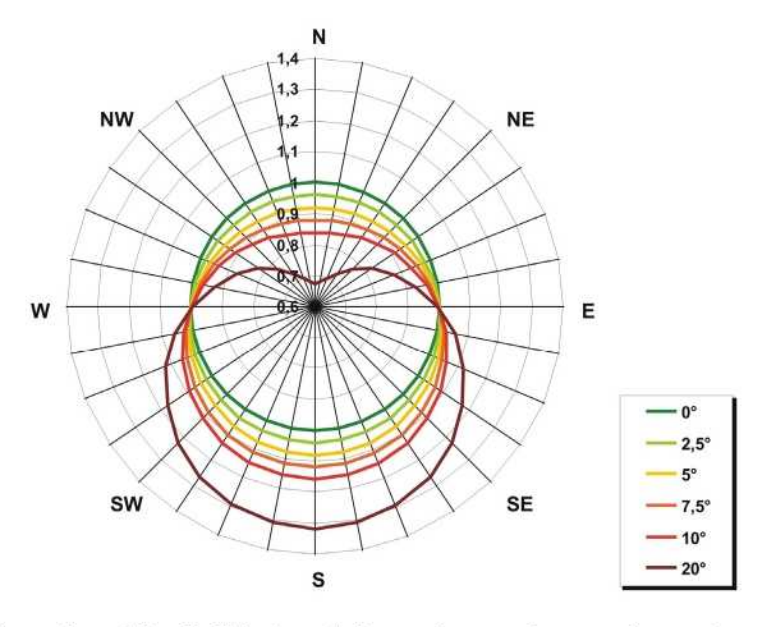


Fig. 3: The value of the Golf-factors f_h depending on slope and aspect.

2.2.3 Groundwater-affected sites

For sites affected by groundwater, the application of Eq. 20 leads to an underestimation of the actual evapotranspiration level, since due to capillary rise, water is constantly available for the evapotranspiration process. It is therefore assumed that the actual evapotranspiration corresponds to a maximum evapotranspiration:

$$ETa_{gw} = ET_{\text{max}} \tag{24}$$

ETagw : Actual evapotranspiration of groundwater affected sites [mm/a]

ET_{max}: Maximum evapotranspiration [mm/a]

The maximum evapotranspiration represents a modification of the potential evapotranspiration, which reflects an evapotranspiration value attainable under the theoretical condition of a grass vegetation with 12 cm height. The actually attainable evapotranspiration level of other land use types, however, can clearly deviate from this value. The maximum evapotranspiration (ET_{max}), which can be lower or higher than the potential evapotranspiration, depends on the type and height of vegetation. The maximum evapotranspiration is cal-

culated from the potential evapotranspiration (ET_0) using the parameter f (ATV-DVWK, 2002):

$$ET_{\max} = f \cdot ET_o \tag{25}$$

The values for the parameter f were determined via regression equations as a function of land use, vegetation height and available field capacity of the soil on the basis of lysimeter and gauge data for different site conditions (ATV-DVWK, 2002). Glugla et al. (1999) assume that the actual evapotranspiration level in lysimeters with sufficient moisture availability, i.e. with high soil-internal capillarity and thus high capillary water rise into the evapotranspiration-affected soil zone, corresponds to the maximum evapotranspiration:

$$f = \frac{ET_{\text{max}}}{ET_o} \approx \frac{ETa_{lysimeter}}{ET_o}$$
 (26)

ETalysimeters : measured evapotranspiration of the lysimeter [mm/a]

A value for f = 1.51 + /- 0.76 was obtained for lysimeters with soils from deep loess (ATV-DVWK, 2002).

For paved and bare sites, Glugla et al. (1999) compared the evapotranspiration values of bare lysimeters with the grass reference evapotranspiration after extensive precipitation events. For areas with deciduous and coniferous forest, observed data from non-weighable lysimeters were used. The actual evapotranspiration results from the difference between corrected precipitation and measured percolation. In this way, Glugla et al. (2002) discovered the following correlation:

$$ET_{\text{max}} = \frac{ETa}{0.8} \tag{27}$$

On the basis of Eq. 27, the parameter *f* for flat regions was calculated as a function of soil properties and rotation age (ATV-DVWK, 2002). The rotation age corresponds here to the stand age to the time of felling. The respective value for f thus corresponds to the average over all development stages up to the stand age upon felling. Fig. 4 shows the dependence of the parameter f on the soil type and the respective rotation age.

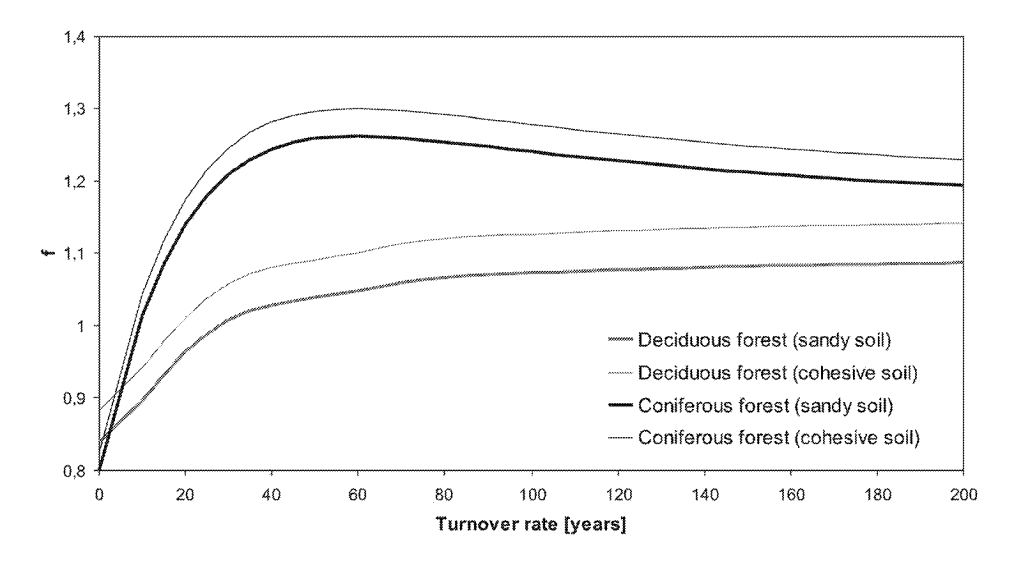


Fig. 4: Long-term means of the parameter f for deciduous and coniferous forests and different soil types depending on the turnover rate.

Furthermore, in determining the maximum evapotranspiration, the influence of slope gradient and aspect is taken into account by an additional factor f_H calculated in analogy to Eq. 28:

$$ET_{\text{max}} = f_H \cdot f \cdot ET_o \tag{28}$$

The equations for calculating the parameter f are listed in Tab. 3. The parameters z_B (average vegetation height of the plant stand) and UA (average rotation age of the plant stand) were estimated on the basis of the landcover categories of the landcover data CORINE (see Chapter 3.2.2).

2.2.4 Urban regions

Due to the variability in the building and settlement structure, it is very difficult to take the influence of pavement in urban regions into account. Presently, a number of studies dealing with this topic are available, but most of them created non-transferable results.

The present methodology is based on studies by Wessolek & Facklam (1997), who investigated the influence of pavement on groundwater recharge in the Berlin area. Accordingly, a correction factor is introduced by Kunkel & Wendland (1998) that reduces evapotranspiration in paved regions (Eq. 29).

Tab. 3: Land use-specific equations for the calculation of parameter f according to ATV-DVWK (2002).

Landuse classes	Equations	
Urban fabric	f = 0.8	
Open spaces	$\Theta_{nFK} \le 8.5 \text{ Vol.\%} \rightarrow f = 0.8$ $\Theta_{nFK} \ge 8.5 \text{ Vol.\%} \rightarrow f = 0.0186 \Theta_{nFK} + 0.6419$	
Pasture (12 cm)	$\Theta_{nFK} \le 11 \text{ Vol.\%} \Rightarrow f_{12om} = 0.0125 \cdot \Theta_{nEK} + 0.7108$ $\Theta_{nFK} \ge 11 \text{ Vol.\%} \Rightarrow f_{12om} = 0.2866 \cdot \ln(\Theta_{nFK}) + 0.6419$	
Pasture (varying)	$\begin{array}{rcl} 5\text{cm} < z_B \le 20\text{cm} & \Rightarrow & f_k = 0.0676 \cdot \ln(z_B) + 0.8321 \\ z_B \ge 20\text{cm} & \Rightarrow & f_k = -0.7 \cdot 10^{.5} \cdot z_B^2 + 0.37 \cdot 10^{.2} \cdot z_B + 0.9661 \\ & & f = f_k(z_B) \cdot f_{12\text{cm}} \end{array}$	
Arable land	$f = 0.221 \ln(\Theta_{nFK}) + 0.431$	
Deciduous forest	Sandy soils (Θ _{nFK} ≤ 16 Vol.%):	
Coniferous forest	$ \begin{array}{lll} \textbf{Sandy soils} \; (\Theta_{nFK} \leq 16 \; Vol.\%); \\ \textbf{UA} \leq 130 \; years \Rightarrow & f = 0.8 \pm 0.2694 \pm 10^{-1} \cdot UA \pm 0.63924 \pm 10^{-3} \cdot UA^2 \pm 0.8052 \pm 10^{-5} \cdot UA^3 \pm 0.5785 \pm 10^{-7} \cdot UA^4 \pm 0.223 \pm 10^{-9} \cdot UA^5 \pm 0.356 \pm 10^{-12} \cdot UA^8 = f_{SL1} \\ \textbf{UA} \geq 130 \; years \Rightarrow & f = 1.35 \pm 0.108 \pm 10^{-2} \cdot UA \pm 0.178 \pm 10^{-5} \cdot UA^2 = f_{SL2} \\ \textbf{Loamy soils} \; (\Theta_{nFK} \geq 16 \; Vol.\%); \\ \textbf{UA} \leq 130 \; years \Rightarrow & f = 1.03 \pm 10^{-2} \cdot UA \pm 0.178 \pm 10^{-5} \cdot UA^2 = 10^{-2} \cdot UA \pm 0.178 \pm 10^{-5} \cdot UA^2 = 10^{-2} \cdot UA \pm 0.178 \pm 10^{-5} \cdot UA^2 = 10^{-2} \cdot UA \pm 0.178 \pm 10^{-5} \cdot UA^2 = 10^{-2} \cdot UA \pm 0.178 \pm 10^{-5} \cdot UA^2 = 10^{-2} \cdot UA \pm 0.178 \pm 10^{-2} \cdot UA \pm 0.178 $	

$$ETa_{urban} = ETa_{RW} - f_v \cdot G \tag{29}$$

ETa_{urban}: Actual evapotranspiration of urban areas [mm/a]

G : Degree of pavement [%] $f_{_{V}}$: Correction factor [-]

The correction factor f_V was determined by a comparison between the actual evapotranspiration calculated according to Eq. 20 for a hypothetically unpaved situation and the evapotranspiration resulting after Wessolek & Facklam (1997) for the Berlin area (Kunkel & Wendland, 1998). A value of 3.44 was thus found for f_V . According to ATV-DVWK (2002), fractions of the paved area can be derived using the CORINE nomenclature.

2.2.5 Deriving the groundwater recharge

The groundwater recharge level is determined in the GROWA model by separating the calculated total runoff into the components of direct runoff and baseflow. According to Peschke (1997) on a long-term average the baseflow component essentially corresponds to the groundwater recharge. Following Dörhöfer & Josopait (1980) and Hennings (2000), the baseflow levels are separated by so-called "baseflow indices" (BFI). In this way, the groundwater recharge level, $GW_{recharge}$, is expressed as a relative fraction of the total runoff level, Q_{total} :

$$GW_{recharge} = BFI \cdot Q_{total} \tag{30}$$

The BFI values are dependent on specific site conditions and are assumed to be nearly constant on a long-term average. In order to enable a differentiated calculation of the groundwater recharge for the total area of the Rur catchment, the BFI values must be spatially distributed to the entire area. A three-step procedure was adopted for this purpose, which will be explained in more detail in the following.

2.2.6 Determining the BFI values from gauge data

In a first step, observed discharge data were used to determine the BFI values arising in the respective catchment areas. In order to achieve an adequate determination of the BFI values the discharge data of a large number of catchments has to be analysed. Since most of the sub-catchments of the Rur basin are strongly influenced by water management activities (e.g. strip mining, water reservoirs), it was necessary to consider a larger region for this purpose. Since the same data base for the GROWA model was available for the Federal State of North-Rhine Westphalia (NRW), it was decided to carry out the BFI determination for this region. In selecting appropriate gauges in NRW, care was taken to ensure that different sizes of catchment areas (from 1.3 to 4783 km²) as well as a broad spectrum of climatological, geological and pedological variability were included. The catchment-area-related BFI values (BFI_{basin}) are determined according to the following relation:

$$BFI_{basin} = Q_G / MQ \tag{31}$$

MQ : Mean annual discharge [m³/sec] Q_G : Groundwater discharge [m³/sec]

In order to determine the groundwater-bearing runoff, Wundt (1958) proposed a method in which the groundwater runoff is derived from the monthly low-water discharges (MoLR) of a prolonged series of years (MoMLR-method):

$$Q_G \approx MoMLR = \sum_{i}^{n} MoLR_i / n \tag{32}$$

In a first approximation, the MoMLR value reflects the groundwater flow of a river for sites that are not significantly anthropogenic affected and which are located in unconsolidated rock regions. In this case the MoMLR value is an appropriate measure of the groundwater recharge for a catchment area. The applications of the GROWA model to the Elbe catchment area (Kunkel & Wendland, 1998) and to Lower Saxony (Dörhöfer et al., 2001) have proved that plausible baseflow fractions can be determined in such regions with the MoMLR-method.

In solid rock regions, however, the MoMLR-values do not correspond to the mean groundwater recharge, since the monthly low-water discharges contain significant fractions of direct runoff (surface runoff and interflow), which are also covered by the MoMLR-method. For this reason, following Kille (1970) and Demuth (1993), a method was applied to the solid rock regions, which allows a reduction of the MoMLR values by the interflow fraction.

The graphical Kille-method is a modification of the Wundt-method, the individual MoMLR values being arranged in ascending order. A relevant example is shown in Fig. 5 for the Rebbelroth (Agger) gauge. In this way, a cumulative frequency is obtained which, according to Demuth (1993), can be divided into two types (type I S-shaped, Type II parabolic). The Kille method can only be applied to type I, the linear section of the distribution being used for fitting a straight line. The MoMLR value reduced by the interflow (MoMLRr) is read in the middle of the distribution on the y-axis according to Kille and corresponds to the mean groundwater recharge.

This procedure was taken up by first forming the cumulative frequency from the MoMLR values as was done by Kille (1970) and Demuth (1993). With the aid of a regression analysis, the linear section of the cumulative frequency is then determined by iteratively reducing the domain of definition of the MoMLR values. For this purpose, first of all the maximum and then the minimum MoMLR values are omitted in each iteration step. This procedure is completed, when a maximum coefficient of determination of the regression straight line is reached.

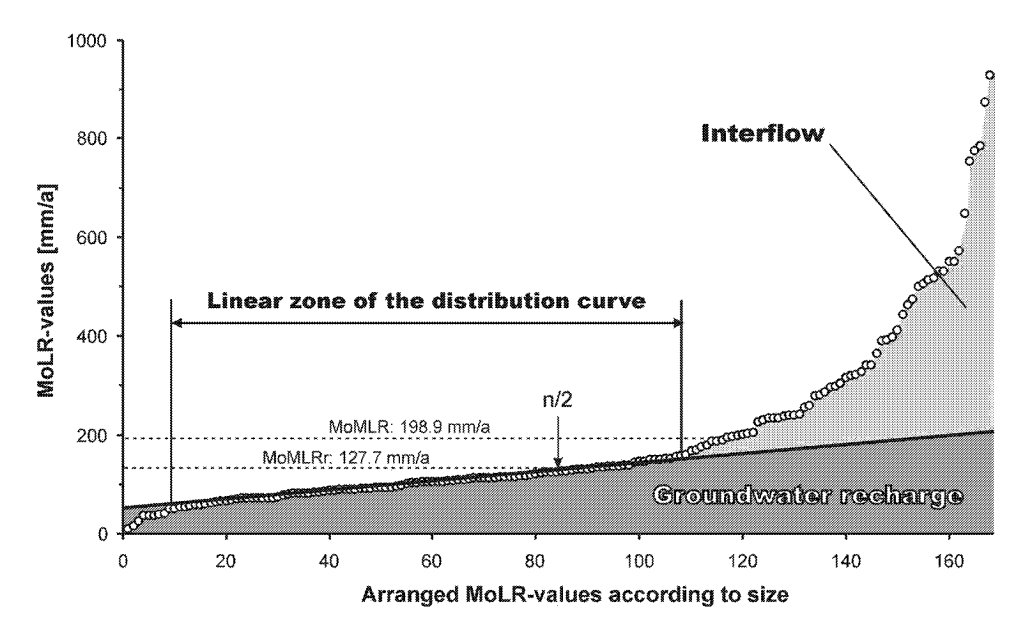


Fig. 5: Separating the interflow component from groundwater recharge in consolidated rock areas (MoMLRr-method).

Finally, the MoMLRr-value is calculated by means of the gradient m, the number of MoLR-values n and the axis intercept y_0 :

$$MoMLRr = m \cdot \frac{n}{2} + y_0 \tag{33}$$

The example of the Rebbelroth (Agger) gauge in Fig. 5 illustrates the difference from the Wundt method. If the MoMLR method after Wundt is used, a very high value (198.9 mm) is obtained for the groundwater recharge level. As can be seen in Fig. 5, this results from the relatively large fraction of exceedingly high MoMLR values, which may exhibit high fractions of direct runoff e.g. due to snowmelt or during periods of heavy precipitation. If the MoMLR method is used, a value of 127.7 mm is determined by eliminating the direct runoff fraction, which corresponds much better to the actual groundwater recharge in the catchment area of the Rebbelroth gauge (Bogena et al., 2003).

2.2.7 Identification of runoff-effective site conditions

After having derived the regional averages of the BFI values for the considered catchment areas on the basis of the runoff data, the next steps are the disaggregation and the transfer to regions for which no suitable gauge data

are available. Therefore runoff-effective regional features and parameters are taken into account.

For this purpose, a hierarchical approach is used, in which the value of a site condition is considered to be exclusively determining for the BFI value. Further site parameters are only considered if the primary site condition is not relevant (see Fig. 6). A total of 21 different site features have been defined, to each of which a BFI value is assigned:

- Two pavement classes for separating the groundwater recharge in urban regions according to their degree of pavement
- Seven classes for including the influence of the geology on groundwater recharge in solid rock regions
- Three classes to differentiate the influence of the depth to groundwater on groundwater recharge in unconsolidated rock regions
- Two classes to reproduce water logging influences on groundwater recharge in unconsolidated rock regions
- Seven classes for including the influence of the different slope gradients on groundwater recharge in unconsolidated rock regions

The hierarchical approach is consequently divided into five steps. First of all, it is assumed in each area element or each grid cell that groundwater recharge is negligible for the paved fraction.

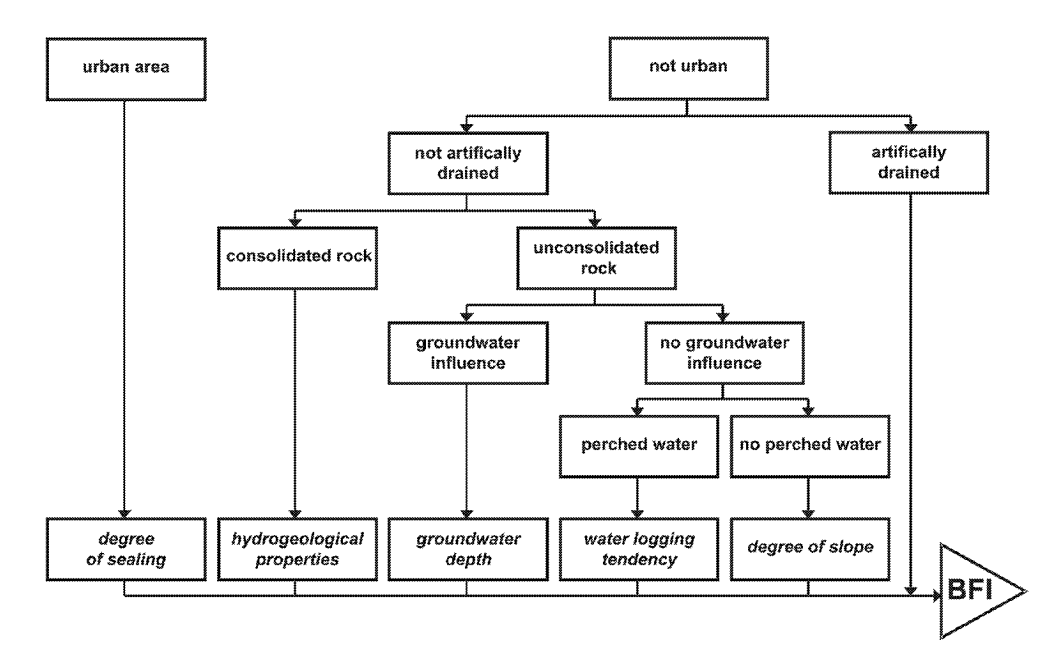


Fig. 6: Site characteristics that determine groundwater recharge in GROWA.

It is then verified for the remaining fraction of the area element whether there is a significant artificial drainage, e.g. pipe or ditch drainage. If this is the case, a corresponding BFI value is estimated. In the case that a detailed information concerning pavement and the remaining landcover is not available, e.g. if the CORINE Landcover data are used, a representative value for the whole area element is used.

If the actual grid cell shows neither pavement or artificial drainage, a differentiation into consolidated rock and unconsolidated rock regions is carried out. In the unconsolidated rock areas, the depth to the groundwater table and the water logging tendency as well as the slope gradient are considered. In the solid rock regions, the hydrogeological rock properties are regarded as the decisive runoff-effective site property.

The degree of pavement is identified using the CORINE Landcover data (see Chapter 3.2.2). The hydrogeological properties were taken from the Hydrogeological Information System HK100 of the NRW Geological Service (see Chapter 3.2.4). The soil-physical and topographic data for the unconsolidated rock regions were taken from the Digital Soil Information System BK50 (see Chapter 3.2.3) and are calculated on the basis of the DGM50 digital terrain model, respectively (see Chapter 3.2.5).

2.2.8 Attribution of area-differentiated BFI values

The application of the GROWA model to the Elbe catchment area (Kunkel & Wendland, 1998) and to Lower Saxony (Dörhöfer et al., 2001) has shown that the use of BFI values from the literature (see Tab. 4) leads to realistic ground-water recharge rates in unconsolidated rock regions. A further calibration of the BFI values on the basis of the MoMLR values measured in the North Rhine-Westphalian unconsolidated rock region was omitted, since many rivers in this region exhibit strongly anthropogenically influenced runoff conditions (e.g. due to massive discharges of strip mine draining waters).

Kunkel & Wendland (1998) established that the BFI values specified in Tab. 4 cannot be used for the solid rock regions, since the influence of the geological subsoil conditions by far predominates that of the soil properties. Several other authors (e.g. Gabriel & Ziegler, 1989, Schwarze et al., 1991) also point out that particular importance must be attributed to the influence of the geological subsoil conditions in quantifying the runoff fractions. For this reason, Kunkel & Wendland (1998) took the geological conditions into account as the central parameter in separating the base flow in solid rock regions.

Tab. 4: BFI-values of the unconsolidated rock areas according to Dörhöfer & Josopait (1980), Hennings (2000) and Wessolek & Facklam (1997).

Degree of sealing	Groundwater depth	Water logging tendency	Slope	Baseflow indices
	>2 m	no water logging	<1 %	1
	1.3 – 2 m	1 (very low)	1 – 3.5 %	0.9
1 (10 – 45 %)				0.82
			3.5 - 7 %	0.67
			7 - 10 %	0.59
	0.8 - 1.3 m	2 (low)	10 – 13 %	0.5
	0.4 - 0.8 m	3 – 4 (medium – high)	13 – 15 %	0.44
	<0.4 m	5 (very high)	>15 %	0.4
II (45 – 75 %)				0.33
III (75 – 90 %)				0.28
IV (>90 %)				0.2

The baseflow fractions in the unpaved solid rock regions of North Rhine-Westphalia were therefore also determined here on the basis of the geological subsoil conditions. For this purpose, nine solid rock units differing in their permeability were taken from the Hydrogeological Map special information system (HK100) (see Chapter 3.2.4). Since so far no characterization of the HK100 geological units is available concerning the distribution of baseflow and direct runoff, adequate BFI values have been determined by calibrating the runoff data of numerous gauging stations in North Rhine-Westphalia (Chapter 3.2.6). Tab. 5 shows the hydraulic conductivity classes of HK100 and the BFI values determined by calibration.

Tab. 5: The classification of the hydrogeological properties of the hard rocks in North Rhine-Westphalia and the associated BFI-values obtained by calibration.

Hydrogeological class	Permeability	k _s -value	Baseflow Indices
(very high	>10 ⁻² m/sec	0.9
****	high	$>10^{-3}-10^{-2} \text{ m/sec}$	0.6
111	medium	>10 ⁻⁴ - 10 ⁻³ m/sec	0.57
IV	moderate	>10 ⁻⁵ - 10 ⁻⁴ m/sec	0.3
V	low	$>10^{-7}-10^{-5}$ m/sec	0.29
VI	very low	>10 ⁻⁹ - 10 ⁻⁷ m/sec	0.18
VII	extremely low	<10 ⁻⁹ m/sec	0.12

Fig. 7 summarizes the procedure in the GROWA model for determining the baseflow fractions.

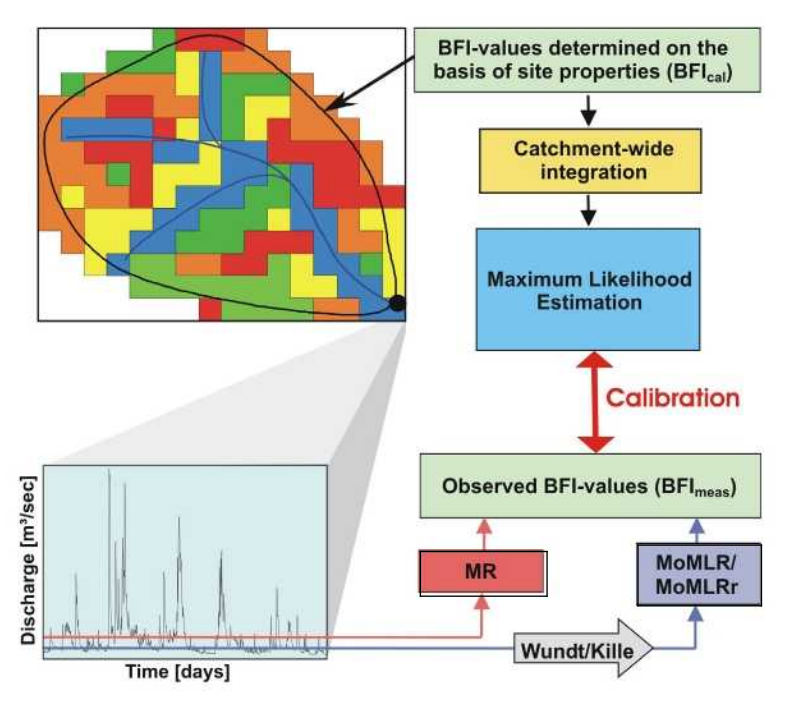


Fig. 7: Procedure in the GROWA model for determining the baseflow fraction.

The calibration is performed in a catchment-area-related manner. For this purpose, the relative area fractions (a_i) of the individual site parameters in each region under investigation were multiplied by the respective (BFI_i), added up and compared with the baseflow indices observed (BFI_{meas}):

$$BFI_{meas} = MoMLR(r)/MR \leftarrow_{compared\ with} \rightarrow BFI_{cal} = \sum_{i=1}^{n} BFI_{i} \cdot a_{i}$$
 (34)

where *MR* denotes the measured long-term average total runoff. The sum runs here across all the 21 site features distinguishable, e.g. in the unconsolidated rock regions across the categories of groundwater and water logging influence shown in Tab. 9 and of the slope gradient. In a next step, only the baseflow indices of the seven site features in solid rock were varied, so that the sum of the square deviations between calculated and measured baseflow fractions assumes the lowest value (maximum likelihood method):

$$\sum_{j=1}^{n} (BFI_{meas} - BFI_{cal,j})^2 = Min$$
(35)

For the calculation of *BFI*_{meas}, as already described, the MoMLR-method was applied to unconsolidated rock regions and the MoMLRr-method to solid rock regions. In this way, a set of BFI values was obtained, which leads to an optimal fit for the ensemble of catchment areas under consideration. This parameter set was then applied area-wide to the whole of North Rhine-Westphalia (Bogena et al., 2004).

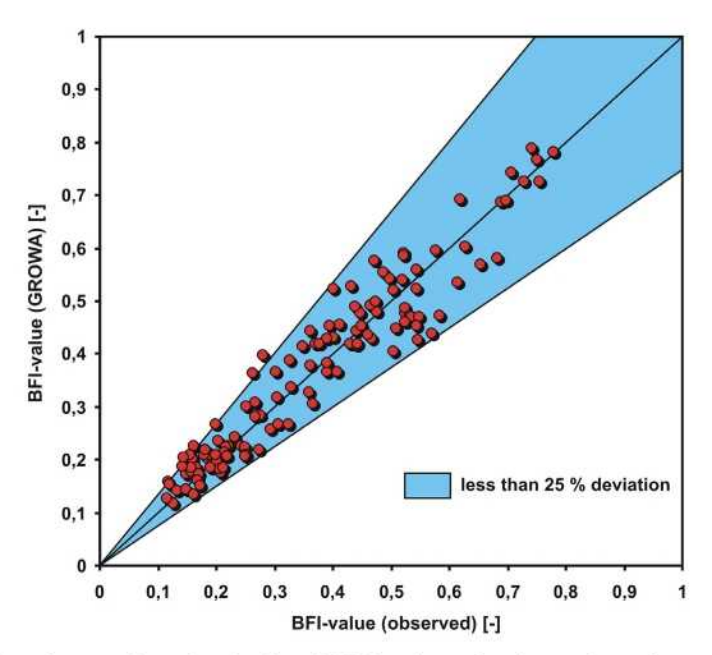


Fig. 8: The observed and calculated BFI-values for the subcatchments in North Rhine-Westphalia.

As is shown by the correlation diagram in Fig. 8, good agreement between calculated and measured baseflow fractions of the total runoff is reached using the method presented. This is also documented by the coefficient of determination ($r^2 = 0.93$) and the mean residue, which only amounts to 12.2 %. The selected approach therefore enables the baseflow fractions of the total runoff both in unconsolidated rock regions and in solid rock regions to be satisfactorily reproduced on a long-term average.

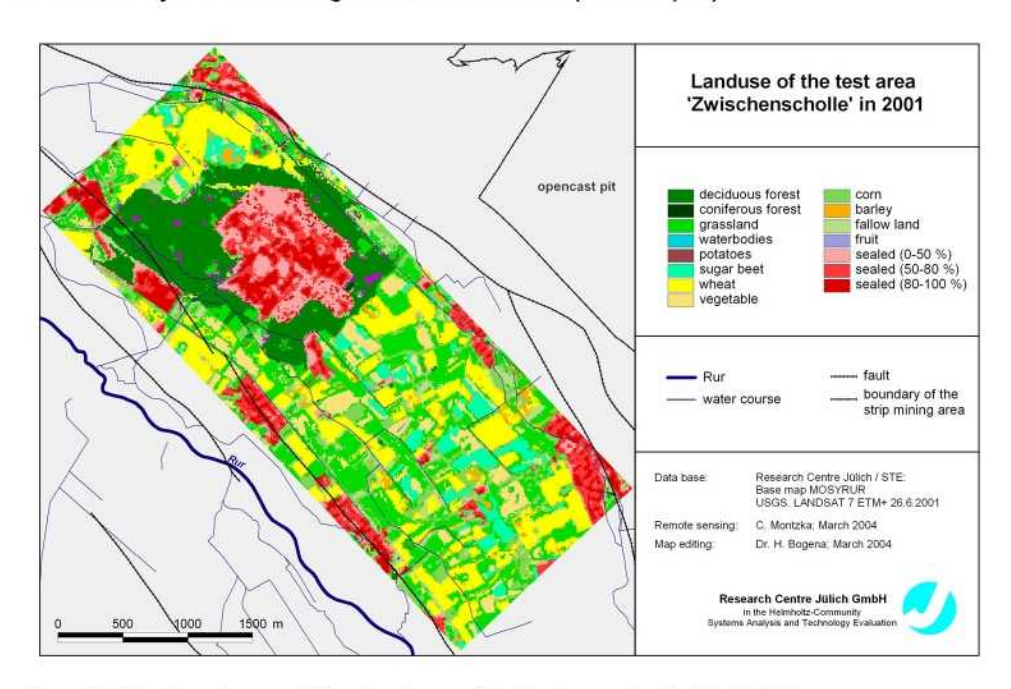
Data preparation and regionalization

3.1 Microscale

In the following, the main features of the 'Zwischenscholle' test area and the pre-processing of input data to generate a dataset for the application of the TRACE model are described. The main focus is on the calculation of the potential evapotranspiration, on the application of Pedotransfer functions to derive the soil hydraulic properties and on the spatial-temporal interpolation of groundwater levels used as vertical boundary conditions.

3.1.1 Material and Methods

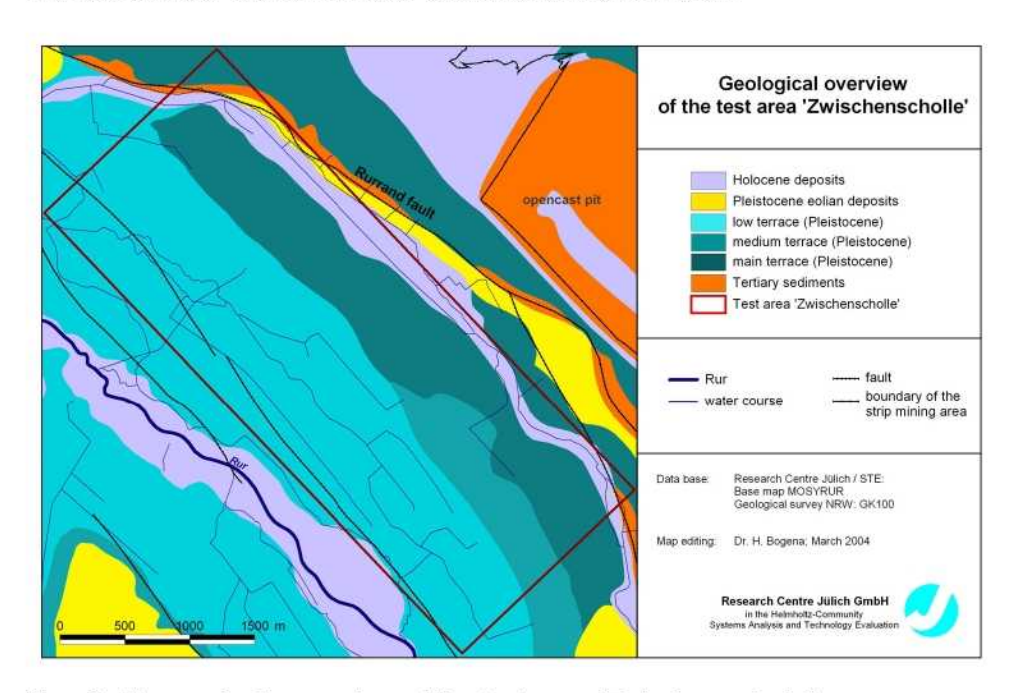
The test area 'Zwischenscholle' is bounded by the Rurscholle on the southwest and the Erftscholle on the northeast. The Zwischenscholle area is lowered against the Erftscholle but lifted against the Rurscholle. The area is characterized by forest and agricultural land use (see Map 2).



Map 2: The land use of the test area 'Zwischenscholle' in 2001.

The western part, which includes the research centre area, is mainly covered by deciduous forest. The eastern part is dominated by agricultural land use. The main crop is sugar beat with an annual turning of winter wheat. Minor crops are corn, potatoes and oat. Urban regions in the area are small villages (Stetternich, Hambach, Niederzier, Krauthausen, Selgersdorf), a network of motorways, and the area of the research centre.

According to Klosterman (1992) the first (unconfined or semi confined) aquifer consists of Quaternary Rhine and Maas sand and gravel sediments (Map 3). The base of the aquifer is build by the Reuver clay. The aquifer thickness varies from few meters in the southwest to 35 m in the northeast. The main groundwater flow direction is from southeast to northwest. The first aquifer is in direct contact with small local creeks and the Rur River.



Map 3: The geologic overview of the test area 'Zwischenscholle'.

Regions with leakage effects from the lower confined aquifer (between 45 and 120 m thick) are found on the Rurrand fault. The Rurrand fault is assumed to be a natural no flux boundary, whereas the Rursprung fault shows a hydraulic connection between the Zwischenscholle area and the Rurscholle area. The southern part of the area is used by the Research Centre for the withdrawal of drinking water from shallow wells. For this purpose two water supply wells are used. The total amount of water withdrawn by these two wells is 33000 m³ per year.

In order to model daily evapotranspiration, daily time series on radiation, air temperature, air humidity, wind speed and precipitation were obtained for the period 1/12/1983-31/11/1993. All of these parameters were measured at the meteorological tower in the Research Centre. In order to calculate the potential evapotranspiration the approach of Penman/Monteith was applied according to the FAO method (Smith, 1996). For periods not all parameters were available the simplified approaches of Makkink (Makking, 1957) or Hamon (Hamon, 1961) were applied to complete the time series on potential evapotranspiration.

In order to derive the soil hydraulic parameters from the textural properties and porosity of the soil Map 1:5000 the Pedotransfer functions (PTF) of Rawls & Brakensiek (1985) were used. Because these PTF calculates the parameters according to the Brooks/Corey approach the pore size index λ [-] and the bubbling pressure ψ_b [L] were transformed to the Mualem/Van Genuchten (Van Genuchten 1980) parameters n [-] and α [cm⁻¹] by using:

$$\alpha = \psi_b^{-1}$$

$$n = 1 + \lambda n$$
(36)

In order to take the coarse fraction (> 2mm) into account the PTF of Brakensiek & Rawls (1994) were applied, too. First the volumetric coarse fraction Z_2 [L³ L⁻³] is calculated from the density of quartz ρ_s [M L⁻³], the dry bulk density of the soil ρ_b [M L⁻³] and the gravimetric coarse fraction Z_1 [M M⁻¹]:

$$Z_2 = \frac{\rho_b}{\rho_s Z_1} \tag{37}$$

The modification of the volumetric water contents (θ_s and θ_r) according to the volumetric coarse fraction is given by:

$$W_{vt} = W_{v<2}(1 - Z_2) \tag{37}$$

where W_{vt} [L^3 L^{-3}] is the modified water content of the total soil and $W_{v<2}$ [L^3 L^{-3}] is the water content of the soil matrix only. The saturated hydraulic conductivity of the soil K_s [L T^{-1}] influenced by the coarse fraction is calculated from the gravimetric coarse fraction and the saturated hydraulic conductivity of the matrix K_m [L T^{-1}]:

$$1 - Z_1 = \frac{K_m}{K_s} \tag{38}$$

The relation between porosity ϕ [L³ L⁻³] and bulk density is given by:

$$\phi = 1 - \frac{\rho_b}{\rho_s} \tag{38}$$

This relation was used to calculate the porosity from the bulk density classes of the soil Map 1:5,000.

In order to calculate the groundwater levels necessary for the vertical boundary conditions in a first step a temporal interpolation was carried out. For a fixed time step interval of 30 days the groundwater level of every available well was linearly interpolated from the measurements of available dates. In a second step the spatial interpolation for the 30 days interval was done using the point dataset generated from the temporal interpolation by applying the inverse distance weighting method (IDW). The output is a raster of the groundwater levels at the grid size chosen for the hydraulic model. The last step is the extraction of the grid cells relevant for the boundary conditions.

3.1.2 Results

To get information on the spatial distribution of land use interviews with farmers were carried out. As this does not provide a complete Map of land use for every year a stochastic distribution approach was chosen. First the land use fraction of every crop was calculated from the interview data. Then the land parcel boundaries were digitized and the forest and built up areas (partially sealed surface) were identified and the land use of these areas was fixed for the whole period 1983-1993. The remaining area (arable land) was used for the stochastic spatial distribution of crops reproducing the calculated land use fractions. Fig. 9 shows the results of this procedure for 1991 to 1993. The interviews with the farmers were also used to fix the dates of sowing and harvest.

Fig. 10 shows the spatial distribution of soil types on the 'Zwischenscholle' test site. Every spatial unit is attributed to one of the 122 representative soil profiles. Even for the areas with 'no soil type' data on texture, organic carbon and coarse fraction is available for pedogenetic soil horizons. For these areas not

a single soil type was chosen during the survey, due to the heterogeneity of soil types in this spatial unit.

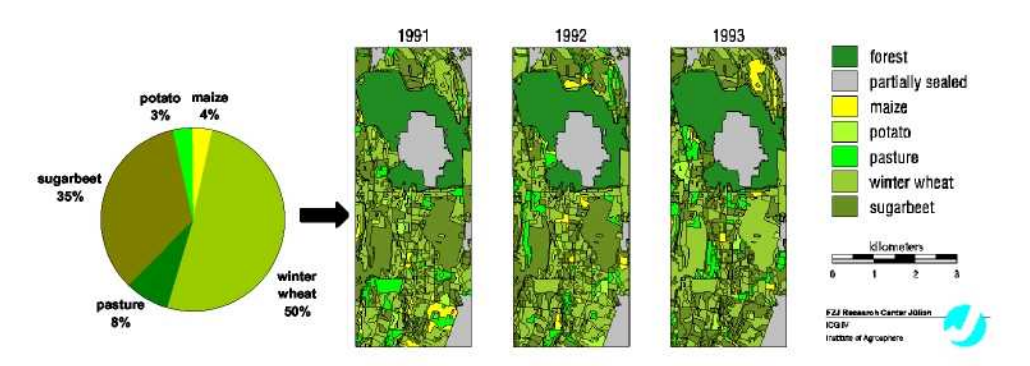


Fig. 9: Spatial distribution of crops; the diagram on the left shows the average fraction of the crops between 1983 and 1993, the right side shows the stochastically generated land use Maps for 3 years.

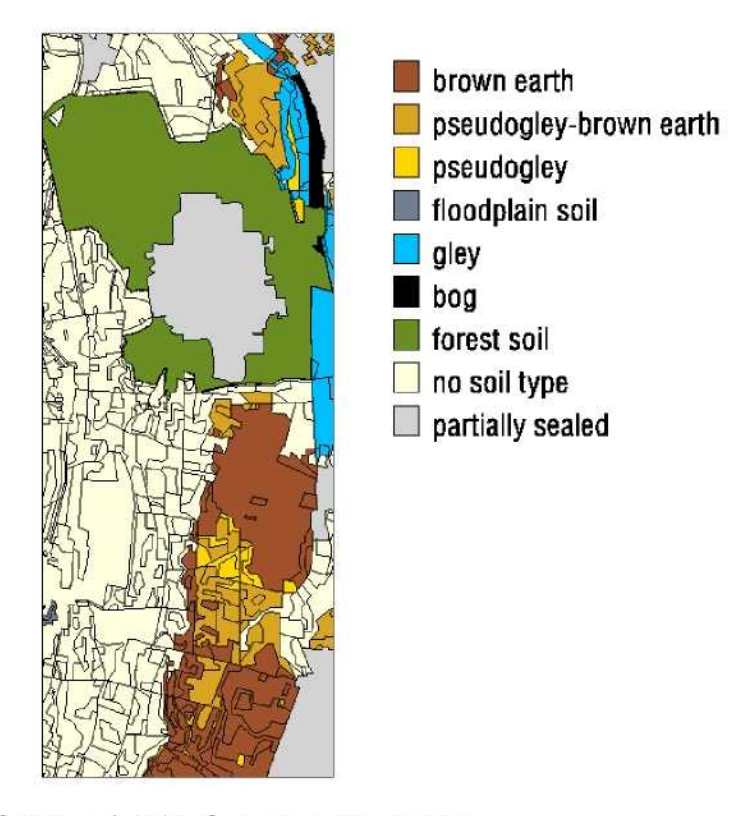


Fig. 10: Soil Map 1:5000, German soil taxonomy.

The results of the PTFs are shown in Fig. 11. For every horizon of the representative soil profiles the parameters according to Mualem/Van Genuchten were derived. The broad range of soil hydraulic properties is visible, although loamy textured soils predominate, resulting in a rather slow decrease of soil moisture with decrease in pressure head and moderate air entry values.

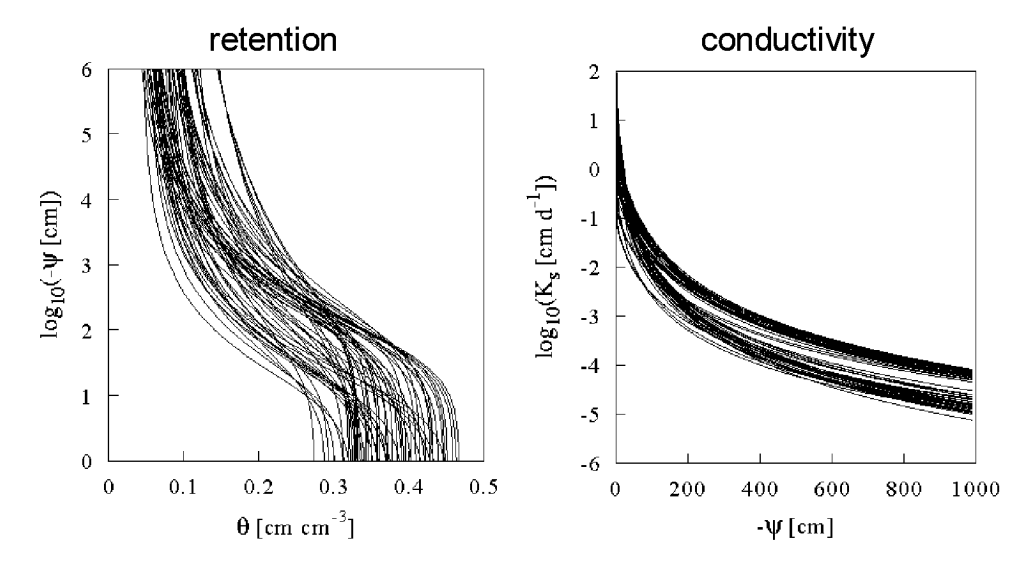


Fig. 11: Conductivity and retention functions according to Mualem/Van Genuchten (Van Genuchten 1980) for the 293 horizons of 122 soil profiles.

The low saturation water contents are mostly found at the bottom of the soil profiles due to large amounts of coarse fractions (gravel). The saturated hydraulic conductivity covers a range of roughly four orders of magnitude.

For the estimation of the hydrogeological situation data of about 350 bore holes was analysed. This data was used to calculate mean properties of the aquifer like porosity and saturated hydraulic conductivity. In addition, the borehole data were used to define the position of soil and aquifer layers necessary for the model geometry. The base of the uppermost aquifer is the Reuver clay. This aquifer base was interpolated from the point data on boreholes (for details on this procedure see Jahn, 2002).

As shown in Fig. 12 the base of the uppermost aquifer is closer to the surface near the River Rur (cross section AA'). In north-western direction the main

trend is also an increase of aquifer thickness (cross section BB'). The geometry of the upper boundary is given by a digital elevation model.

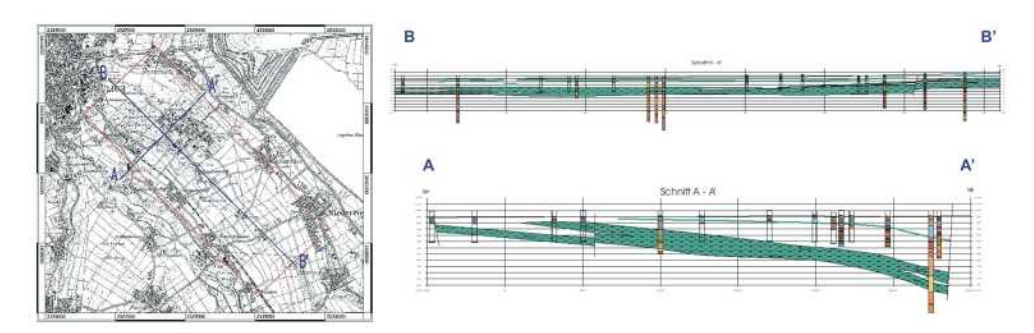


Fig. 12: Cross sections of the hydrogeological model.

An example of an interpolated groundwater level is given in Fig. 13. The main groundwater flow direction is northwest. This groundwater level calculated for the first date at the beginning of the model period was taken as initial condition for the hydraulic model after spatial transformation.

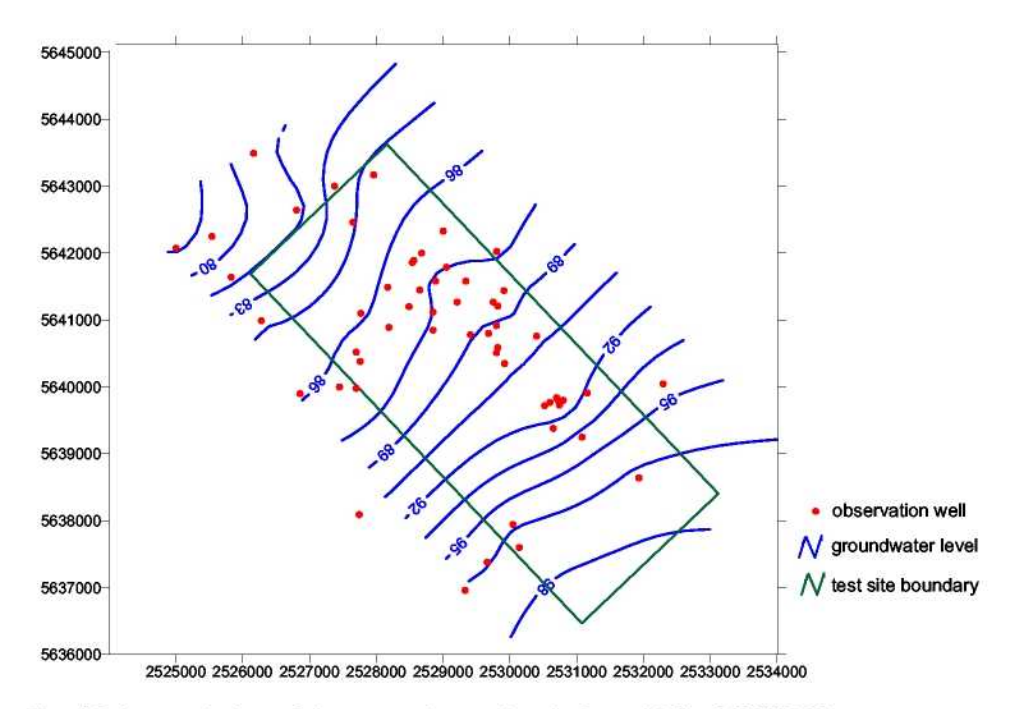


Fig. 13: Interpolation of the groundwater levels [m asl.] for 1/12/1983.

The mean precipitation measured at the meteorological tower for the model period 12/1983 –11/1993 is 712 mm/a. Single events can have up to 55 mm/d (see Fig. 14). The mean of potential evapotranspiration for the model period is 559 mm/a. The occurrence of negative potential evapotranspiration rates (see Fig. 14) is linked with the method used for the estimation of the potential evapotranspiration. Only the Penman/Monteith approach estimates negative potential evapotranspiration due to a negative radiation balance. Thus the process of evapotranspiration is reverted and thawing occurs. The amounts of thawing are rather small, and in a yearly water balance not significant. In terms of long-term water balance the mean difference between precipitation and potential evapotranspiration on a yearly base is 153 mm/a, which can be seen as the minimum of groundwater recharge.

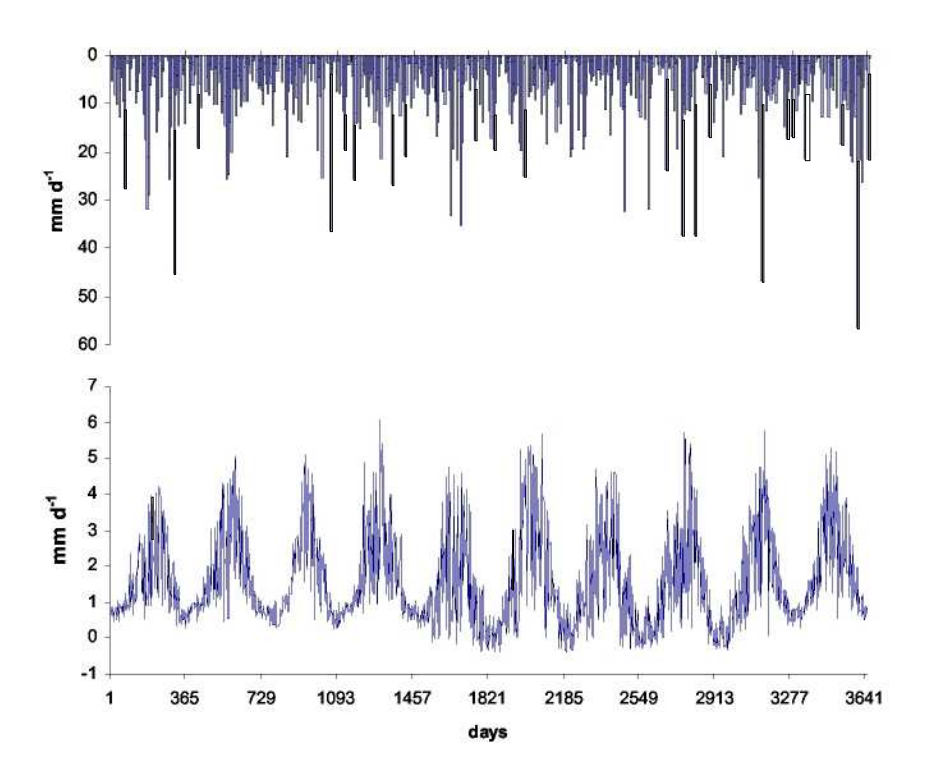


Fig. 14: Meteorological data: Dec 1st 1983 to Nov 30th 1993 (upper graph: precipitation, lower graph: potential evapotranspiration for grass using Penman/Monteith, Makkink or Hamon).

3.2 Macroscale

The model GROWA was used in order to determine the water balance at the macroscale, thus for the Rur basin. For the application of the GROWA model spatially distributed climatic, hydrological, pedological, topographic and hydrogeological basic data are needed. The datasets used for this study are described in this chapter with respect to origin, determination methodology and precision. Furthermore, special procedure steps in data processing are explained and the specific regional features described. All the databases used in this study originate from data stocks made available by the federal and state authorities (see Tab. 6).

The climatic parameters were processed by the German Meteorological Services (DWD). The pedological and hydrogeological parameters were derived by the NRW Geological Service. Datasets from the NRW Land Surveying Office were used as topographic site conditions. Hydrological data bases were made available by the NRW State Environmental Agency, by the national environmental agencies in NRW and by various water associations. Detailed explanations concerning the individual data stocks are to be found in Bogena et al., 2003. All data stocks were embedded in the Geographic Information System ArcView® and in the Access database system. Data storage as well as analysis and the evaluation of results takes place in ArcView®.

Tab. 6: Database of the GROWA water balance model.

	Data base	Scale / spatial resolution	Data source
Climate data	Precipitation (May – October) Precipitation (November – April) Potential evapotranspiration	1000 x 1000 m²	German Meteorological Survey
Soil data	Effective field capacity Rooting depth Capillary rise Groundwater depth Influence of perching water	1:50,000	Geological Survey of NRW
Soil cover	CORINE land cover	25 ha	Federal Statistical Office
Geology	Classes of permeability	1:100,000	Geological Survey of NRW
Topography	Slope Aspect	50 x 50 m²	Geological Survey of NRW
Malisladian data	Catchment areas	1:25,000	Environmental Agencies and
Validation data	Daily runoff 1979 - 1999		Water associations of NRW

3.2.1 Climatic data bases

All the climatic data were provided by the German Meteorological Services (DWD). These were the following digital datasets of the period 1979-1999:

- mean level of precipitation in the hydrological six summer months
- mean level of precipitation in the hydrological six winter months
- average annual potential level of evapotranspiration after Wendling

The basis for establishing the area-wide climate data is the climate and precipitation stations of the DWD. The station values were regionalized by DWD using the IDW method (inverse distance weighting interpolation) and including an elevation correction (see also Müller-Westermeier, 1995 and Wendling, 1995). With this method the DWD first established datasets for the different months of the period 1979-1999. The average annual precipitation level in the hydrological six summer months (1979-1999) and the average annual precipitation level in the hydrological six winter months (1979-1999) were derived by averaging and adding up these basic grids. The dataset for the potential evapotranspiration after Wendling was treated analogously.

For modelling a uniform grid with a grid width of 50 m was chosen. However, the DWD data were available in the 1 km grid format, so that a disaggregation of the DWD grid data had to be carried out. The method of ordinary kriging (Matheron, 1963) was used for this purpose. The climate data presented in the following are thus the original DWD data disaggregated to a 50 m grid.

Level of precipitation

The method for determining the water balance values incorporates the average precipitation levels in the hydrological six summer months and hydrological six winter months. In order to describe the precipitation conditions in the Rur catchment, the annual precipitation levels (Map 4) and the ratio between summer and winter precipitation (Map 5) of the reference period will be dealt with in more detail in the following.

In the northern part of the Rur basin the annual precipitations are relatively uniform distributed in space and ranges between 700 mm/a in the North and 900 mm/a near Aachen. In the southern part of the Rur catchment a clear differentiation of the precipitation levels is observed. Due to the marine air flowing in predominantly from southwest to northwest, a significant precipitation shadowing effect can be observed: The precipitation levels in the crestal regions of the Rhenish Massif ("Hohes Venn") are higher than those on the eastern sides (lee regions). Whereas annual precipitation levels of 1200 mm/a

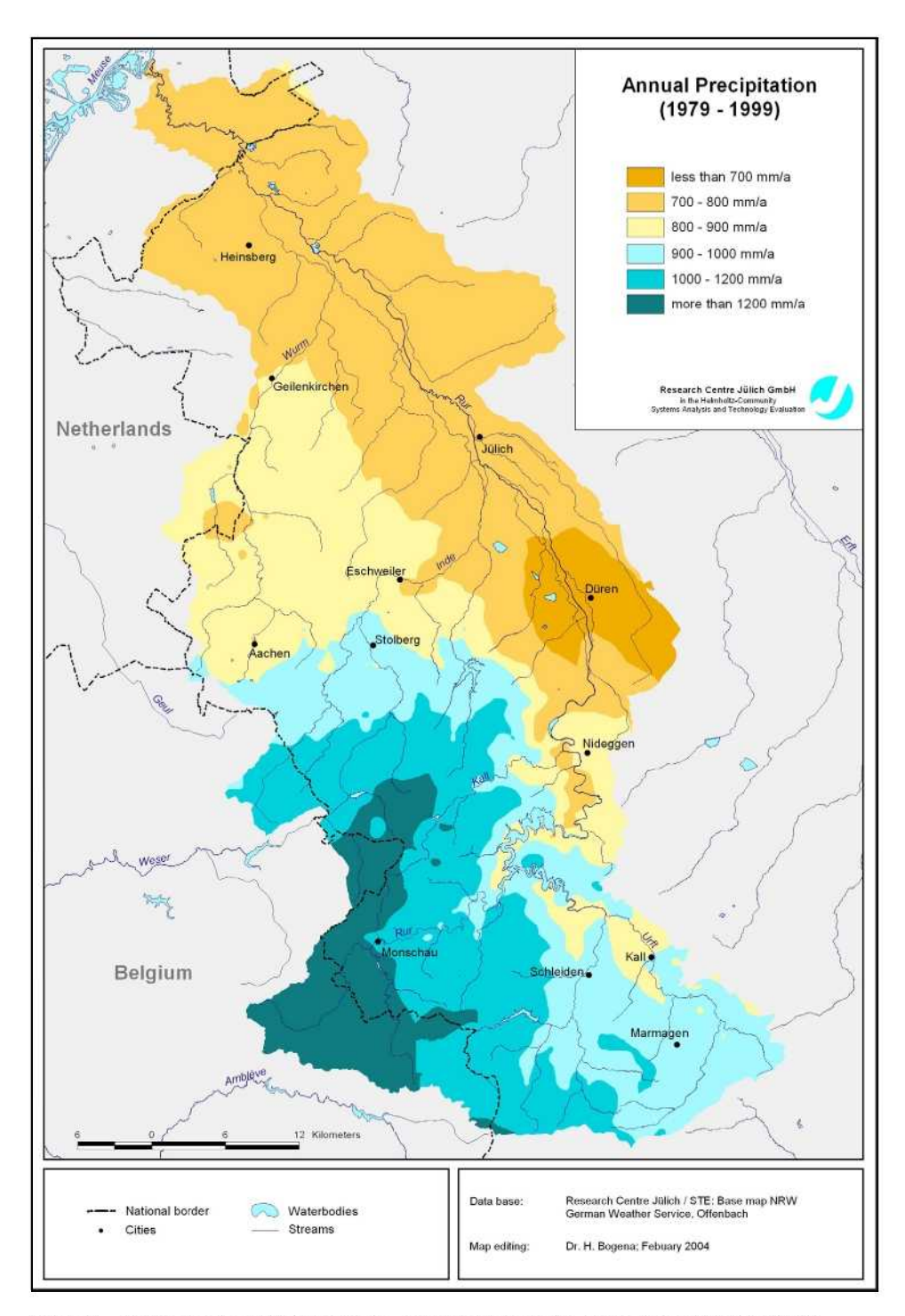
and more can occur in the crestal regions, leeward precipitation levels below 700 mm/a occur around Düren (see Map 4). This example demonstrates that the windward and lee effects should be taken into account in a consideration of the dependence of the precipitation level on the topographic elevation.

Map 5 shows the ratio of summer and winter precipitation in the period 1979-1999. At a ratio of 100 % the precipitation level in the hydrological six summer months (May to October) is the same as in the hydrological six winter months (November to April). Winter precipitation predominates at values below 100 %, summer precipitation at values above 100 %. The precipitation ratios observed range from below 85 % to above 110 %. In the middle part of the catchment of the Rur River, a fairly balanced precipitation ratio is to be observed. In the upland areas, however, winter precipitation is clearly predominant. Consequently, the highest precipitation levels fall in the period of the lowest evapotranspiration potential. Due to the low transpiration rates in winter and the associated high soil moisture, a large portion of the precipitation water can rapidly become runoff-effective. In contrast, in the northern part of the catchment of the Rur River the highest precipitation levels occur in summer and thus at the time of the highest potential evapotranspiration. In this case, an effective buffering of precipitation events can be assumed, resulting in rather smoothed hydrographs.

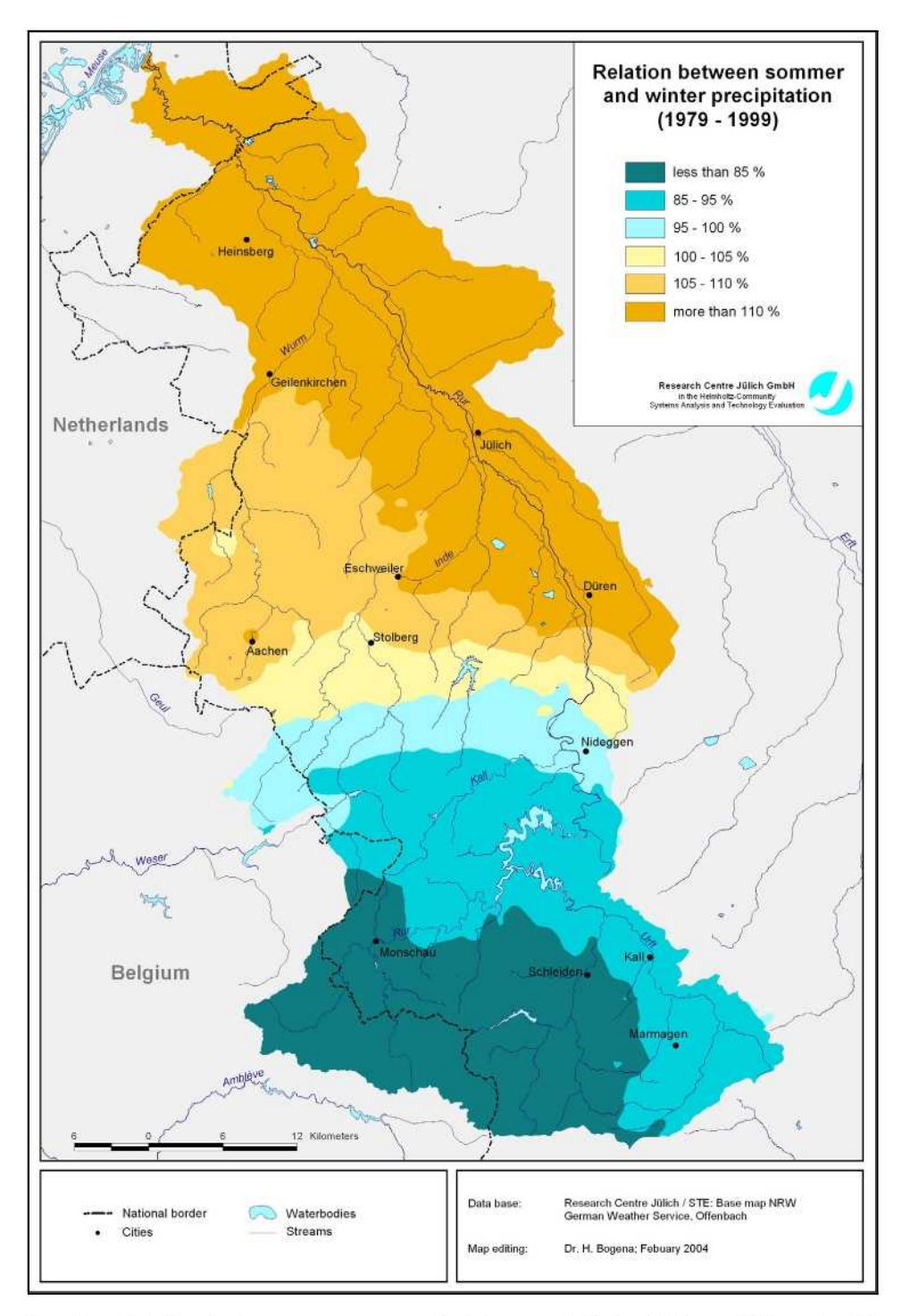
Potential evapotranspiration

Due to the high measurement effort, often models are used in order to determine evapotranspiration rates. The potential evapotranspiration describes the evapotranspiration amount under given climatic conditions that may arise from a defined soil surface in the case of unlimited water resources and, therefore, results from meteorological data alone. In order to enable a uniform calculation, the boundary conditions (vegetation, land use and soil properties) must be defined.

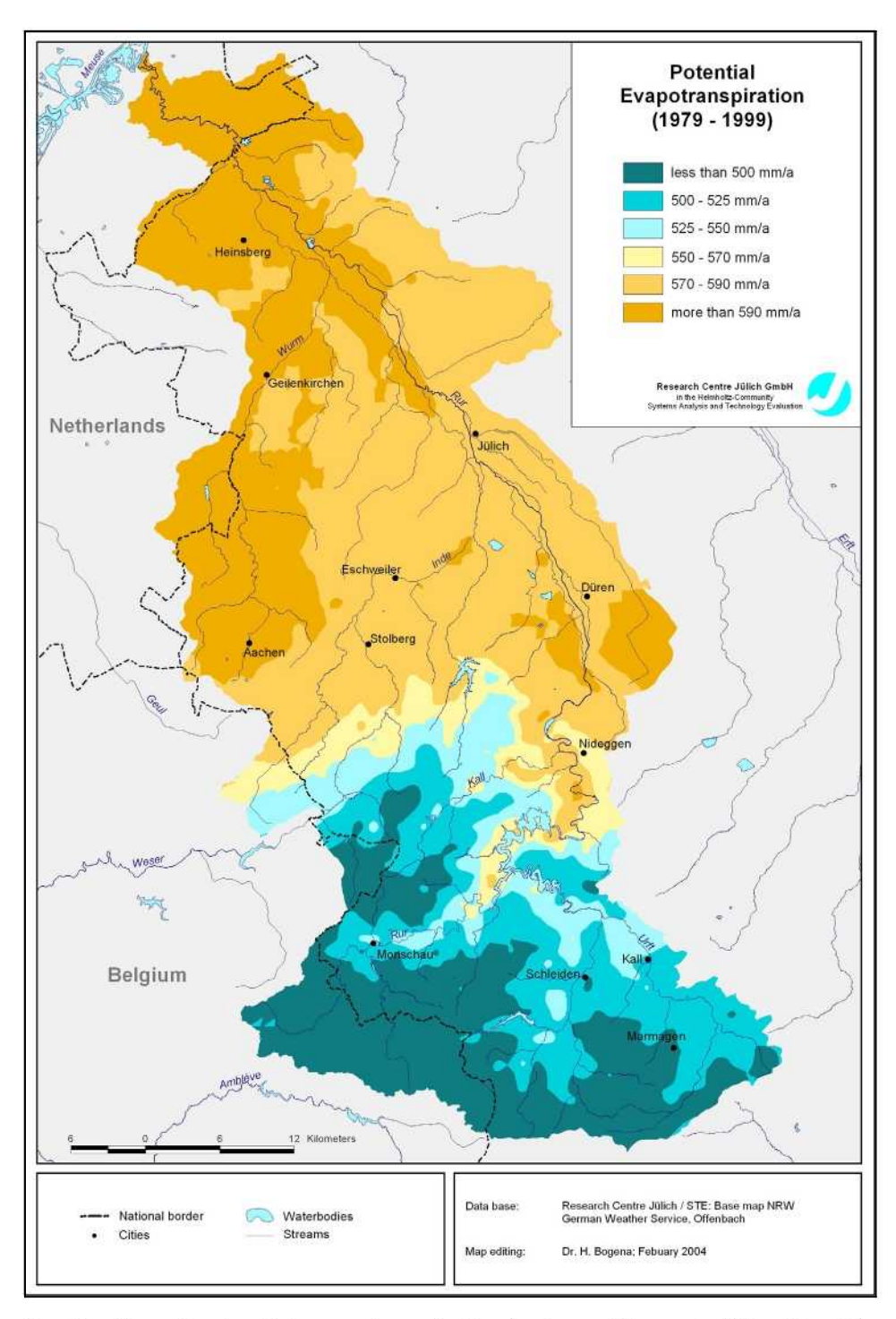
The FAO (Food and Agriculture Organization) recommends the grass reference evapotranspiration, which is based on the Penman-Monteith relation (Allen et al., 2000), as an internationally uniform standard. The following boundary conditions were defined in this connection: all-year grass cover (12 cm height), no drought stress (at least approx. 50 % of the available field capacity) and a mean albedo of 0.23.



Map 4: Annual precipitation in the catchment of the Rur River (1979-1999).



Map 5: Relation between summer and winter precipitation in the catchment of the Rur River (1979-1999).



Map 6: Annual potential evapotranspiration in the catchment of the Rur River (1979-1999).

Potential evapotranspiration

Due to the high measurement effort, often models are used in order to determine evapotranspiration rates. The potential evapotranspiration describes the evapotranspiration amount under given climatic conditions that may arise from a defined soil surface in the case of unlimited water resources and, therefore, results from meteorological data alone. In order to enable a uniform calculation, the boundary conditions (vegetation, land use and soil properties) must be defined.

The FAO (Food and Agriculture Organization) recommends the grass reference evapotranspiration, which is based on the Penman-Monteith relation (Allen et al., 2000), as an internationally uniform standard. The following boundary conditions were defined in this connection: all-year grass cover (12 cm height), no drought stress (at least approx. 50 % of the available field capacity) and a mean albedo of 0.23.

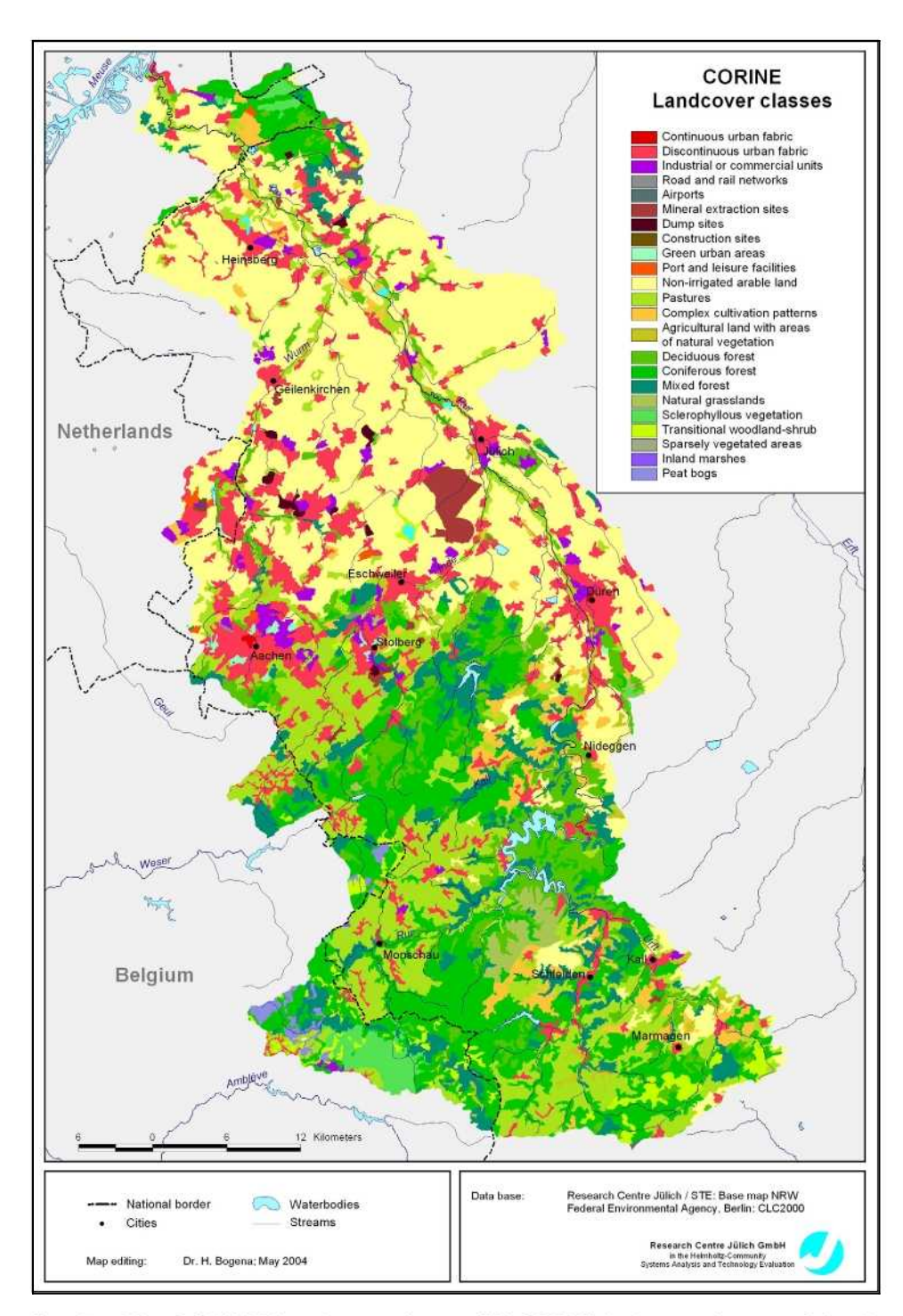
3.2.2 Landcover data

The landcover data used in this study were determined by the Federal Statistical Office within the framework of the EU programme CORINE (Coordination of Information on the Environment). The aim of this programme was to establish uniform and comparable landcover data for the entire region of the European Union. In Germany, a basic data stock is available for the statistical information system on land use (STABIS) and other national geographic information systems. Data collection was effected on a 1:100,000 scale additionally using topographic Maps (TK100) and panchromatic aerial photographs (Statistisches Bundesamt, 1997). Areas with homogeneous landcover of a minimum size of 25 ha or a minimum width of 100 m for linear objects were included. The second evaluation of the CORINE Landcover was based on satellite images from the years 1990 to 2000 (CLC2000). The data stock of CLC2000 contains 44 landcover categories of which 25 occur in the Rur basin (see Map. 7). The total area and area fraction of the CLC2000 Landcover categories are listed in Tab. 7:

Tab. 7: Landcover categories in the catchment of the Rur River (CLC2000).

ID	CORINE Land cover class	Total area [km²]	Percentage of area [%]
1.1.1	Continuous urban fabric	1.22	0.05
1.1.2	Discontinuous urban fabric	262.11	11.14
1.2.1	Industrial or commercial units	31.33	1.33
1.2.2	Road and rail networks and associated land	1.03	0.04
1.2.4	Airports	2.33	0.10
1.3.1	Mineral extraction sites	25.42	1.08
1.3.2	Dump sites	6.20	0.26
1.3.3	Construction sites	0.61	0.03
1.4.1	Green urban areas	5.65	0.24
1.4.2	Sport and leisure facilities	3.17	0.13
2.1.1	Non-irrigated arable land	779.38	33.12
2.3.1	Pastures	368.82	15.67
2.4.2	Complex cultivation patterns	67.70	2.88
2.4.3	Land principally occupied by agriculture, with significant areas of natural vegetation	26.64	1.13
3.1.1	Broad-leaved forest	165.30	7.02
3.1.2	Coniferous forest	351.98	14.96
3.1.3	Mixed forest	168.85	7.17
3.2.1	Natural grasslands	19.92	0.85
3.2.2	Sclerophyllous vegetation	29.66	1.26
3.2.4	Transitional woodland-shrub	11.56	0.49
3.3.3	Sparsely vegetated areas	1.76	0.07
4.1.1	Inland marshes	0.33	0.01
4.1.2	Peat bogs	8.55	0,36
5,1.1	Water courses	0.06	0.002
5.1.2	Water bodies	13.92	0.59

The GROWA model differentiates between the following landcover units: paved areas, vegetation-free areas, grassland, arable land, deciduous forest, coniferous forest and water surface. For the evapotranspiration calculation, the more differentiated CORINE Landcover categories must be allocated to the corresponding land use units or prorate combinations of these have to be formed. For this purpose, the 25 categories that occur in the Rur basin according to CLC2000 were subsumed under these seven land use groups on the basis of a recommendation by ATV-DVWK (2002). The key used for this allocation is shown in Tab. 8:



Map 7: The CORINE Landcover classes (CLC2000) in the catchment of the Rur River.

Tab. 8: Percentages of the landcover units of the CLC classes used in the GRO-WA model, as well as the parameters plant height Z_B and turnover rate (UA) according to ATV-DVWK (2002).

CLC class	Paved areas	Open spaces	P	asture	Arable land		duous rest		iferous orest	Water
[%]	[%]	[%]	Z₅ [cm] [%]	[%]	UA [a]	[%]	UA [a]	[%]		
1.1.1	80		10	12		10	100			
1.1.2	35		20	12	20	15 10	100 30			
1.2.1	85		10	12		5	100			
1.2.2	50	20	20	12		10	100			
1.2.3	80	10	10	12						
1.2.4	30		70	12						
1.3.1		70	25	12						-5
1.3.2		80	20	12						
1.3.3	20	80								
1.4.1			50	12		50	100			
					_	10	100			
1.4.2	15		60	12	5	10	30			
2.1.1					100.					
2.2.2						100	20			
2.3.1			100	20						
2.4.2			35	20	40	25	10			
2.4.3			35	20	40	15	50	10	50	
3.1.1						100	155			
3.1.2								100	85	
3.1.3						50	155	50	85	
3.2.1			100	12						
3.2.2			50	20		50	50			
3.2.4						50	15	50	10	
3.3.1		100								
3.3.3		50	50	12						
4.1.1			50	20	40	10	50			
4.1.2			100	20						
5.1.1										100
5.1.2										100

The frequency distribution obtained on the basis of this land use grouping is shown in Fig. 15. More than one third of the region of the Rur catchment (37.1 %) is represented by the "arable land" landcover unit. The major portion of this landcover group is to be found in the lowland regions in the northern part of the Rur catchment.

The forest categories "deciduous forest", "coniferous forest" are covering a total area of 807 km² in the Rur catchment (34.3 %). This landcover group is the second largest area fraction in the Rur catchment and predominates in the upland regions. The landcover category "pasture" only accounts for approx. 21.9 % and, thus, is also an important landcover category, especially in the upland areas. The paved areas in the Rur catchment occupy a noteworthy area fraction (approx. 5.1 %), but are manly allocated in the northern part of the region. Open spaces (1.0 %) are mainly caused by open cast mining, e.g. "Tagebau Inden" with an area of 1370 ha in 2003 (RWE Power, 2004). Sur-

face waters are taken up to a great extent by the water reservoirs located the upland areas.

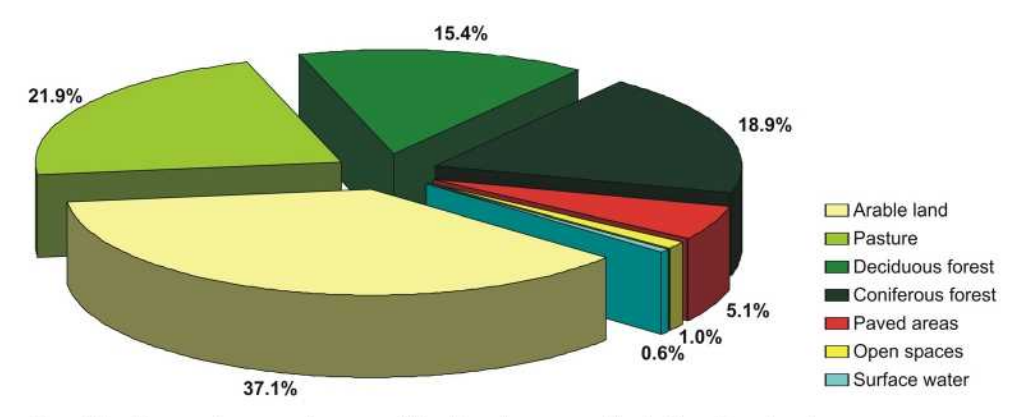


Fig. 15: Percentages of area of the landcover units in the Rur basin.

3.2.3 Soil data

The water and matter balance is particularly governed by pedological factors. For example, the evapotranspiration rate is controlled by the water stored in the rhizosphere, the so-called plant available soil water content (W_{pl}). This soil hydrological parameter enters in the calculation of the water balance values (Chapter 2.2.1). Information about the available field capacity, effective rooting depth and capillary rise is required to derive this parameter. The soil data is also important for separating the baseflow fraction from the total runoff level (Chapter 2.2.7).

All pedological parameters were taken from the soil map of North Rhine-Westphalia BK50 on a scale of 1:50,000. The scale of this map gives an overview of the soils in the Rur catchment and their regional significance with adequate precision. BK50 describes each soil unit by the soil type, the groundwater and waterlogging influence, the geogenesis or rock type with its stratigraphy and the soil type stratification down to 2 m depth (Schrey, 1994). The soil type stratification contains quantified information on the soil texture, humus and lime contents and thickness for each layer. Moreover, each unit is described by classified data on the sorption capacity, water storage capacity and permeability. On this basis, in conjunction with characteristics from the pedological mapping instructions (AG Boden, 1994), the evaluations presented here are calculated.

Groundwater level

The groundwater near the surface essentially determines the development and properties of soils and, thus their opportunities for agricultural use or melioration requirements. The groundwater level varies more or less strongly during of a year as a function of weather, of the substratum, the terrain location and vegetation. Apart from the mean groundwater level, the amplitude of its variations is also shown. The variations are very strong downwards, above all under forest, and the wet phases of the soils characterized by waterlogging are shorter than under agricultural use.

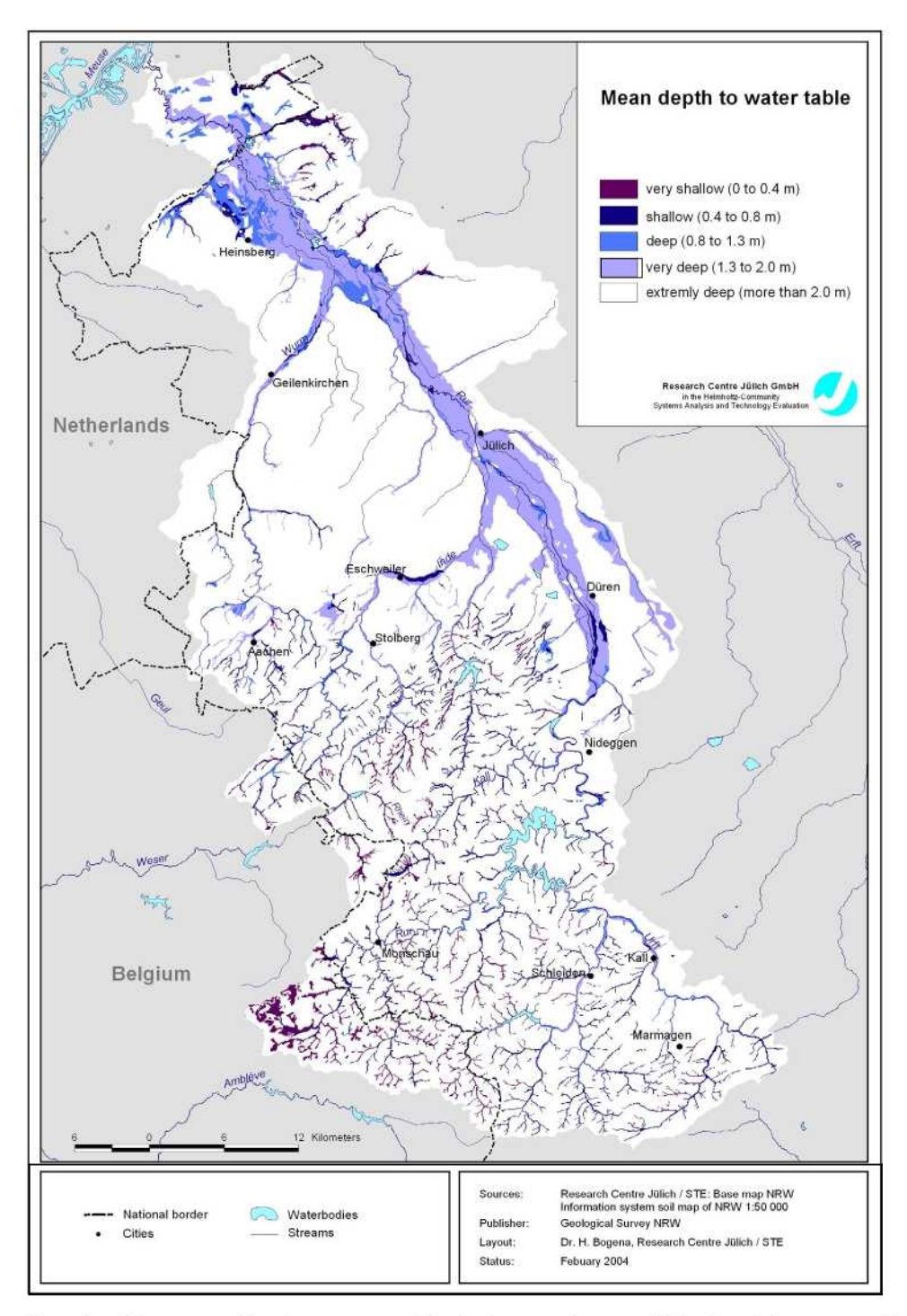
The groundwater level can be anthropogenically influenced by subsidence, drainage, recipient regulation, groundwater withdrawal, industry or as subsidence in open-pit lignite mining and by near-surface groundwater backflows in front of constructions such as motorways or canals.

The groundwater stage characterizes the mean depth to groundwater including the closed capillary fringe in decimetres below ground level (GL) with a normal variation amplitude related to the hydrological six summer months (May to October). Groundwater-free soils are given groundwater stage "0". In the soil unit symbol, the numerical groundwater stage is preceded by "G" for groundwater or "H" for slope groundwater and by a further letter for the level of the mean variation range (see Tab. 9).

Map 8 shows the mean depth to the groundwater in decimetres below ground level. Areas with a depth to groundwater of less than 0.4 m, relevant for the identification of near-groundwater sites, occur in the floodplain meadows of almost all rivers and in the bog region of the Hohes Venn in the southwest of the Rur catchment.

Tab. 9: Coding of the depth to water table and the groundwater stage.

Description	very shallow	shallow	deep	very deep	extremely deep
mean range below ground surface [m]	0 – 0.4	0.4 - 0.8	0.8 – 1.3	1.3 – 2.0	more than 2.0
normal fluctuating	GW1	GW2	GW3	GW4	not documented
lowered and normal fluctuating	not documented	GA2	GA3	GA4	GA5
risen and normal fluctuating	GH1	GH2	GH3	GH4	not documented
strongly upward fluctuating	GO1	GO2	GO3	GO4	not documented
strongly downward fluctuating	GU1	GU2	GU3	GU4	not documented
strongly upward and downward fluctuating	GS1	GS2	GS3	GS4	GS5



Map 8: The mean depth to water table in the catchment of the Rur River according to BK50.

Sites with a medium to deep depth to groundwater are widespread in the alluvial plains of the rivers Rur, Inde and Wurm. In the upland regions, the soils of the river plains are frequently affected by groundwater. In the region of the Jülich fertile plains, in contrast, hardly any site is groundwater-affected. An exception is the region of the "Zwischenscholle", where due to an tectonic uplift of a water-impermeable rock layer groundwater is kept near the surface.

Waterlogging tendency

The waterlogging stage describes the type and degree of waterlogging of perched- and retained-water-affected soils relative to the whole soil profile. Perched-water-free soils are given waterlogging stage "0". The coding of the waterlogging stages is listed in Tab. 10.

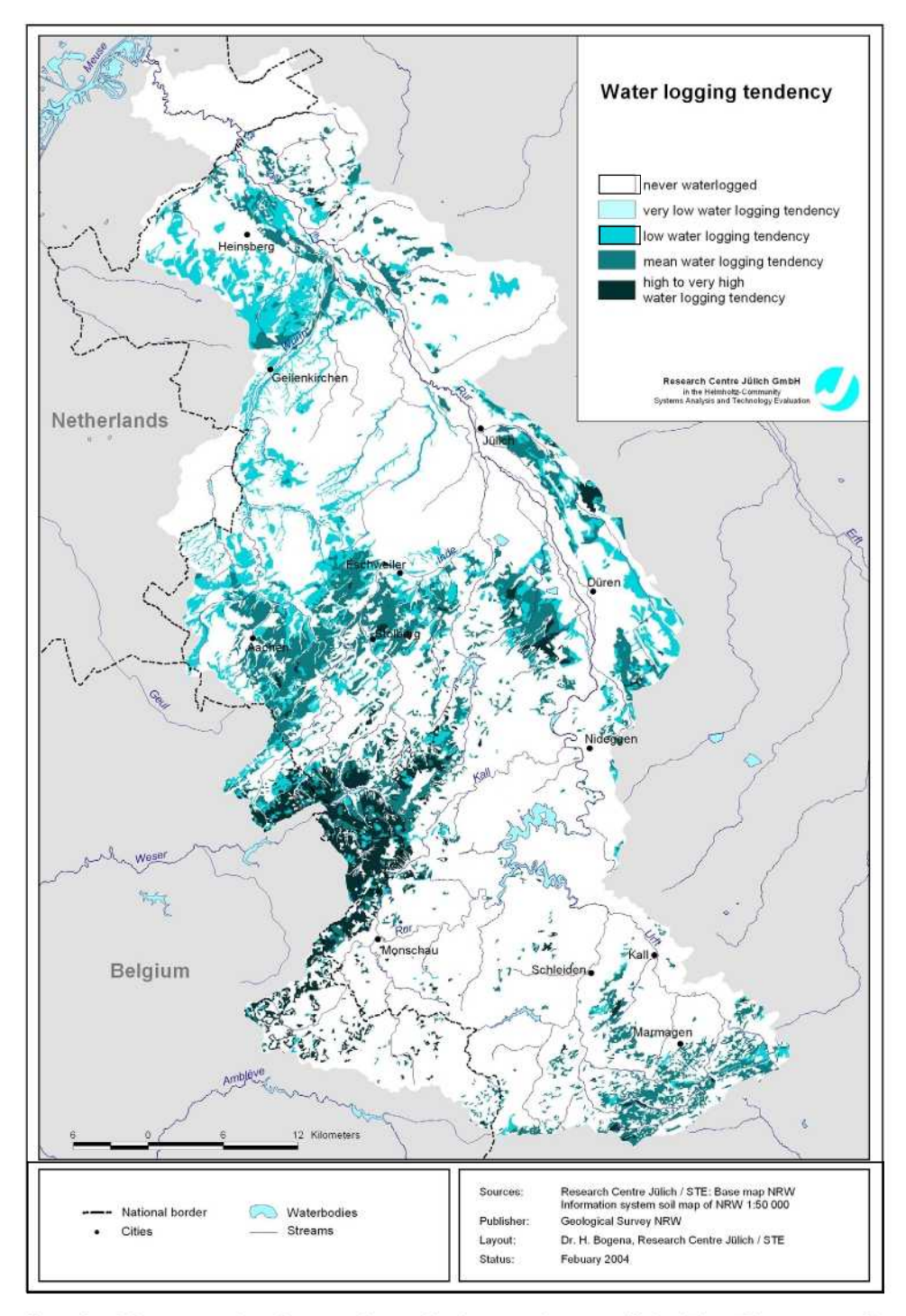
Tab. 10: Coding of the degree of the water logging tendency.

Description	very low	low	mean	distinct	very distinct
waterlogging	SW1	SW2	SW3	SW4	SW5
waterlogging at slopes	SH1	SH2	SH3	SH4	SH5
hygroscopic water	SP1	SP2	SP3	SP4	SP5

Map 9 shows the waterlogging tendency of the perched- and retained-water-affected soils in the catchment of the Rur River. The map indicates that strongly affected soils are predominantly located in the upland region Hohes Venn. Soils with a mean water logging tendency can be found in the northern part of the Rur catchment, in a band stretching from Aachen to Düren, and in the Eifel region south of Marmagen.

Plant available water in the effective rhizosphere

The plant available soil water corresponds to the available field moisture capacity in the effective rhizosphere (Schrey, 1996), added by the annual capillary rise of groundwater into the rhizosphere in the case of soils close to groundwater.



Map 9: The water logging tendency in the catchment of the Rur River according to BK50.

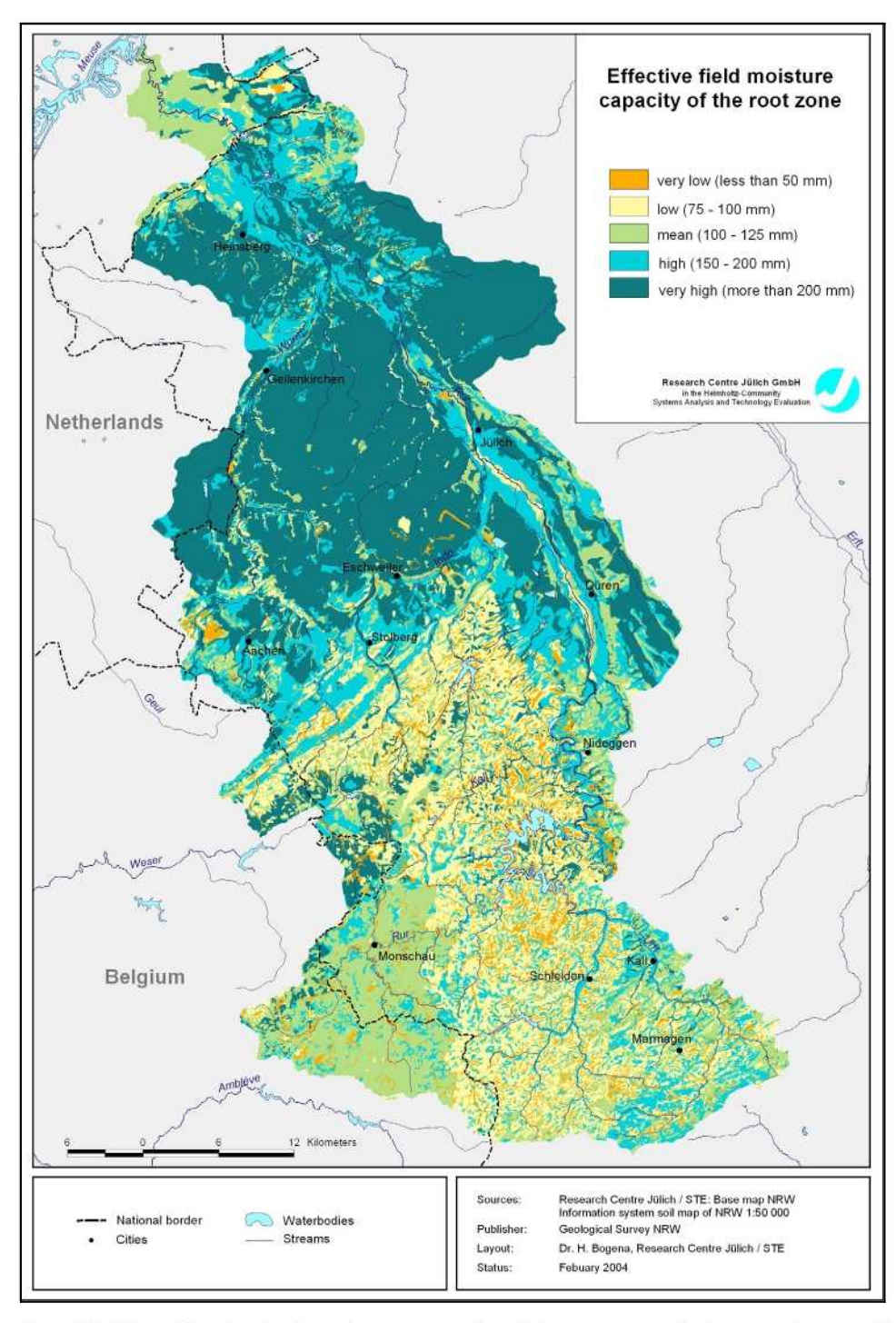
The available field moisture capacity is that part of the field capacity that can be reached by vegetation and is stored in the medium-sized pores with tensions of pF 1.8 to 4.2. Depending on the soil type layer, it is calculated from the fraction of soil types with medium compactness corrected by volume-percentage deductions for the skeletal fraction (without available field capacity) or additions for the humus contents. The available field capacity of the effective rhizosphere *FCeff* is obtained from the sum of the available field capacity per soil type layer across the mean effective rooting depth.

The mean effective rooting depth is land use-dependent. Within the framework of this study, the landcover categories of arable land, pasture and forest were distinguished in calculating the available field capacity. The CORINE landcover dataset CLC2000 was used for the spatial differentiation of the land use categories (see Chapter 3.2.4). The calculation of the available field moisture capacity is performed separately for each land use category assuming a maximum rooting depth of 1.1 m for arable land, 0.8 m for pasture and 1.5 m for forest. In those cases in which rooting is limited (e.g. because of low depth to groundwater, small soil thickness etc.) the rooting depth is correspondingly lower.

Map 10 shows the available field capacity of the effective rhizosphere determined according to this method. For the Dutch areas in the northeast of the Rur catchment and for individual urban areas the data of the 1:1,000,000 digital soil survey Map (BÜK1000) of the Federal Institute for Geosciences and Natural Resources were used, since these areas were not documented by data in BK50.

In the Rur catchment, soils of high available field capacity are often associated with the occurrence of loess. Especially in the Northern part of the catchment the loess coverage shows high thicknesses, e.g. the Jülich fertile plain. Here, mean available field capacities above 200 mm are abundant. Significantly lower available field capacities are to be found in the upland regions in the southern part of the Rur catchment. Here, the field capacity ranges between 50 and 150 mm and can locally fall below 30 mm.

The capillary rise of groundwater into the rhizosphere depends on the distance between the bottom limit of the rhizosphere and the temporally varying groundwater surface, on the water content in the rhizosphere and on the soil types.



Map 10: The effective field moisture capacity of the root zone in the catchment of the Rur River according to BK50.

The capillary rise is high for small distances or soils rich in clay or silt and low for large distances or sandy soils. The average annual water reaching the soil through capillary rise CR_{annual} is calculated from the rise rate CR_{rate} and the duration of capillary rise D_{CR} :

$$CR_{annual} = CR_{rate} \cdot D_{CR} \tag{37}$$

Values for the capillary rise rate are available in the BK50 soil information system. For the determination of the capillary rise, standards are specified by NIBIS (Lower Saxonian soil information system) (Müller, 1997) for cereals, corn and pasture, which are listed in Tab. 11:

Tab. 11: Calculation of the duration of capillary rise after NIBIS (Müller, 1997).

1 -1 -1	CR _{rate}	D-1-4	Dui	ration of capil	lary rise D _{CR}	[d/a]
Landuse	[mm/d]	Relation	$FC_{eff} = 0$	FC _{eff} =100	$FC_{\text{eff}} = 200$	$FC_{eff} = 300$
	<= 1	0.14 · FC _{eff} + 14.3	14.3	28.3	42.3	56.3
	2	$0.13 \cdot FC_{eff} + 23.4$	23.4	36.4	49.4	62.4
Cereals	3	$0.10 \cdot FC_{eff} + 35.0$	35.0	45.0	55.0	65.0
	4	0.07 · FC _{eff} + 44.4	44.4	51.4	58.4	65.4
	>=5	60.0	60.0	60.0	60.0	60.0
	<= 1	0.20 · FC _{eff} + 16.6	16.6	36.6	56.6	76.6
	2	0.18 · FC _{eff} + 32.8	32.8	50.8	68.8	86.8
Corn	3	$0.16 \cdot FC_{eff} + 45.3$	45.3	61.3	77.3	93.3
	4	0.11 · FC _{eff} + 62.5	62.5	73.5	84.5	95.5
	>=5	90.0	90.0	90.0	90.0	90.0
	<= 1	$0.25 \cdot FC_{eff} + 19.5$	19.5	44.5	69.5	94.5
	2	0.23 · FC _{eff} + 38.7	38.7	61.7	84.7	107.7
Pasture	3	0.21 · FC _{eff} + 59.4	59.4	80.4	101.4	122.4
	4	0.18 · FC _{eff} + 81.0	81.0	99.0	117.0	135.0
	>=5	120.0	120.0	120.0	120.0	120.0

These parameters were generalized to the following equation (Bogena et al., 2003):

$$D_{CR} = (a + 0.02(1 - CR_{rate})) \cdot FCeff + CR_{rate} \cdot b$$
(38)

FCeff : Field capacity of the effective rhizosphere [mm]

a,b : Land use specific coefficients [-]

Tab. 12 lists the constants a and b for calculating capillary rise duration:

Tab. 12: Coefficients for the calculation of the duration of capillary rise according to equation 38.

Landuse	а	Ď
Cereals	0.14	12
Corn	0.20	16
Pasture	0.25	20

The CORINE landcover dataset CLC2000 is used for the spatial differentiation of land use (see Chapter 3.2.2), distinguishing between the categories of arable land, pasture and forest. Due to the lack of differentiation between corn and cereals in CORINE, a mean value of the constants of cereals and corn was formed for the crop areas. The constants for intensive pasture were used for the categories of pasture and forest. Furthermore, it has to be taken into account that capillary rise only occurs in the case of water deficiency. On average, water deficiency is given in the case that the evapo-transpiration in the summer months is higher than the precipitation level in this period. A measure of this is the climatic water balance of the six summer months, CWB_{Su} , which results from the difference between average precipitation level in summer, P_{Su} , and potential evapotranspiration in summer, $ETpot_{Su}$:

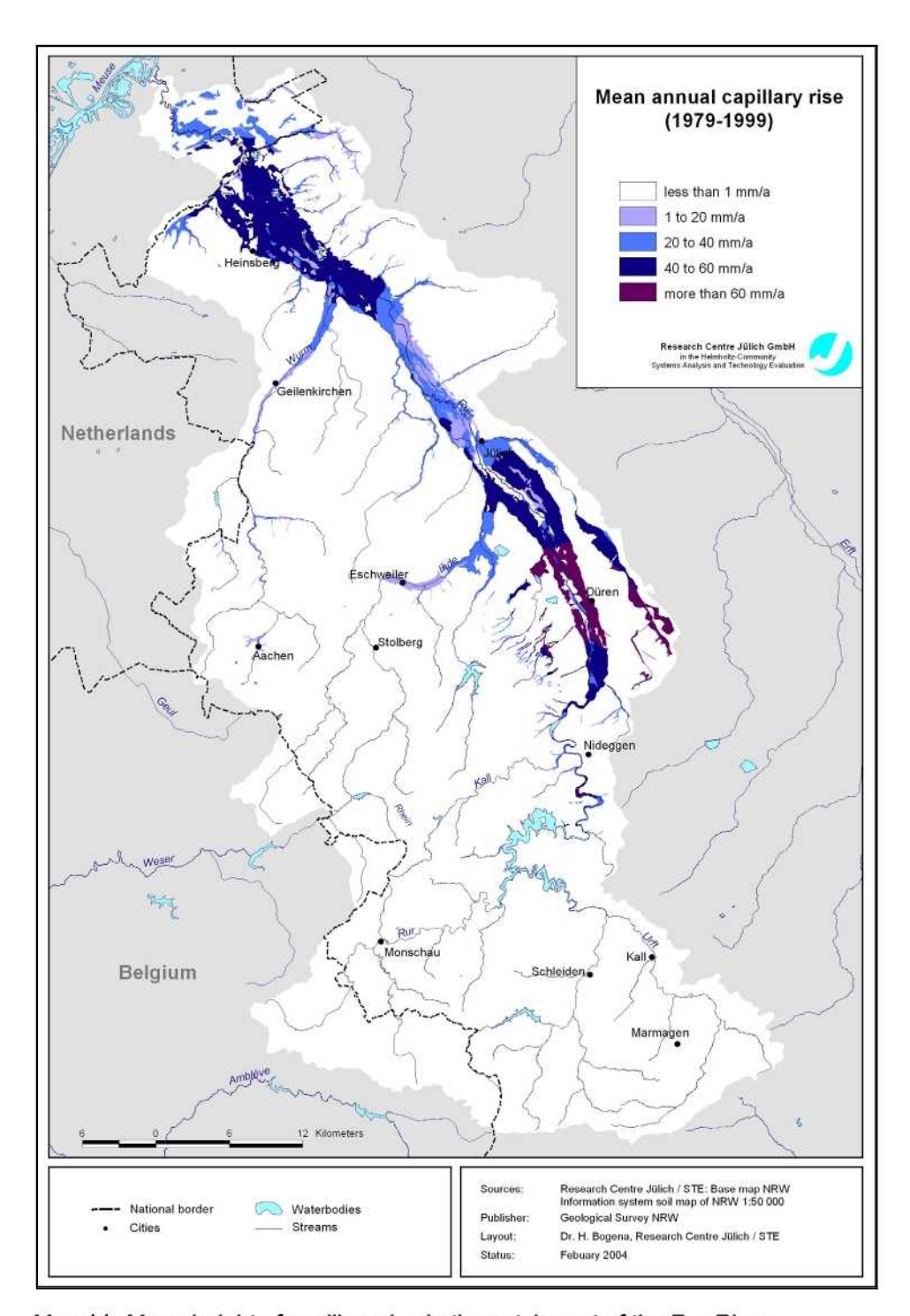
$$CWB_{Su} = P_{Su} - ETpot_{Su}$$
 (39)

The average annual capillary rise is thus calculated as follows:

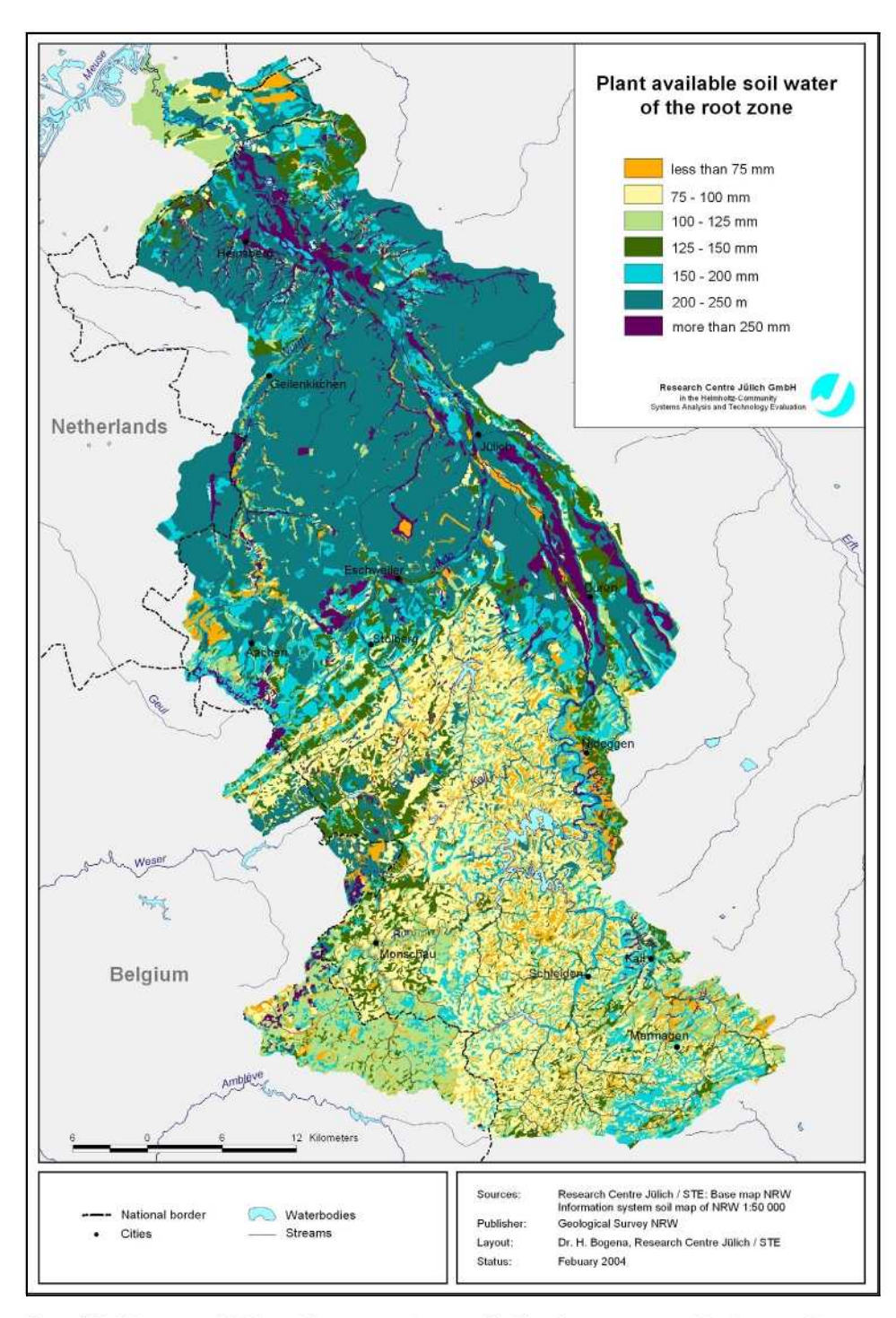
$$CR_{annual} = \begin{cases} 0 & for \ CWB_{Su} \ge 0 \\ CWB_{Su} & for \ CWB_{Su} < 0 \quad and \ CR_{rate} \cdot D_{RC} \ge CWB_{Su} \\ CR_{rate} \cdot D_{RC} & for \ CWB_{Su} < 0 \quad and \ CR_{rate} \cdot D_{RC} < CWB_{Su} \end{cases}$$

$$(40)$$

The result of the calculation is shown on Map 11. The spatial distribution of the sites affected by capillary rise is almost congruent with the distribution of the groundwater-affected sites, since capillary rise is linked to small groundwater depths. Due to the climatic and soil-physical conditions, however, the direct correlation between groundwater level and capillary rise may be less significant. For example, the alluvial soils of the Rur basin exhibit relative low groundwater levels (1.3 to 2 m), so that low capillary rise would have to be expected. Due to the favourable soil-physical conditions of the soils and the relative high evapotranspiration deficiency in the six summer months, nevertheless, capillary rise rates of more than 20 mm/a frequently occur.



Map 11: Mean height of capillary rise in the catchment of the Rur River.



Map 12: Plant-available soil water volume of effective root zone in the catchment of the Rur River.

The sum of the available field capacity of the root zone and the mean annual capillary rise of groundwater into the rhizosphere gives the plant-available soil water W_{pl} .

$$W_{pl} = FCeff + CR_{annual} (39)$$

This is the only soil-physical quantity that enters in the calculation of actual evapotranspiration according to Renger & Wessolek (1996) (Chapter 2.2.1) and, therefore, it is of special importance. Map 12 shows the spatial distribution of the plant-available soil water volume in the effective rhizosphere. The regions whose soils primarily originate from loess-containing parent substrata generally exhibit high plant-available soil water volumes. Thus, for some regions of Rur catchment, average values of over 250 mm/a are reached (e.g. some parts of the alluvial plain of the Rur River).

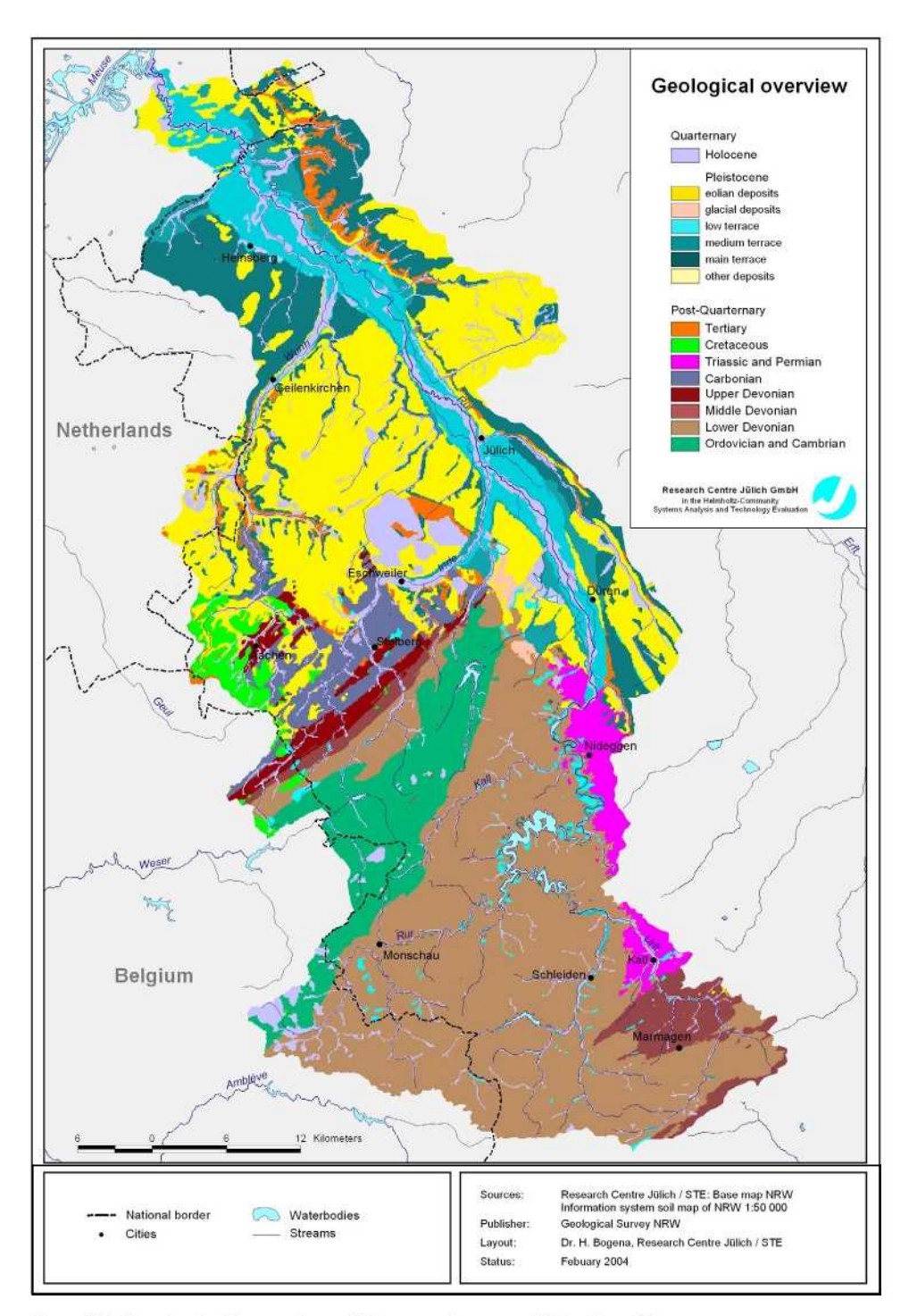
In the case of very small soil thicknesses, e.g. for the soils in the upland region, and for soils with sandy parent substratum, e.g. in the northern Dutch part of the Rur catchment, the plant-available soil water volumes can partly amount less than 100 mm/a.

3.2.4 Hydrogeological data base

Hydrogeological data provide information about groundwater flow through the consolidated and unconsolidated rocks and thus can be used for the spatial-related interpretation of the relevant runoff components. Within the framework of the present study, the geological units of the solid rock areas form the basis for the separation procedure for calculating the groundwater recharge (see Chapter 2.2.5). The specialized information system Hydrogeological Map 1:100,000 was developed by the Geological Service of NRW (GD NRW) as part of the activities for the European Water Framework Directive. It is available in its first extended version, in which the geometries shown are identical to those of Geological Map 1:100,000 (GK100) (GD NRW, 2003).

Geological overview

Map 13 shows a survey of the geological conditions in the catchment of the Rur River on the basis of the GK100. The stratigraphic division was performed as a function of the near-surface occurrence of the rock formations. The Palaeozoic and Mesozoic solid rocks, outcropping mainly in the southern part of the Rur catchment, occupy an area fraction of about 47 % throughout the catchment area (Fig. 16).



Map 13: Geological overview of the catchment of the Rur River.

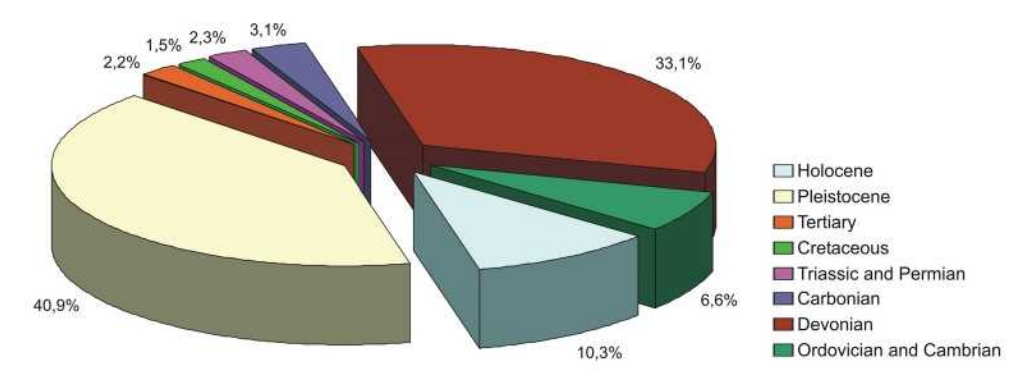


Fig. 16: Frequency distribution of the main stratigraphic units in the Rur catchments.

The Palaeozoic solid rocks of the Rhenish Massif formed in the course of Variscan orogenesis occupy the largest area fraction (33 %). Predevonian solid rocks only outcrop in some locations, e.g. in the region of Hohes Venn in the form of Cambrian and Ordovician clay slates and quartzites (6.6 %).

The Rhenish Massif is predominantly formed of Devonian and Carboniferous sedimentary rocks, which can show thicknesses of several thousand metres. These are alternating sequences of silt- and mudstones as well as sandstones and greywackes with small cavity and groundwater storage volumes. Water flow in these rocks is primarily linked to tectonic faults and jointing. Due to their mostly strong karstification, the Middle and Upper Devonian carbonate rocks (e.g. in the "Sötenicher Kalkmulde" to the north of Marmagen and the Givetian reef limestone "Massenkalk" to the south of Stolberg) can exhibit a higher groundwater storage volume.

Mesozoic solid rocks outcrop in the east border of the Rur catchment between the localities Nideggen and Kall. These are primarily rocks from the Lower Triassic Age, which consists mostly of semisolid sandstones of the Lower Triassic stage are superimposed by Triassic limestones.

Approximately 53 % of the near-surface rocks in Rur basin are formed from unconsolidated sediments. These are mainly Quaternary deposits. Thick Tertiary unconsolidated rock deposits are above all present in the northern part of the Rur catchment, but are mostly covered by Pleistocene terrace deposits (sands and gravels of the main, middle and lower terraces of the rivers Maas and Rur) and by aeolian deposits (loess and dune sands).

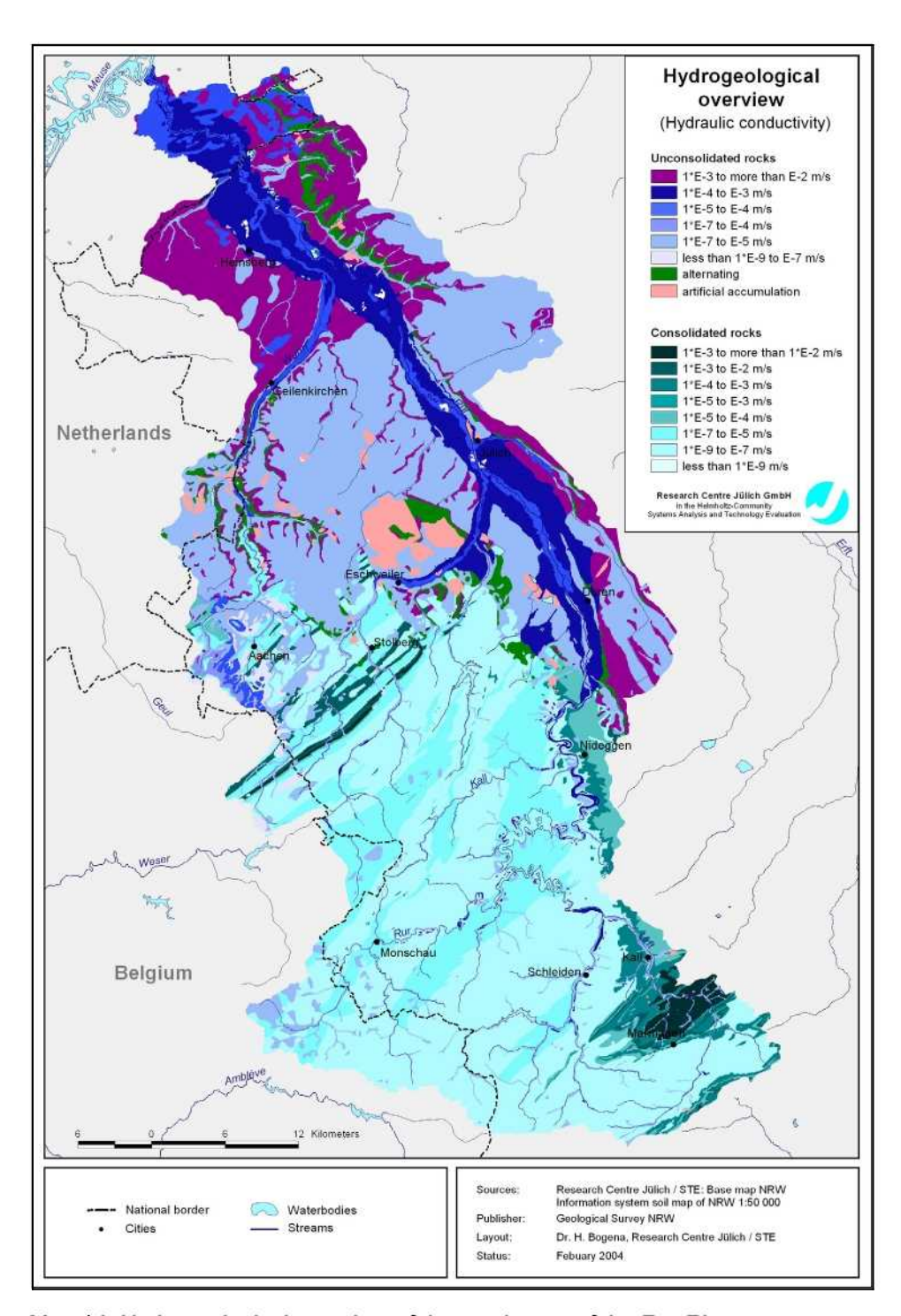
Hydraulic conductivity of water-bearing rocks

Gabriel and Ziegler (1989) point out that the special lithologic character of the rock complexes is more important for hydrogeological assessment than their stratigraphic position. This applies, in particular, to the quantification of the baseflow fractions in solid rock (see Chapter 2.2.7). For this reason, hydrogeological characteristics of the HK100 specialized information system derived on the basis of the GK100 were used to determine the groundwater recharge. The rocks that outcrop near the surface have been assessed with respect to their permeability, to their geochemical characteristic and to their cavity volume. As far as the geological map information is adequate, an evaluation of the covering strata was also performed. Since the HK100 information system is a generalized synoptic representation, the assessment of the permeability of the consolidated and unconsolidated rock units is based on maps, as well as on evaluations and representations on other scales. Furthermore, the relevant geologists' regional knowledge and experience have been incorporated.

Pumping test evaluations and sieve analyses form the bases of the actual data for the unconsolidated rocks. In this respect, a method is applied which is based on the algorithm of Beyer (1964) and which allocates typical permeability coefficients to the granulometric curves. For solid rocks, jointing and the degree of separation are estimated. For stratified unconsolidated rocks, especially if less permeable clay or silt bands are intercalated, the vertical permeability is often one to two orders of magnitude lower.

Map 14 shows the hydraulic conductivities of the water-bearing rock strata in the catchment of the Rur River. The hydraulic conductivities of the Quaternary deposits frequently range between 10⁻⁴ m/sec and 10⁻² m/sec depending on the lithologic character of the sediments. In regions where the loess forms thick covering strata (e.g. the Jülicher fertile plains) clearly lower conductivities (10⁻⁷ m/sec to 10⁻⁵ m/sec) are present. Furthermore, areas with artificial accumulations frequently occur, which cannot be assigned to a conductivity class due to the heterogeneous substrata.

In the region around Aachen, Upper Cretaceous unconsolidated clay and silt rocks are outcropping featuring hydraulic conductivities from 10⁻⁸ m/sec up to 10⁻⁶ m/sec. These strata are covered by sandy unconsolidated rocks that exhibit conductivities of 10⁻⁶ m/sec to 10⁻⁴ m/sec, whereas the marly deposits can have significantly higher conductivities (between 10⁻² m/sec and 10⁻⁴ m/sec).



Map 14: Hydrogeological overview of the catchment of the Rur River.

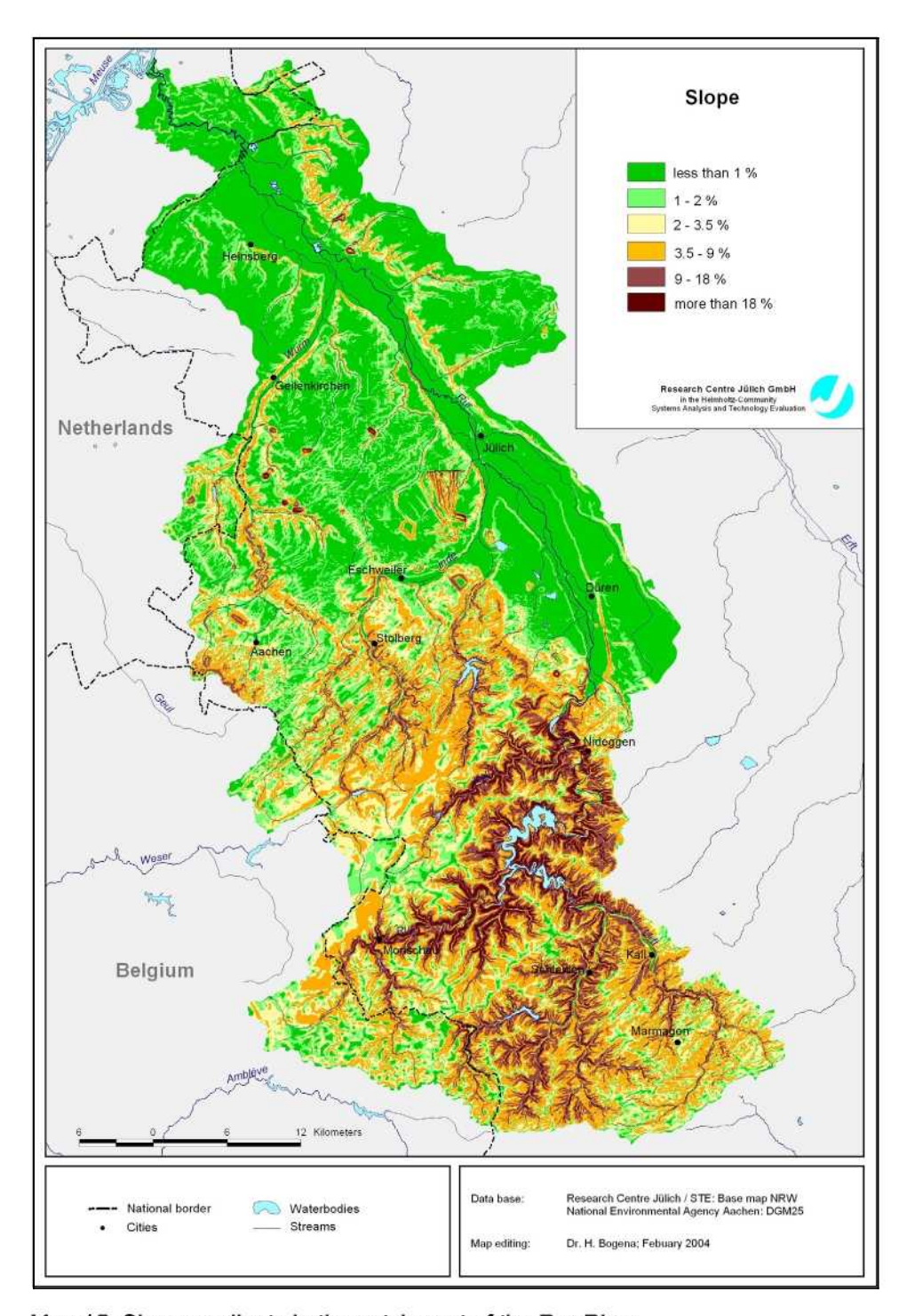
The Triassic semisolid sandy rocks form a yielding aquifer. A primary fast flow system, similar to a karst aquifer, can be differentiated from a secondary flow system having a more effective retention. These rocks have hydraulic conductivities ranging from 10⁻⁵ m/sec to 10⁻² m/sec. Much higher hydraulic conductivities are to be expected for the Triassic limestones and dolomites due to karstification (mostly more than 10⁻² m/sec).

The groundwater in Palaeozoic consolidated rocks of the Rhenish Massif circulates mainly through a system of narrow fissures. Therefore, these rocks have in part extremely low hydraulic conductivities (less than 10⁻⁹ m/sec to 10⁻⁵ m/sec) depending on the fracture permeabilities. Very low groundwater recharge rates are to be expected here, as was also shown by studies on dryweather flow (e.g. summarised in Bogena et al., 2003). In contrast, the often karstified Middle and Upper Devonian massive limestones, located in of Stolberg, and the partly karstified limestones of the lime troughs situated in the North Eifel ("Sötenicher Kalkmulde") have very high hydraulic conductivities (10⁻³ m/sec up to more than 10⁻² m/sec).

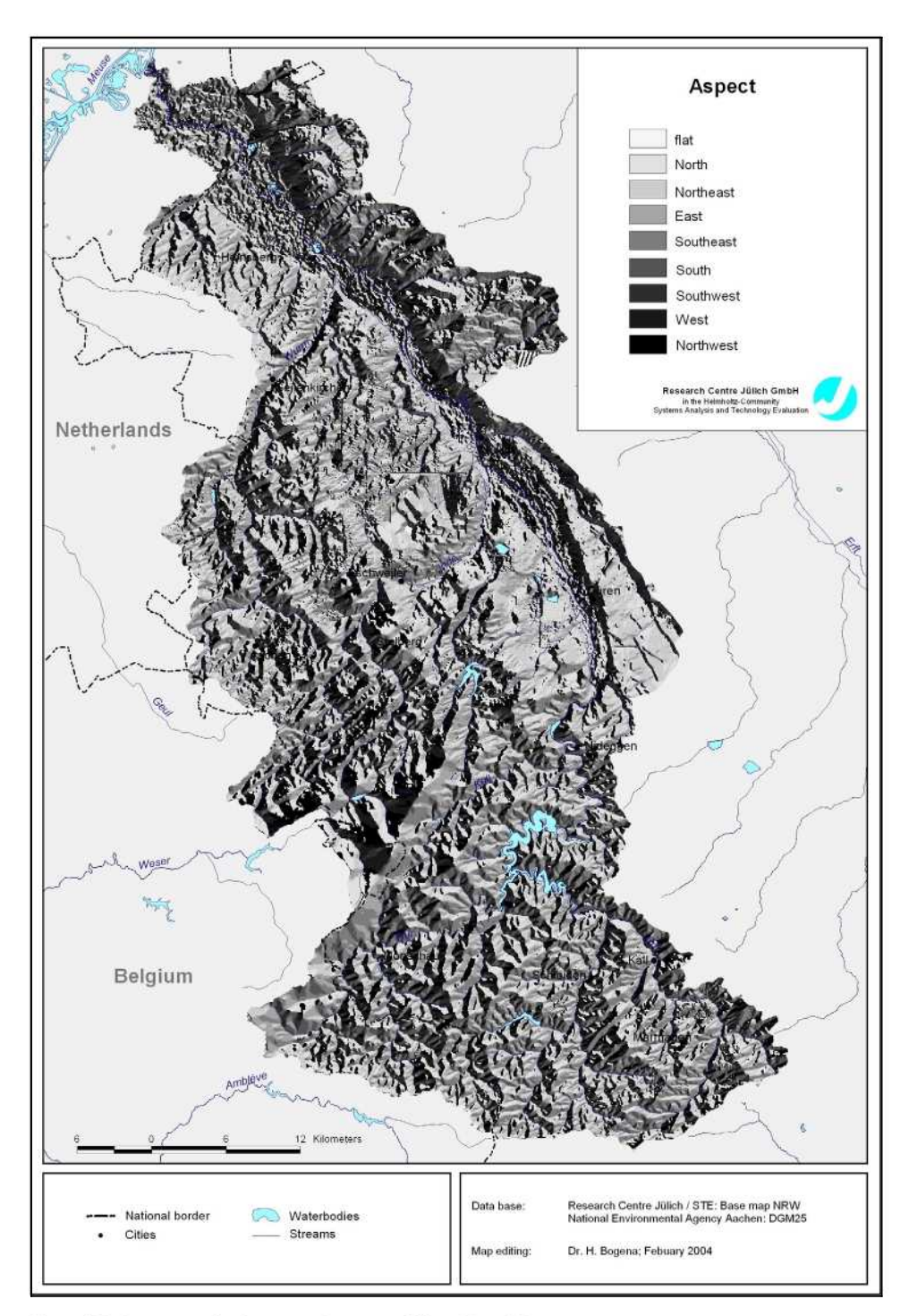
The Predevonian solid rocks (Cambrian and Ordovician age) exhibit very low permeabilities ranging from 10⁻⁸ m/sec down to 10⁻¹⁰ m/sec. According to Loosen (2003), noteworthy groundwater flow is only possible in a 20 m to 50 m thick loosening zone that super-imposes these almost impervious rocks.

3.2.5 Topographic data

The topography has a great influence on the determination of the water balance. Firstly, the slope gradient and aspect are effecting the level of actual evapotranspiration and, secondly, the slope gradient serves as an input parameter for determining the baseflow fraction of total runoff (see Chapter 2.2.7). An area-wide digital terrain model with a resolution of 50 m was made available by the StUA Aachen. On the basis of this terrain model, the aspect and slope gradient were derived area-wide for the catchment of the Rur River. The slope gradient calculated from the DGM50 (Map 15) clearly maps the geological structures in the Rur catchment. Particularly flat regions with slope gradients of less than 1 % are the lowlands in the northern part of the catchment area, which are often associated with the occurrence of unconsolidated rocks.



Map 15: Slope gradients in the catchment of the Rur River.



Map 16: Aspects in the catchment of the Rur River.

The higher relief energy of the Rhenish Massif region clearly distinguishes itself from the lowland regions by gradients mostly above 3.5 %. Here, on the one hand, the distribution of the differently morphologically effective rock strata and, on the other hand, the river system that deeply cuts into the mountains are clearly reflected. The highest slope gradients are reached in the region around the water reservoir "Rurtalsperre", where the maximum values can exceed 30 %.

Map 16 shows the aspect which also reflects the structure of the land surface in the Rur catchment in a high resolution manner. For example, the relatively broad valley of the Rur River and the highly resolved river system in the upland landscapes can be recognized.

3.2.6 Discharge data

Measured gauge runoff values were used for the calibration of the GROWA model and the final validation of the model results. As already explained in Chapter 2.2.5, data from gauging stations distributed in the entire federal state of North Rhine-Westphalia were used for the model calibration. These were made available by numerous institutions (water associations, environmental state agencies and the Federal Institute of Hydrology) (Tab. 11). For data storage and analysis of the gauge data, an extensive database was built up, which currently contains daily runoff values from 268 gauging stations in the federal states of North Rhine-Westphalia and Rhineland-Palatinate in daily resolution. On the basis of this data pool, a selection of gauge measuring stations was made that can be utilized for modelling the water balance (Tab. 13). In selecting the gauges, on the one hand, care was taken to ensure that as different sizes of catchment areas as possible (from 1.3 to 4,783 km²) and a wide range of climatological, geological and pedological site situations were included. On the other hand, only those gauges were selected for which a continuous acquisition of measured data over at least ten years within the period under consideration (1979-1999) was available.

Moreover, catchment areas expected to be significantly affected in their natural runoff processes by anthropogenic influences, e.g. by dams or mining, were not considered any further. After extensive analyses 125 gauges were selected for model calibration. For detailed information see Bogena et al. (2004). Some of the gauge values had to be corrected. In order to eliminate the influence of dam management from the Opladen/Wupper gauge, the runoff quantities of the Glüder/Wupper gauging station located further above were

subtracted on a daily basis and the effective subcatchment area size determined. This correction was necessary because the flow of this section of the river Wupper has been considerably influenced by the low-water augmentation of the Wupper dam since 1987. For the Weeze/Niers and Goch/Niers gauges, the discharge quantities into the Niers canal were taken into account. The discharge quantities were also available in daily resolution. The catchment area above ground of the Schwaney gauge significantly deviates from the runoff-effective catchment area due to karst. On the basis of a comparison with the neighbouring catchment area (gauging station: Altbeken 2) the actual size of catchment area was estimated (17.7 km² instead of 29.5 km²). From the runoff data of the Dedenborn/Rur and Gemünd/Urft gauges, allowances of 15 and 8 %, respectively, had to be abstracted, which the Eifel-Rur water association had assessed to take the respective dam area into account.

Tab. 13: Institutions in North Rhine-Westphalia and Rhineland-Palatinate that delivered gauging data.

No.	Name of the institution	Number of allocated gauging stations	Number of used gauging stations for calibration
1	German Federal Institute of Hydrology	7	1
	Water associations NRW		
2	Wasserverband Eifel-Rur	5	2
3	Erftverband	70	4
4	Wahnbachverband	2	2
5	Aggerverband	8	6
6	Wupperverband	.8	5
7	Ruhrverband	10	6
8	Bergisch-Rheinischer Wasserverband	16	4
	Environmental agencies NRW		
9	StUA Aachen	42	1
10	StUA Köln	22	15
11	StUA Siegen	15	9
12	StUA Krefeld	21	7
13	StUA Düsseldorf	10	.2
14	StUA Duisburg	.5	2
15	StUA Herten	14	12
16	StUA Hagen	9	7
17	StUA Lippstadt	20	10
18	StUA Münster	20	14.
19	StUA Bielefeld	14	9
20	StUA Minden	6	6
	Rhineland-Palatinate		
21	Water management administration RP	2	1
	Total number;	268	125

Model results

4.1 Microscale

Fig. 17 shows the temporal variability of the green leaf area index LAl_{green} [L² L⁻²] calculated with TRACE for grass, potato, maize, sugar beet and winter wheat. It is clearly visible, how the LAl_{green} differs between the years due to the influence of the meteorological conditions and their effect on plant growth.

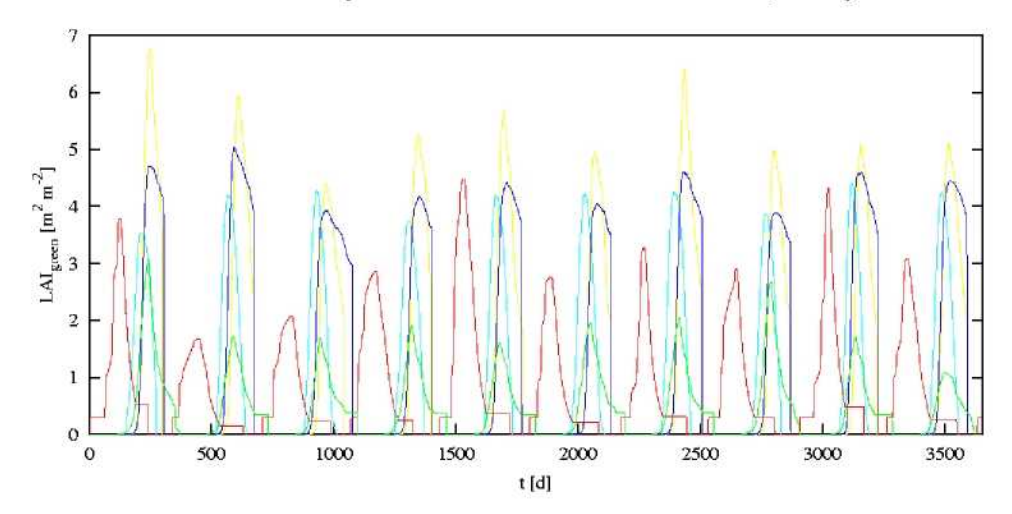


Fig. 17: The development of the green leaf area index of the crops relevant for the test site 'Zwischenscholle' for the 10 years model period 1983-1993 (Green=pasture, cyan=potato, yellow=maize, blue=sugar beet, red= winter wheat).

The highest LAI_{green} were calculated for maize. For winter wheat the intermediate periods without growth during the winter can be detected. These simulations were carried out in a one-dimensional mode with the representative soil profile 'agr2' (see Tab. 12) in order to check the implementation of SUCROS to TRACE and the linking to the water flow modules. The plant database of Van Hemst (1988) was used in order to parameterize the SUCROS module.

Tab. 14: Soil properties of the profile 'Agr2'.

horizon	clay [%]	silt [%]	C _{org} [%]	θ_s [m ³ m ⁻³]	θ_r [m ³ m ⁻³]	α [m ⁻¹]	n [-]	K_s [m d ⁻¹]	thickness [m]
1	13.0	78.5	2.3	0.395	0.044	2.040	1.3381	0.0491	0.2
2	19.0	37.5	0.2	0.298	0.069	4.160	1.3289	0.1102	1.0

Fig. 18 shows the results of this one-dimensional simulation runs concerning the pressure head distribution in the soil profile. The years 1984 and 1988 can be summarized as rather wet years, with high precipitation and only little evapotranspiration. Furthermore differences in root water extraction between plants are clearly visible.

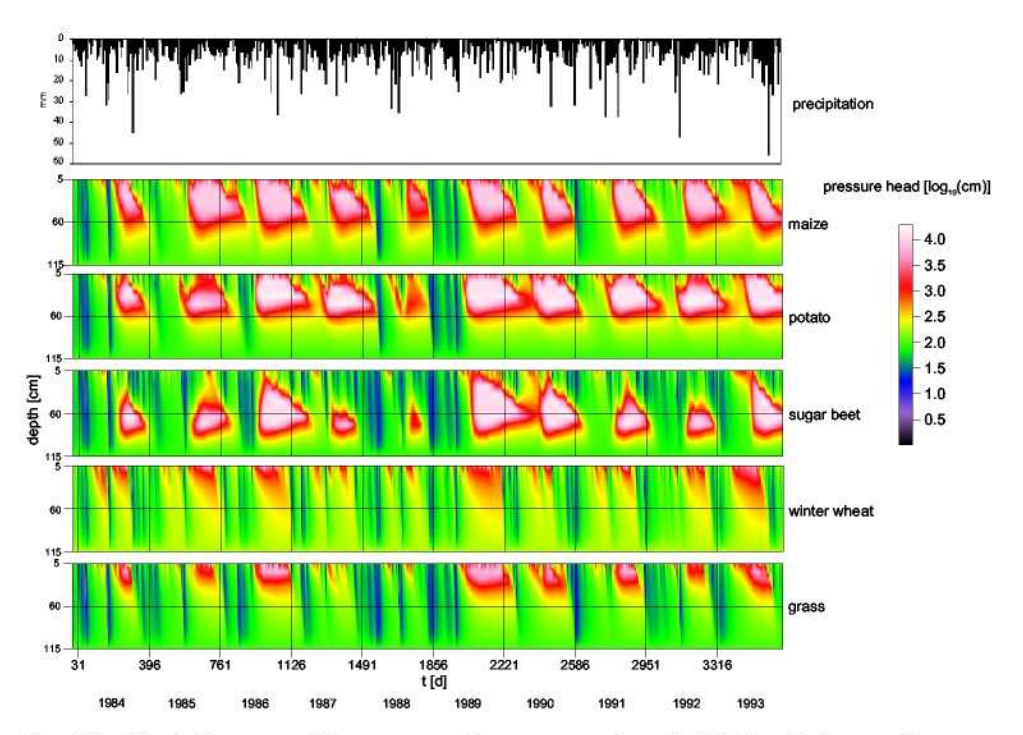


Fig. 18: The influence of the crop on the pressure head; 1D-Simulations with TRACE were carried out with the same soil hydraulic properties and atmospheric boundary conditions.

Fig. 19 shows an example of xy-Maps depicting the pressure head at the soil surface, and evaporation and transpiration for two dates of the modelling period. Here a full 3-dimensional model was built, and the data described in section 2.3 was used to check the performance of the plant module linking. The main differences at the first date 1/7/1984 occur between the forest and the crops. The forest shows high transpiration rates and low evaporation rates, resulting in a rather wet soil at the surface. Basically, the same is true for the second date two months later, but due to the dry climatic conditions the soil at the surface is much dryer than at the first date. At beginning of September the winter wheat is close to harvest, thus the pattern with transpiration close to zero follows the spatial distribution of winter wheat.

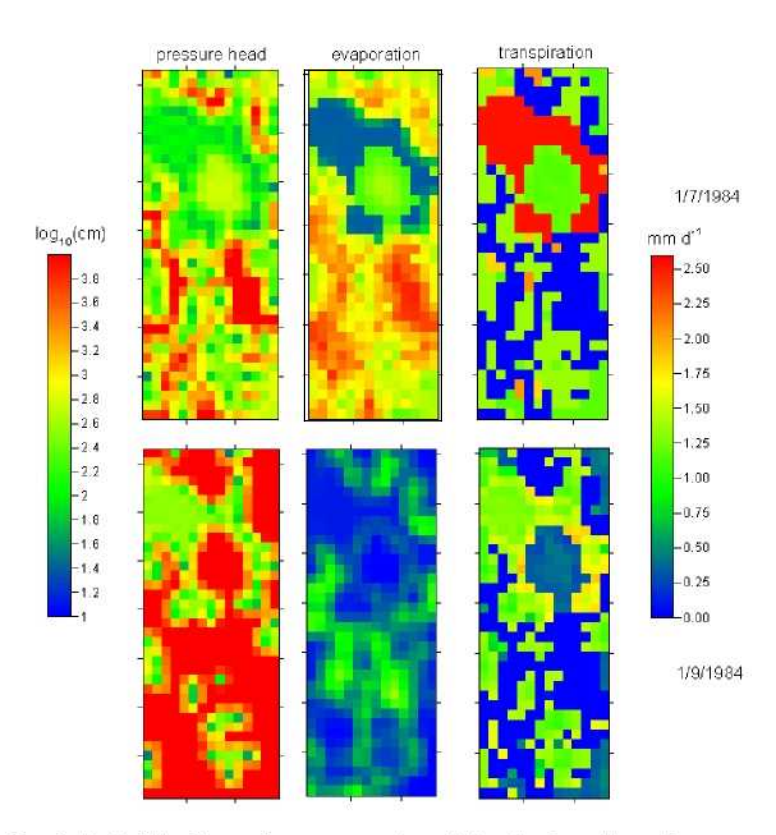
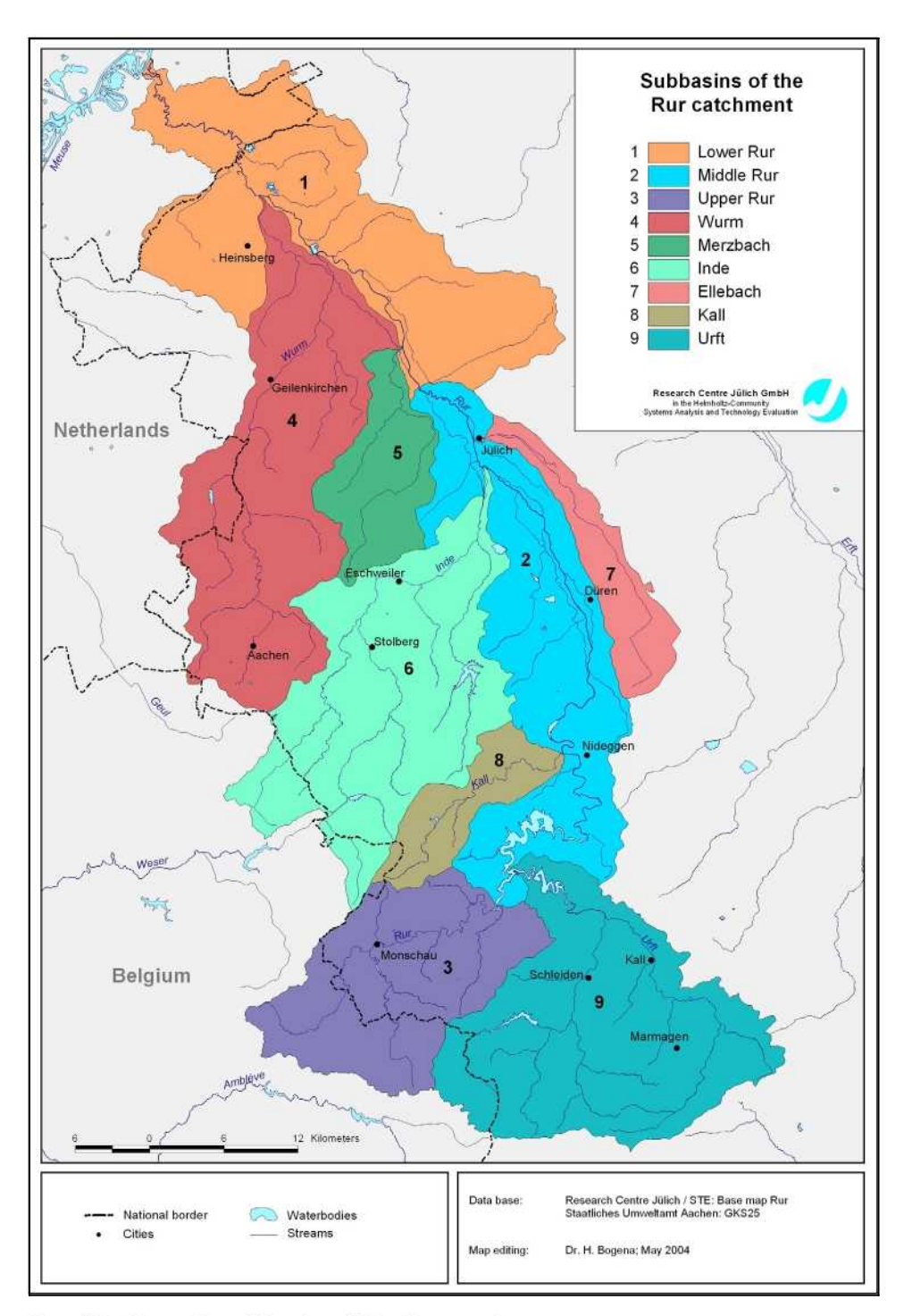


Fig. 19: Spatial distribution of pressure head [cm] at soil surface, evaporation [mm d⁻¹] and transpiration [mm d⁻¹] for two dates (Herbst et al. 2003).

4.2 Macroscale

The GROWA model calculates actual evapotranspiration as well as total runoff and direct runoff in addition to groundwater recharge. These water balance data directly result from the calculation procedure. The water balance data for the catchment of the Rur River are presented as maps and described in Chapters 4.2.1 to 4.2.4. Chapter 4.2.5 contains an evaluation based on the runoff components, which allow a more in-depth and more extensive assessment of the water balance situation in the Rur catchment, e.g. with a view to the description of the condition of water resources in terms of volume. These quantities are the regionally dominant area drainage, the exchange frequency of soil water and the river basin-related water budget balances. Additionally, a statistical analysis on the basis of the main subbasins of the Rur catchment (see Map 17) is carried out in order to provide an overview of their hydrological characteristics.



Map 17: The main subbasins of the Rur catchment.

4.2.1 Actual evapotranspiration

The frequency distribution of the calculated actual evapotranspiration levels for the Rur catchment (Fig. 20) shows that about 80 % of the values are in a relatively narrow range between 400 and 600 mm/a. The frequency distribution is almost symmetrical, the mean value of the actual evapotranspiration levels is 507 mm/a.

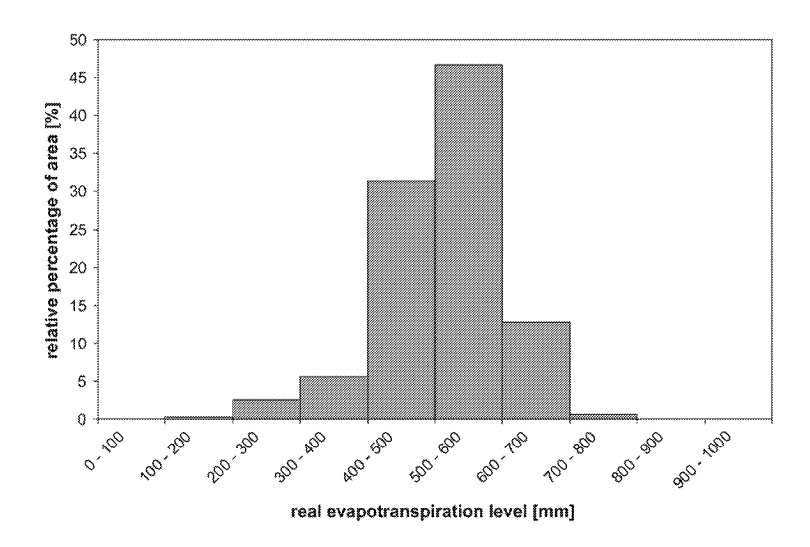
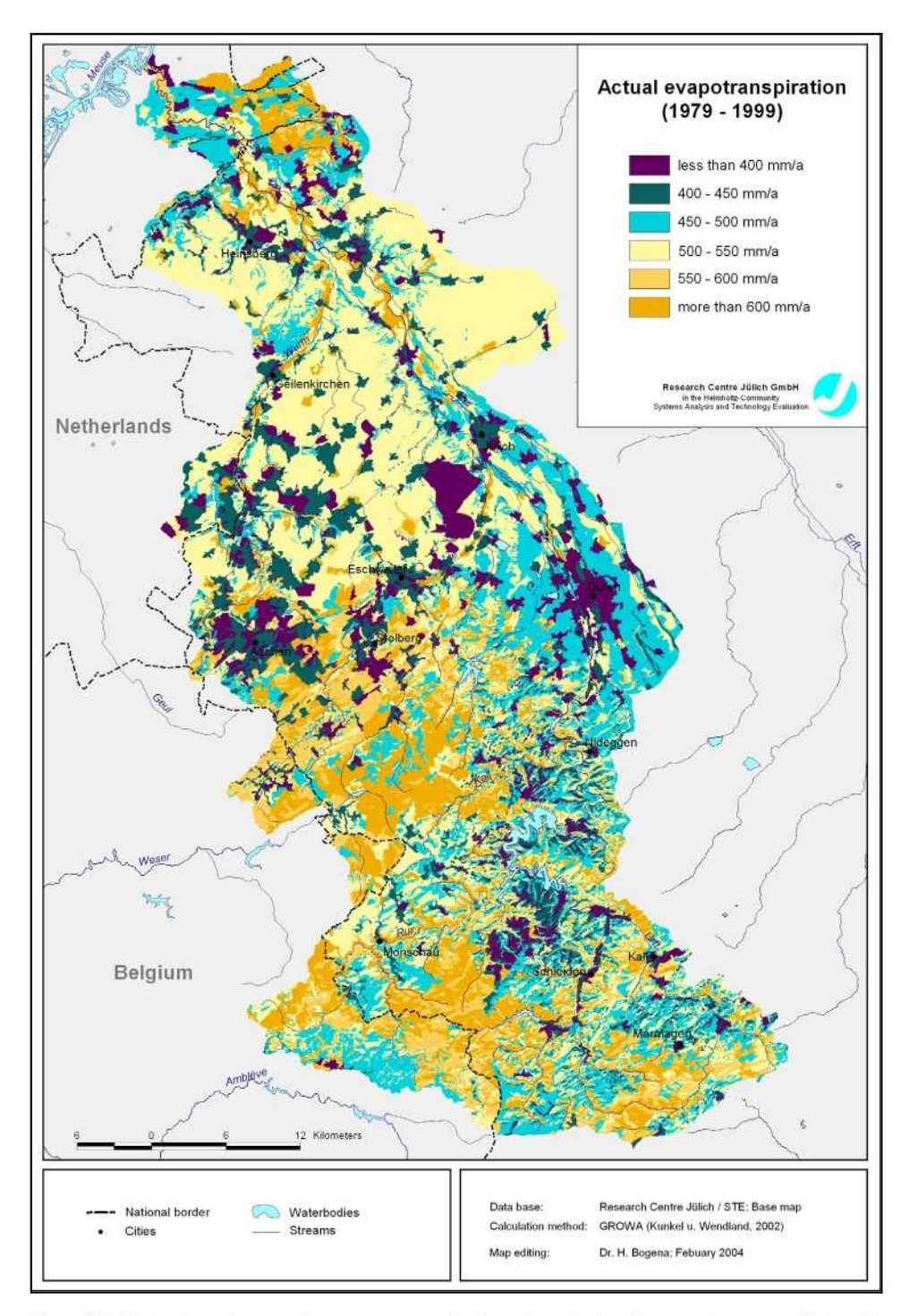


Fig. 20: Frequency distribution of the calculated actual evapotranspiration levels in the Rur basin.

Map 18 shows the actual evapotranspiration levels of the period 1979-1999 calculated for the catchment of the Rur River. Actual evapotranspiration values of more than 550 mm/a prevail only in the upland regions (Eifel, Hohes Venn). This is attributable to the high annual precipitations and the relatively high forest fraction. Low actual evapotranspiration levels below 400 mm/a were especially calculated for the urbanised regions like Aachen and for the mineral extraction sites, e.g. the open-pit mine Inden having an operation area of approx. 1400 ha in the year 2003 (RWE Power, 2004). Depending on the degree of pavement, evapotranspiration in the city centres decreases to values below 300 mm/a.

In the lowland region in the northern part of the Rur catchment, relatively low actual evapotranspiration values (500 to 550 mm/a) are obtained for ground-water distant and unsealed sites, although the potential evapotranspiration is quite high (up to more than 590 mm/a).



Map 18: Calculated actual evapotranspiration levels in the catchment of the Rur River.

This is due to the low annual precipitation amount. Therefore not enough water is available to exhaust potential evapotranspiration.

Tab. 15 shows the actual evapotranspiration levels as mean values and ranges calculated for the main subbasins of the Rur catchment. Instead of the often used arithmetic mean, the median was specified here and for the model results discussed in Chapters 4.2.1 to 4.2.4. The median is much less sensitive to extreme values, especially for asymmetrical distributions, and thus better suited for characterizing the values typical of a region. In the case of the actual evapotranspiration levels, however, the arithmetic mean and the median are nearly identical due to the symmetrical distribution. The range is the difference between the highest and lowest calculated value.

Tab. 15: Ranges and medians of calculated actual evapotranspiration levels of the subbasins of the Rur catchment.

Subbasin	Range	Median
Lower Rur	644 mm/a	515 mm/a
Middle Rur	708 mm/a	488 mm/a
Upper Rur	634 mm/a	530 mm/a
Wurm	609 mm/a	512 mm/a
Merzbach	533 mm/a	511 mm/a
Inde	754 mm/a	547 mm/a
Ellebach	480 mm/a	477 mm/a
Kall	622 mm/a	515 mm/a
Urft	768 mm/a	519 mm/a
Rur catchment	794 mm/a	514 mm/a

Tab. 15 shows that within the main sub-basins large ranges of the actual evapotranspiration occur between approx. 530 mm/a in the Merzbach sub-basin and approx. 770 mm/a in the Urft subbasin. Especially in the hilly regions, there may be great differentiations of evapotranspiration depending on aspect and slope gradient. Thus, in the upland region of the Rhenish Massif, large differences in evapotranspiration can occur between northerly and southerly exposed slopes with otherwise identical characteristics. Actual evapotranspiration levels above 900 mm/a are calculated for coniferous forest in several locations. Groundwater-affected sites in the lowland regions also exhibit high actual evapotranspiration rates, since an additional supply from the groundwater takes place and, in addition, the water storage capacity of the soil is relatively high.

4.2.2 Total runoff

Fig. 21 shows the frequency distribution of the calculated total runoff levels for the Rur catchment. In contrast to the relatively symmetrical distributed evapotranspiration levels, a distinct positive skewness is encountered here. High total runoff levels compared to low total runoff levels occur with increased frequency.

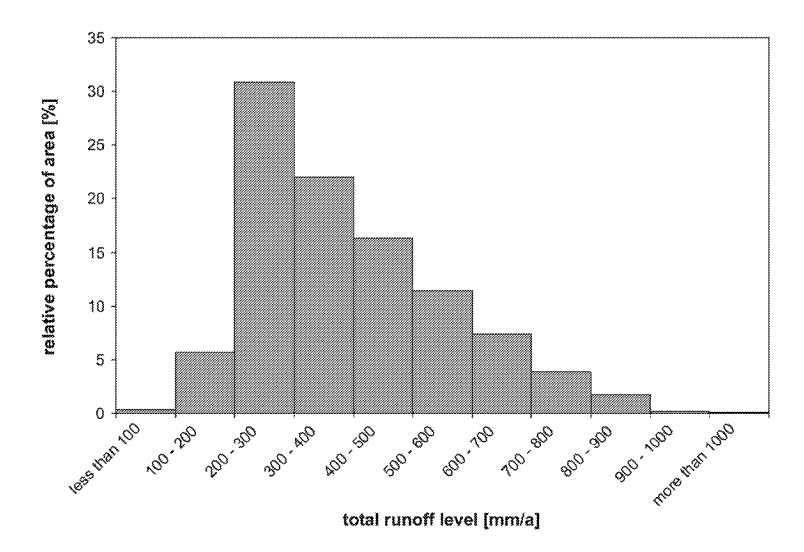
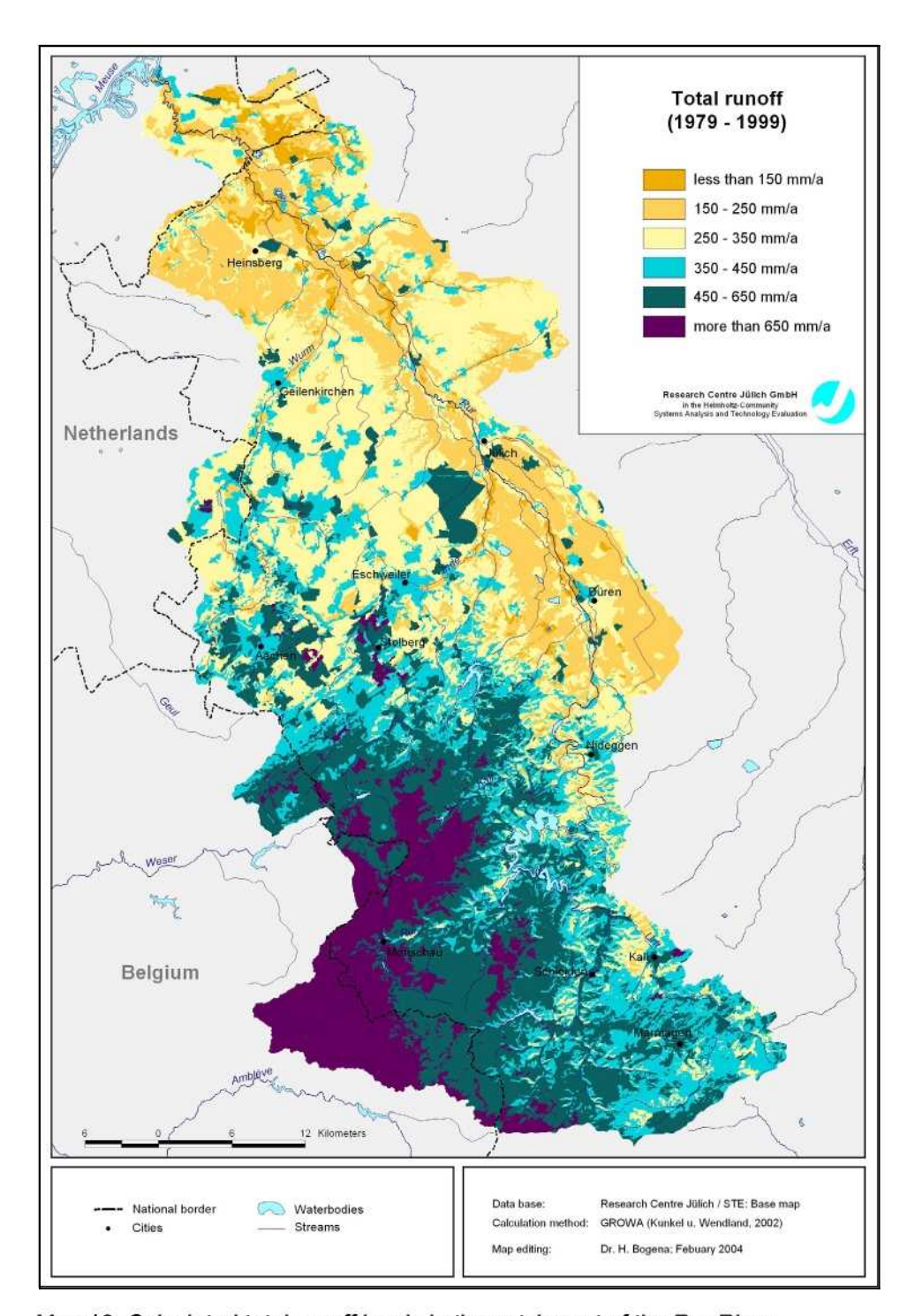


Fig. 21: Frequency distribution of the calculated total runoff levels in the Rur basin.

In this case, the median of the total runoff level of 353 mm/a calculated for the whole catchment of the Rur River is approx. 40 mm/a lower than the arithmetic mean. The maximum of the distribution is formed by the class from 200 to 300 mm/a, in which approx. 31 % of the total values are found. Low total runoff levels below 200 mm/a were only calculated for about 6 %, whereas areas with negative water balances are negligible (less than 0.02 %).

The spatial distribution of the total runoff levels is shown on Map 19. In contrast to the very homogeneously distributed evapotranspiration levels, a pronounced bisection of the land area is visible for total runoff levels. In the low-land regions in the northern part of the Rur catchment total runoff levels of less than 350 mm/a are dominating. Values of less than 250 mm/a are to be found in the region around Heinsberg. In contrast to this, total runoff levels above 450 mm/a are predominating in the upland regions and in elevated upland regions (e.g. Hohes Venn) values of even more than 650 mm/a can be reached. The urbanized regions and the strip mining areas are characterized by total runoff levels between 450 and 650 mm/a.



Map 19: Calculated total runoff levels in the catchment of the Rur River.

Tab. 16 shows the statistical data of the total runoff distribution for the main subbasins of the total area of the Rur catchment. The medians of the total runoff values vary significantly. The Ellebach, Lower Rur, Middle Rur and Merzbach subbasins exhibit the lowest medians with values below 300 mm/a. The highest values are found in the Upper Rur subbasin, where the median of the total runoff levels reaches nearly 700 mm/a.

Tab. 16: Ranges and medians of the calculated total runoff of the subbasins of the Rur basin.

Subbasin	Range	Median
Lower Rur	622 mm/a	250 mm/a
Middle Rur	836 mm/a	291 mm/a
Upper Rur	916 mm/a	686 mm/a
Wurm	619 mm/a	312 mm/a
Merzbach	580 mm/a	291 mm/a
Inde	854 mm/a	421 mm/a
Ellebach	468 mm/a	222 mm/a
Kall	999 mm/a	580 mm/a
Urft	736 mm/a	455 mm/a
Rur catchment	1162 mm/a	353 mm/a

The runoff levels, which occur within the main subbasins, display wide scattering. Even in the climatically relatively homogeneous lowland regions (e.g. the Lower Rur subbasin), the differences between the highest and lowest calculated value can amount to 600 mm/a and more. This reflects the often changing small-scale pedological and hydrological conditions as well as the land-cover taken into account in the calculation.

4.2.3 Groundwater recharge

Fig. 22 shows the frequency distribution of the groundwater recharge levels calculated for the catchment of the Rur River. Instead of a positive skewness as observed for the total runoff a bimodal frequency distribution is visible here. The first maximum of the distribution is formed by the class of 100-150 mm/a, in which approx. 24 % of the values are found, whereas the second maximum is formed by the class 200-250 mm/a (approx. 19 %). Groundwater recharge rates above 350 mm/a only play a minor role in the Rur catchment and only occur in karstified regions and vegetation-free sites (e.g. mineral extraction locations).

Map 20 shows the spatial distribution of the groundwater recharge levels in the Rur catchment for the period 1979-1999. Important to note is that the groundwater recharge levels are clearly higher in the unconsolidated rock regions than in the solid rock regions. The opposite behaviour was found for the total runoff levels.

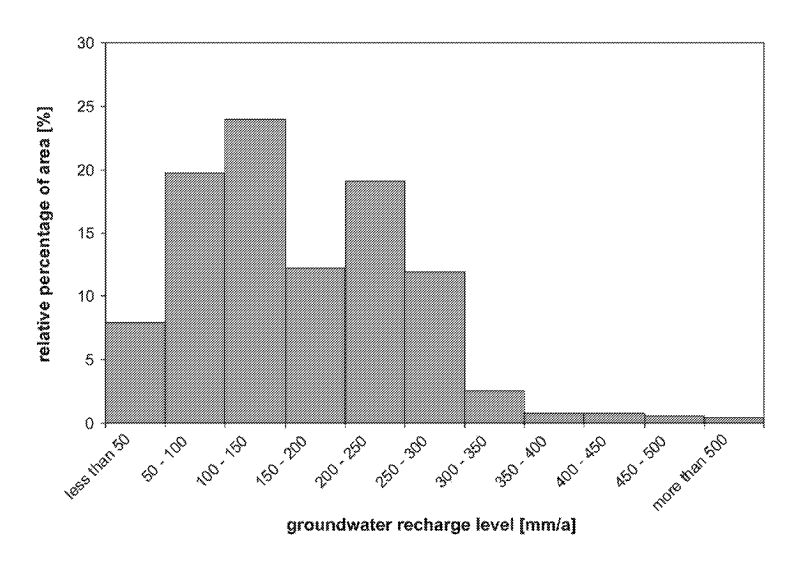
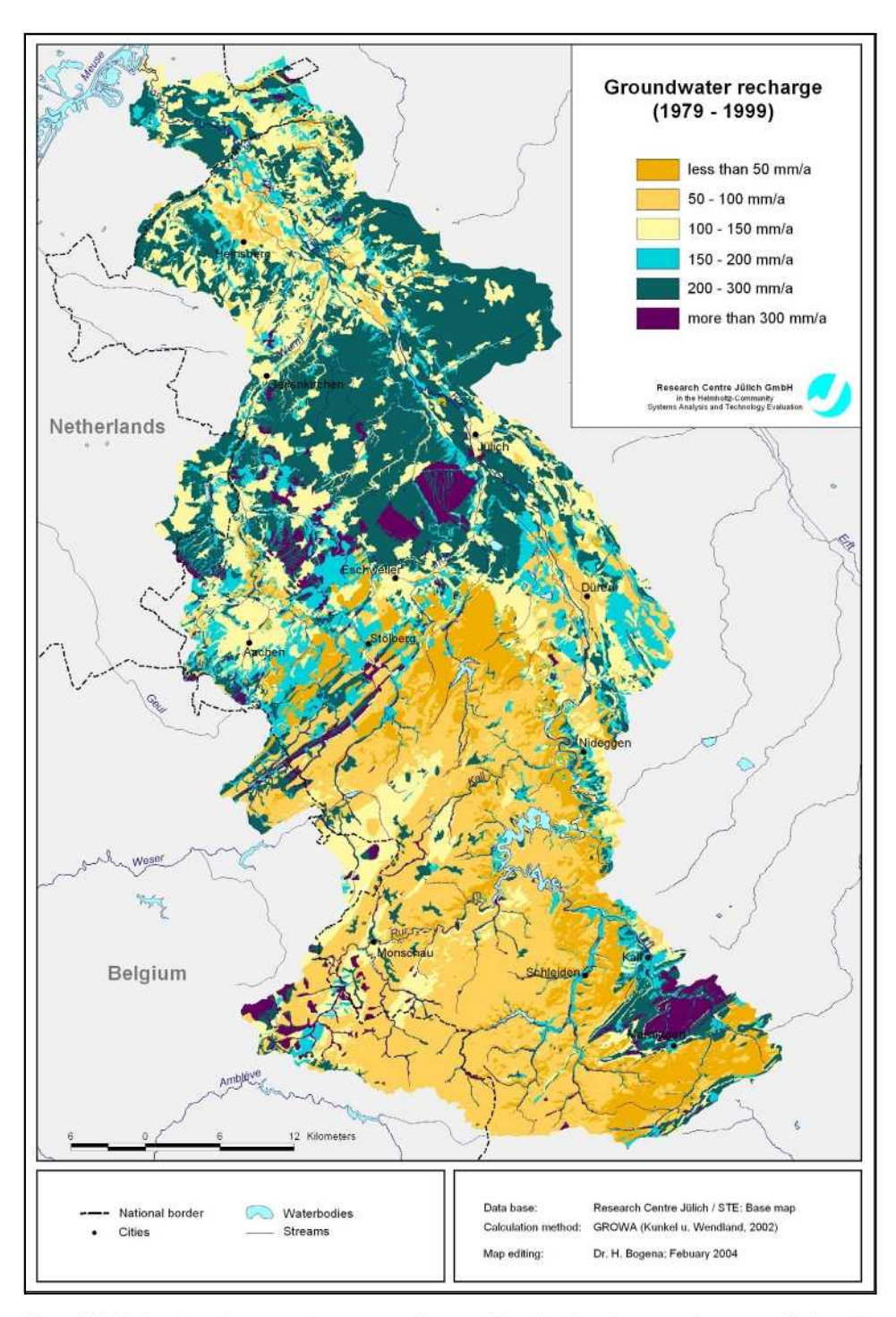


Fig. 22: Frequency distribution of the calculated groundwater recharge levels in the Rur basin.

Apart from the meteorological boundary conditions, in the consolidated rock region the groundwater recharge is primarily determined by the hydrogeological properties of the outcropping rock strata. Thus, the groundwater recharge levels in the impervious Lower and Upper Devonian solid rocks of the Rhenish Massif are mostly in the range of values below 100 mm/a. Only the Middle to Upper Devonian karstified carbonate rocks in the south of Stolberg and the partially karstified limestones in the lime troughs of the North Eifel show groundwater recharges of more than 300 mm/a. In the unconsolidated rock region, groundwater recharge levels between 200 and 300 mm/a occur to a large extend and are mainly associated with the occurrence of Loess.

Tab. 17 shows the variances and medians of the distribution of the groundwater recharge levels for the main subbasins.



Map 20: Calculated groundwater recharge levels in the catchment of the Rur River.

Tab. 17: Ranges and medians of the calculated total runoff levels of the subbasins of the Rur catchment.

Subbasin	Range	Median
Lower Rur	537 mm/a	202 mm/a
Middle Rur	606 mm/a	112 mm/a
Upper Rur	850 mm/a	90 mm/a
Wurm	582 mm/a	161 mm/a
Merzbach	574 mm/a	243 mm/a
Inde	670 mm/a	100 mm/a
Ellebach	243 mm/a	132 mm/a
Kall	657 mm/a	81 mm/a
Urft	667 mm/a	65 mm/a
Rur catchment	942 mm/a	126 mm/a

The highest medians (243 mm/a and 202 mm/a) are reached in the Merzbach and the Lower Rur subbasins. In the Wurm and Ellebach subbasins, where also unconsolidated rocks are predominate, the medians are slightly lower with values around 150 mm/a. The reason for this finding is the relatively large occurrence of groundwater- and waterlogging-affected soils in these regions, which are accompanied with high direct runoff fractions.

The lowest mean groundwater recharge level is reached in the Urft and Kall subbasins (median: 65 mm/a and 81 mm/a). In these subbasins impermeable Devonian solid rocks are predominate. The small pore volume and the associated low hydraulic conductivity of these rocks lead to relatively high interflow rates and, therefore only a relatively small fraction of the runoff contributes to groundwater recharge. Additionally, these subbasins are situated in the lee site of the high mountains of the Hohes Venn, thus receiving relatively low annual precipitation rates compared to the south-western part of the catchment.

4.2.4 Direct runoff

Fig. 23 shows the frequency distribution of the direct runoff levels calculated for Rur catchment. The maximum of the distribution is formed by the class from 0 to 50 mm/a, in which approx. 28 % of the values are found. About half of all calculated direct runoff levels are above 200 mm/a. The maximum values can exceed 800 mm/a (less than 0.1 %).

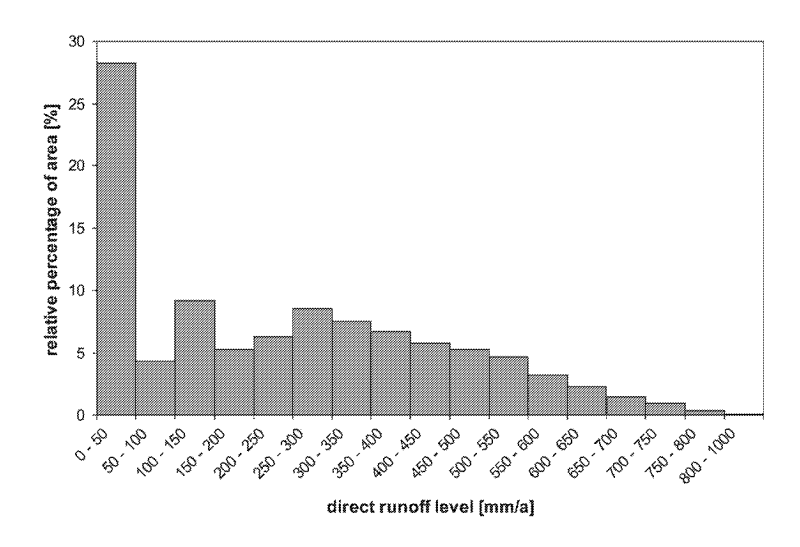
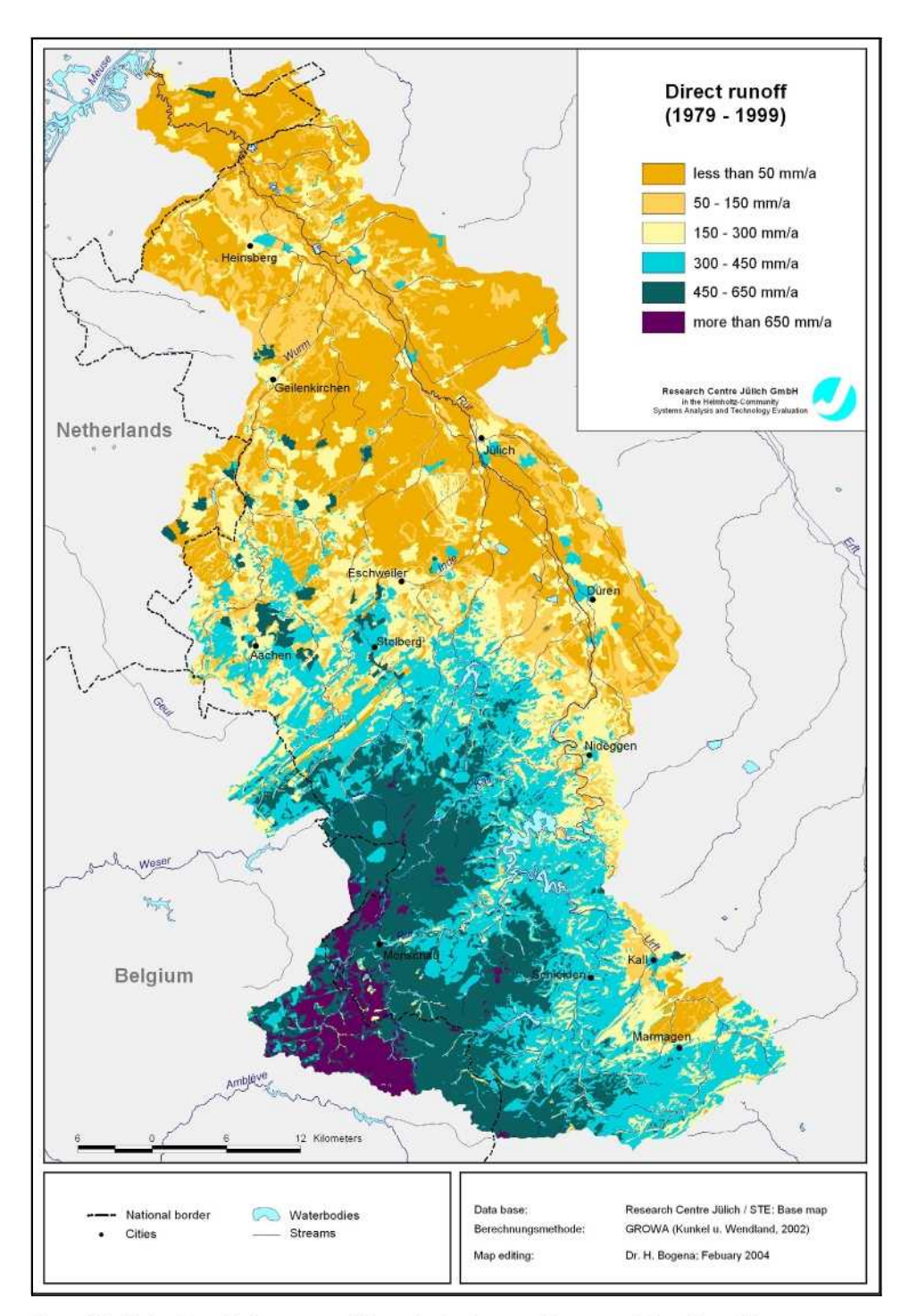


Fig. 23: Frequency distribution of the calculated direct runoff levels in the Rur basin.

Map 21 displays the spatial distribution of the calculated direct runoff levels. A pronounced bisection of the land area similar to that observed for the total runoff level is also visible for the direct runoff levels.

In the lowland regions, values below 50 mm/a predominantly occur, whereas the urbanized areas show values between 150 – 300 mm/a. Also the steep slopes of the open mine pits reveal high direct runoff levels (up to 300 mm/a and more). In contrast to this, direct runoff levels of more than 400 mm/a dominate in the upland regions and even peak values of more than 650 mm/a can be reached in elevated upland regions. Besides the high annual precipitations, the cause is above all the low hydraulic conductivity of the subsoil.

Tab. 18 shows the statistical values of the frequency distributions of the calculated direct runoff levels for the main subbasins of the Rur catchment and the whole region. The medians of the direct runoff values vary significantly. The subbasins of the lowland region exhibit the lowest medians with values below 100 mm/a, in which the Lower Rur subbasin shows by far the lowest values (15 mm/a). The highest values of 450 mm/a and more are found in the subbasins Kall (480 mm/a) and Upper Rur (561 mm/a).



Map 21: Calculated direct runoff levels in the catchment of the Rur River.

Tab. 18: Ranges and medians of the calculated total runoff levels of the subbasins of the Rur catchment.

Subbasin	Range	Median
Lower Rur	472 mm/a	15 mm/a
Middle Rur	638 mm/a	168 mm/a
Upper Rur	856 mm/a	561 mm/a
Wurm	566 mm/a	122 mm/a
Merzbach	570 mm/a	38 mm/a
Inde	679 mm/a	328 mm/a
Ellebach	430 mm/a	83 mm/a
Kall	773 mm/a	480 mm/a
Urft	757 mm/a	363 mm/a
Rur catchment	875 mm/a	227 mm/a

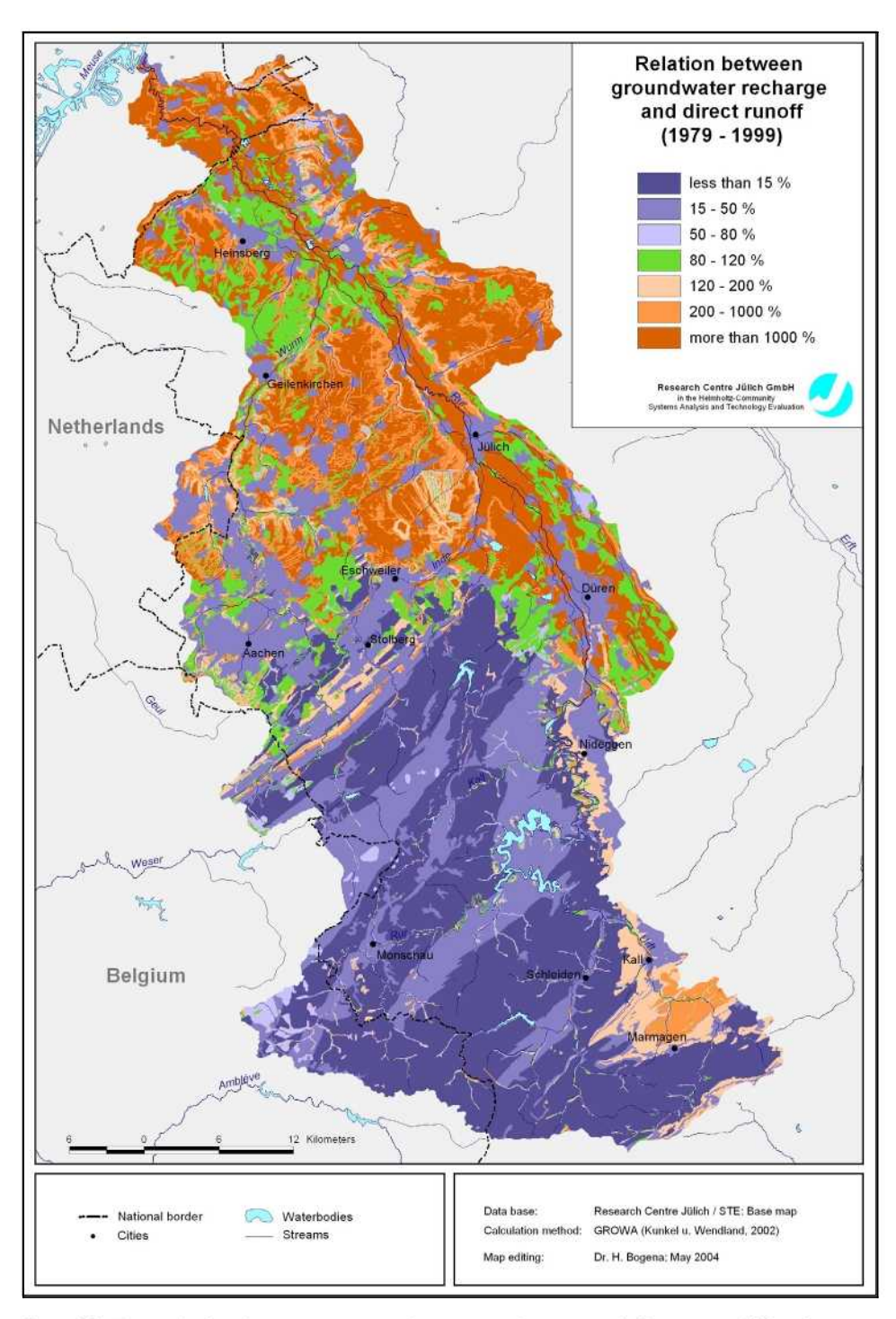
The runoff levels occurring within the main subbasins display wide scattering. In the climatically uniform and in terms of natural area relatively homogeneous lowland regions, the differences between the highest and lowest calculated value are less than 600 mm/a, whereas in the upland regions differences of typically more than 750 mm/a can occur.

4.2.5 Predominating runoff components

On the basis of spatial distributed determined direct runoff and groundwater recharge levels the predominate runoff components can be identified in an area differentiated way. In this study, the relation between the groundwater recharge to the direct runoff (GD-relation) serves as a measure for the determination of the regional prevailing process of runoff generation. In the case that the GD-relation is higher than 100 %, groundwater recharge is prevailing. Otherwise, the predominating proportion of the total runoff is transported to the receiving stream by overland flow and interflow.

Map 22 shows the GD-relations calculated on the basis of the GROWA results presented in Chapter 5.2.3 and 5.2.4. In the groundwater distant and flat regions in the northern part of the Rur catchment with outcropping unconsolidated rocks, the GD-relations are reaching to a large extend values significantly above 500 %. Here, the main portion of the natural discharge is therefore formed by groundwater flow.

In case of water logging tendency or groundwater influenced unconsolidated rock regions, the proportion of groundwater flow is significantly reduced (GD-relation: 80-120). That means that approximately half of the total runoff is discharged as direct runoff.



Map 22: The relation between groundwater recharge and direct runoff for the period 1979 – 1999.

In the consolidated rock regions of the Rur catchment a completely different discharge pattern is to be found. In most cases the GD-relation is lower than 100 %. Hence, the predominating portion of the total runoff is discharged by overland flow and interflow into the receiving streams. In regions where Palaeozoic non-carbonate rocks are present, the proportion of direct runoff is four times higher than the proportion of groundwater recharge. However, the karstified carbonate rocks form an exception. Due to the high hydraulic conductivities of these geologic formations, the proportion of direct runoff is highly increased and therefore the values of GD-relation are exceeding 200 % and, in part, even 500 %.

Model Validation

5.1 Microscale

The validation of water flow and transport processes at regional scale is a difficult task. Thus in a first step the TRACE model is validated at the microscale by means of lysimeter data. The main advantages of a lysimeter experiment are the controlled boundary conditions and the opportunity to measure actual evapotranspiration, soil moisture and drainage for a well-established soil volume.

The TRACE model was tested using lysimeter data (Pütz 1993) provided by FZ Jülich. The lysimeters contained an Orthic Luvisol, sampled a few kilometres north-western of the test area Zwischenscholle. This soil type approximates some of the soil types found at the test site Zwischenscholle. The lysimeter station was located at the test site in the Research Centre Jülich providing relevant meteorological data for the test site. The lysimeter experiment covers a period of 627 days. The lysimeter data were used to check the applicability of the plant database (Van Heemst 1988) to the test site 'Zwischenscholle', to identify the crucial parameters by calibration, and to control if all relevant processes are described properly with TRACE.

5.1.1 Measurements and model input

Five undisturbed soil cores (free draining lysimeters) containing an Orthic Luvisol were monitored for water and pesticide transport. The cores were 1.1 m long and had a surface area of 1.0 m². For the Orthic Luvisol three pedogenetic soil horizons were distinguished (see Table 1). The winter wheat was harvested and soil samples were taken at 3rd of August 1989 (252 days after application). In the following vegetation period winter barley was cropped and harvested on the 11th of May 1990.

Tale 40. Dks	·-:	ا حداد ما حاد		-£46-	Outleie Lindeal
1ab. 19: Pn	vsicai and	cnemicai	properties	or the	Orthic Luvisol.

Soil horizon	clay	silt	sand	ρ _b	foc	pH
	[%]	[%]	[%]	[kg m ⁻³]	[%]	[CaCl ₂]
A _p 0-0.4 m	15.4	78.2	6.4	1.57·10³	1.0	7.2
A _I 0.4-0.6 m	21.9	77.1	1.0	1.59·10 ³	0.4	6.9
B _t 0.6-1.1 m	26.1	73.4	0.5	1.67·10 ³	0.3	6.6

 ρ_b = bulk density, f_{oc} =organic matter content

The next vegetation was oat, which was harvested at the 13th of August 1990, when a last soil sampling was carried out 627 days after the application. From the 25th of November 1988 until the 13th of August 1990 the meteorological parameters precipitation, humidity, air temperature, wind speed and radiation were monitored on a daily basis. Roughly every three days soil moisture was measured at the depths 25 cm and 85 cm below soil surface with a neutron probe. Leachate was collected on a three weekly basis. The amount of drainage was measured directly while the actual Evapotranspiration (Et_a) was calculated from the soil water balance.

The soil water retention function was described using the van Genuchten (1980) model with parameter m=1 (Equation. 4). The soil hydraulic properties listed in Table 2 have already been used by Vereecken and Kaiser (1999). They derived the soil hydraulic properties from the soil properties listed in Table 1 with the Pedotransfer functions (PTF) of Vereecken et al. (1989 and 1990) and fitted the θ_r and α values.

Tab. 20: Retention parameters, hydraulic conductivity parameters and dispersivity λ for the soil horizons of the Orthic Luvisol.

depth	θ_{s}	Θ_{t}	α	n	K _s	b	С	λ
[m]	[cm ³ cm ⁻³]	[cm ³ cm ⁻³]	[cm ⁻¹]	[-]	[cm d ⁻¹]	[cm ⁻¹]	[-]	[cm]
0-0.4	0.39	0.01	0.0036	0.82	84.09	1.044	1.55	1.7
0.4-0.6	0.40	0.07	0.0037	0.79	126.63	1.688	1.45	1.7
0.6-1.1	0.38	0.10	0.0015	0.75	39.80	1.854	1.41	1.7

The potential reference evapotranspiration Et_p was calculated according to the approach of Penman/Monteith (Monteith 1975). Potential evapotranspiration and precipitation are applied as the upper boundary condition, while a seepage face is applied to the lower boundary at the bottom of the lysimeter. The seepage face boundary is characterized by a no-flow boundary for unsaturated conditions:

$$q(z,t) = 0 \quad \text{for} \quad h < 0 \tag{41}$$

If the seepage face becomes saturated, the boundary turns into a prescribed head boundary with h(z,t)=0. The vertical lysimeter wall is set as a no-flow boundary condition. The spatial discretization in vertical direction is 1 cm resulting in 110 finite elements.

In order to evaluate the model performance in total three criteria were calculated. A commonly used criterion for model validation is the *root mean square error* (RMSE), where the root of the mean squared residuals is calculated. The RMSE has the unit of the considered variable. The squared residuals are also used for the second criterion applied, which is the *Coefficient of Model Efficiency* (CME) (Nash & Sutcliffe, 1970). Here they are used to determine the proportion of the deviation from the observed mean, which can be explained by the model:

$$CME = \frac{\sum_{i=1}^{n} (x_o(t) - x_{omean})^2_i - \sum_{i=1}^{n} (x_o(t) - x_s(t))^2_i}{\sum_{i=1}^{n} (x_o(t) - x_{omean})^2_i}$$
(42)

where x_0 is the observed value, x_s is the simulation result at time t and x_{omean} is the arithmetic mean of the observed values. The CME is a dimensionless criterion that can have negative values. The highest value possible is 1, indicating that observation and model are completely in agreement. The *Index of Agreement* (IA) can have values between 0 and 1(Willmott, 1981):

$$IA = 1 - \frac{\sum_{i=1}^{n} (x_o(t) - x_s(t))^2 i}{\sum_{i=1}^{n} (|x_o(t) - x_{omean}| + |x_s(t) - x_{omean}|)^2 i}$$
(43)

Because they are dimensionless, the CME and the IA can be used to compare the model quality between different variables, while the RMSE gives an idea about the model error in the units of the variable under consideration.

5.1.2 Lysimeter experiment

Fig. 24 shows a comparison between observed and modelled cumulative actual evapotranspiration. In general the model matches the measurements, which show only small standard deviations, except for the two drying periods with high evapotranspiration demands.

During the first spring period (1989) TRACE slightly underestimates the amount of actual evapotranspiration. The calculation of selected model performance criteria with the mean of the measured actual evapotranspiration

and the corresponding model results (Tab. 21) reveals that TRACE reproduces the temporal course of evapotranspiration quite well.

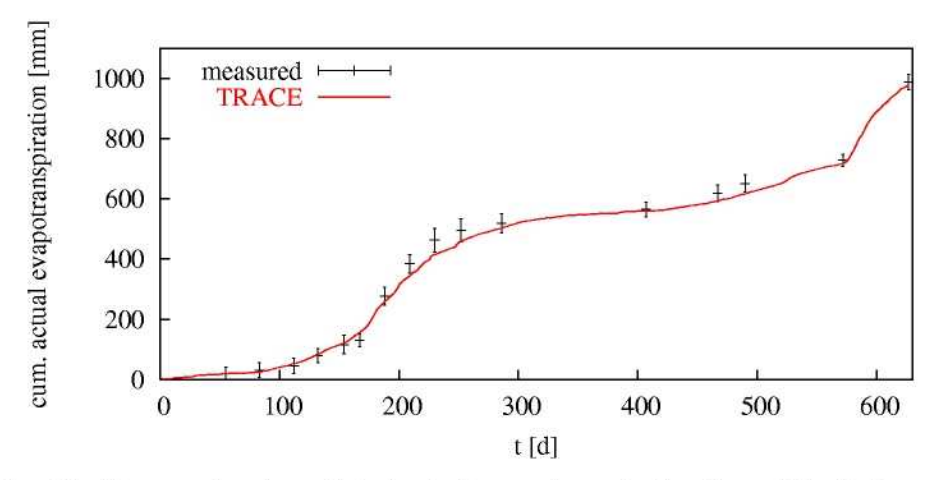


Fig. 24: Measured and predicted actual evapotranspiration (cumulative). Bars are standard deviations of measurements.

Tab. 21: Quantification of the model performance concerning water flow

	RMSE ^a	CME ^b	ΙA ^c
drain [mm]	10.2	0.58	0.89
Et _a [mm]	17.1	0.96	0.99
θ _{25cm} [-]	0.025	0.93	0.98
θ _{85cm} [-]	0.031	0.79	0.94

^a Root mean square error, ^b Coefficient of model efficiency, ^c Index of Agreement

The only parameters that were calibrated are the maximum rooting depth and the crop conversion factor (Doorenbos and Pruitt 1977, see section 3.2.2). For the winter wheat the initial root depth of 85 cm was changed to 108 cm, and the initial scaling factor for the potential evapotranspiration of 1.2 was changed to 1.3. The rooting depth of winter barley was changed from 100 cm to 90 cm and the crop conversion factor was reduced from 1.1 to 0.65. For oat the initial rooting depth of 80 cm was changed to 100 cm and the initial crop conversion factor of 1.0 was increased to 1.3.

A comparison of calculated and observed volumetric soil moisture at two depths is shown in Fig. 25 and Fig. 26. For the depth of 25 cm during the drying period of spring 1989 TRACE reproduces the drying quite accurately.

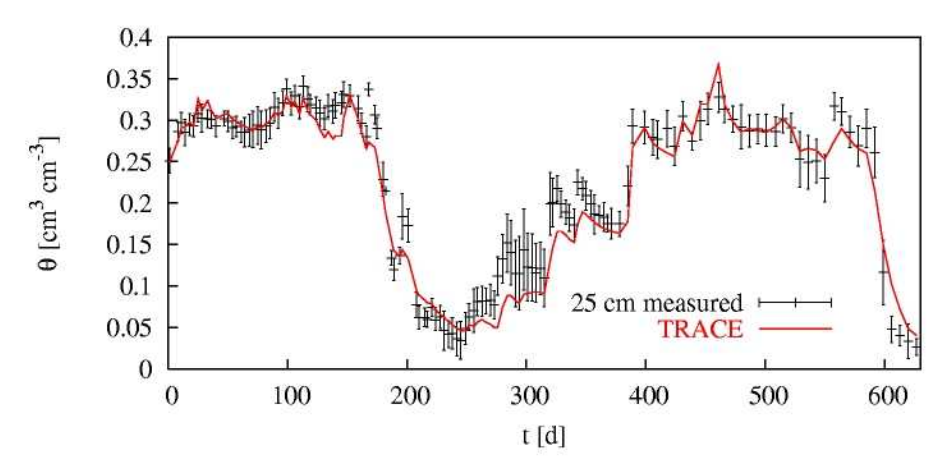


Fig. 25: Measured and predicted soil moisture for the depth of 25 cm. Bars are standard deviations of measurements.

During the following wetting period (autumn and winter 1989) TRACE slightly underestimates the re-wetting. In general, for the depth of 25 cm the model is basically in accordance to the measurements, which is supported by the CME of 0.93 (see Tab. 24).

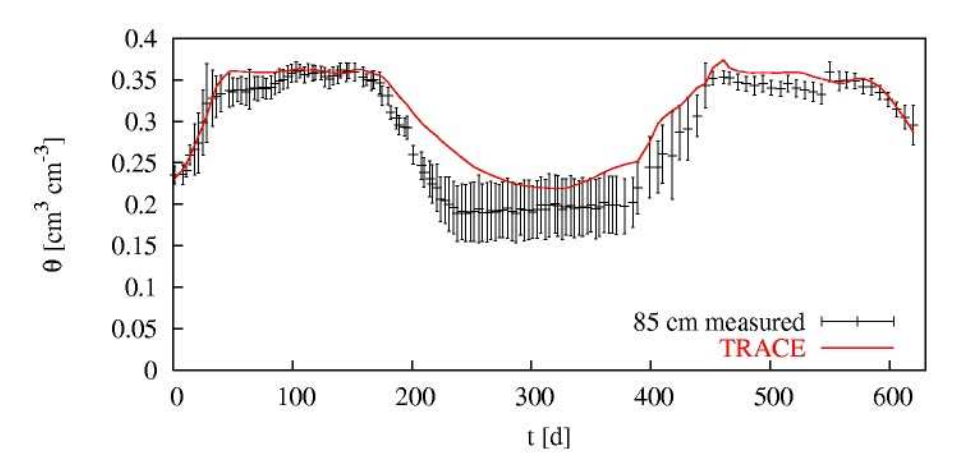


Fig. 26: Measured and predicted soil moisture for the depth of 85 cm. Bars are standard deviations of measurements.

Compared to the measurements at the depth of 85 cm the results of TRACE show too high soil water contents during spring and summer 1989. The measurements exhibit a high standard deviation during the summer 1989 when the

soil was very dry. In the following vegetation period (spring and summer 1990) the results of TRACE match the measurements. During this second period the effect of drying is much less pronounced.

Fig. 27 shows the comparison between modelled and measured cumulative drainage. During winter 1988/1989 the highest amount of drainage was measured. TRACE underestimates this amount slightly. In relation to the mean the standard deviation of the measured drainage is higher than the standard deviation of the measured evapotranspiration. During the second period of drainage (winter 1989/1990) compared to the measurements TRACE overestimates the amount of drainage.

The overall water balance is well reproduced with TRACE. The measured actual evapotranspiration for the whole modelling period is 990 mm, whereas TRACE calculates an amount of 977 mm. The deviation between the measured drainage amount of 158 mm and the amount predicted with TRACE (163 mm) is equal to an error of 3.4 %. The measured precipitation is 1067 mm, thus the change in soil moisture is slightly underestimated with TRACE. The measured change in soil moisture is -82 mm, whereas TRACE calculated an amount of -73 mm.

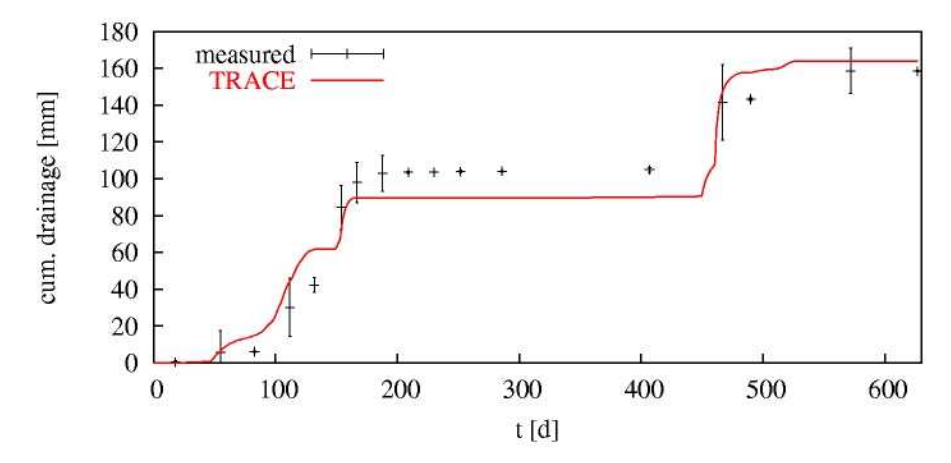


Fig. 27: Measured and predicted drainage (cumulative). Bars are standard deviations of measurements.

Basically, the water flow measurements are well reproduced with TRACE. The estimated overall water balance is very close to the measurements. The actual evapotranspiration is slightly underestimated, while the amount of drainage is slightly overestimated. Nevertheless the calculated model performance indices

indicate that all relevant processes and state variables (evapotranspiration, drainage and soil moisture) are well described. Calibration of rooting depth and the crop conversion factor significantly improved the model results.

Compared to the crop conversion factor, the calibration of the rooting depth was of minor importance. The crop conversion factor was increased during the calibration procedure, except for the winter barley. The decrease of the crop conversion factor for winter barley during calibration can be explained by the fact, that during the experiment the winter barley suffered from a plant disease resulting most likely in a reduction of transpiration. The increase of the crop conversion factor for winter wheat and oat was necessary to reproduce the drying of the soil during the spring periods. This is done successfully for the soil moisture at 25 cm depth. But the decrease during the first spring in the soil moisture at 85 cm depth is not that well reproduced, which might be attributed to a compensation mechanism.

The plant adapts to the low soil moisture near the surface by taking out more water at deeper soil layers. This process is yet not considered in TRACE. In general we conclude that the plant database (Van Heemst 1988) provides useful estimates for the plant parameters. However care should be taken not to underestimate the transpiration by using crop conversion factors that are too small. The inability of the model to correctly calculate the soil water uptake might also be due to incorrect estimates of the potential evapotranspiration for the reference vegetation. If this method is not well adapted, changing the crop conversion factor is only a re-calibration of the errors made during the calculation of the potential evapotranspiration.

5.1.3 Field experiment

In order to check the estimated groundwater levels of the model, a comparison with measured groundwater levels was carried out (see Fig. 20). Time series of the measured groundwater levels of selected wells were compared to the calculated levels of the closest located grid node. Wells were selected, which are located rather in the middle of the test area than close to the boundary, since the model results and measured heads are supposed to be very similar near the boundary, where the measurements are used for the imposed boundary condition.

The RMSE (root mean square error) between the model results and the corresponding wells 20111, 20232, 20255 and 20244 were 0.41, 0.68, 0.33 and 0.42 m, respectively. Fig. 20 also shows that the deviations between the

model and the measurements are much smaller than the deviations between the different measured locations. TRACE reproduces the temporal course of the groundwater levels well. Year 5 (1988) shows the highest groundwater levels for the wells 20232, 20255 and 20244, which is well reproduced by TRACE.

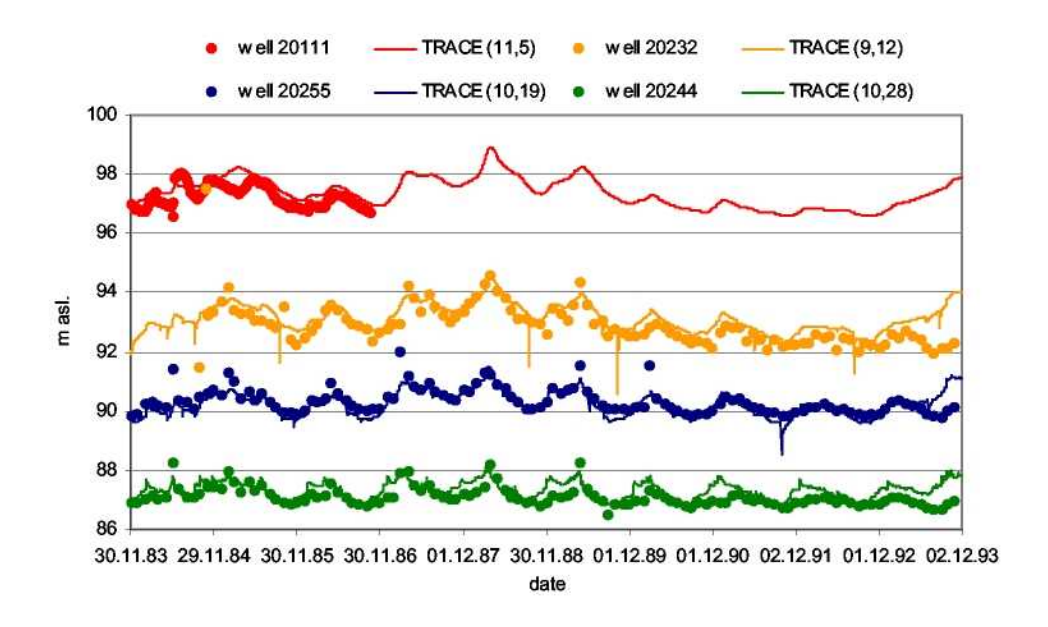


Fig. 28: Comparison between measured and simulated total head [m above sea level] for four selected locations.

According to Fig. 20 and the RMSE given above, the reproduction of the total heads by TRACE is seen as adequate, having in mind that no calibration was carried out. Further, the measurements and the model results are at different scales. The measurements are at point scale, while the model result is supposed to cover an area of 40,000 m².

5.2 Macroscale

A validity check was also performed on the macroscale in order to verify the quality of the water balance modelling for the entire Rur catchment. In principle, several methods are applicable here. The most reliable validation method is a comparison of the model results for as many percolation water rates as

possible determined by lysimeter experiments as it was undertaken for the TRACE model (see Chapter 5.1).

However, this type of validation is not practicable for a large-scale approach since, as a rule, not enough lysimeter stations are available to obtain statistically supported information for the whole Rur catchment and the site combinations that occur. For this reason, the reliability of the calculated runoff levels was verified by a comparison with runoffs measured at gauging stations. The procedure used is schematically shown in Fig. 29:

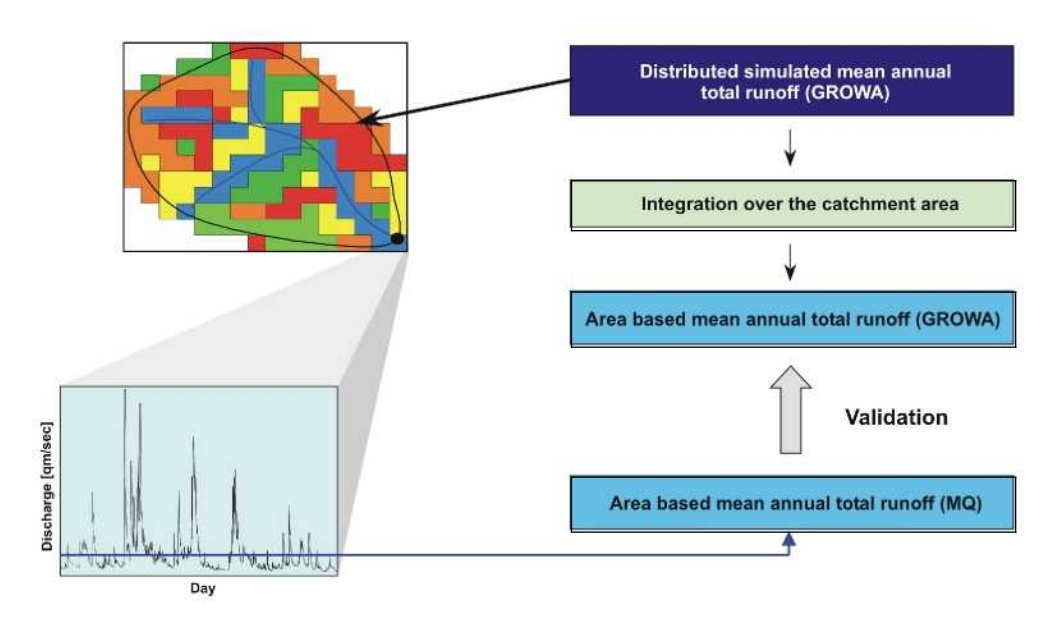
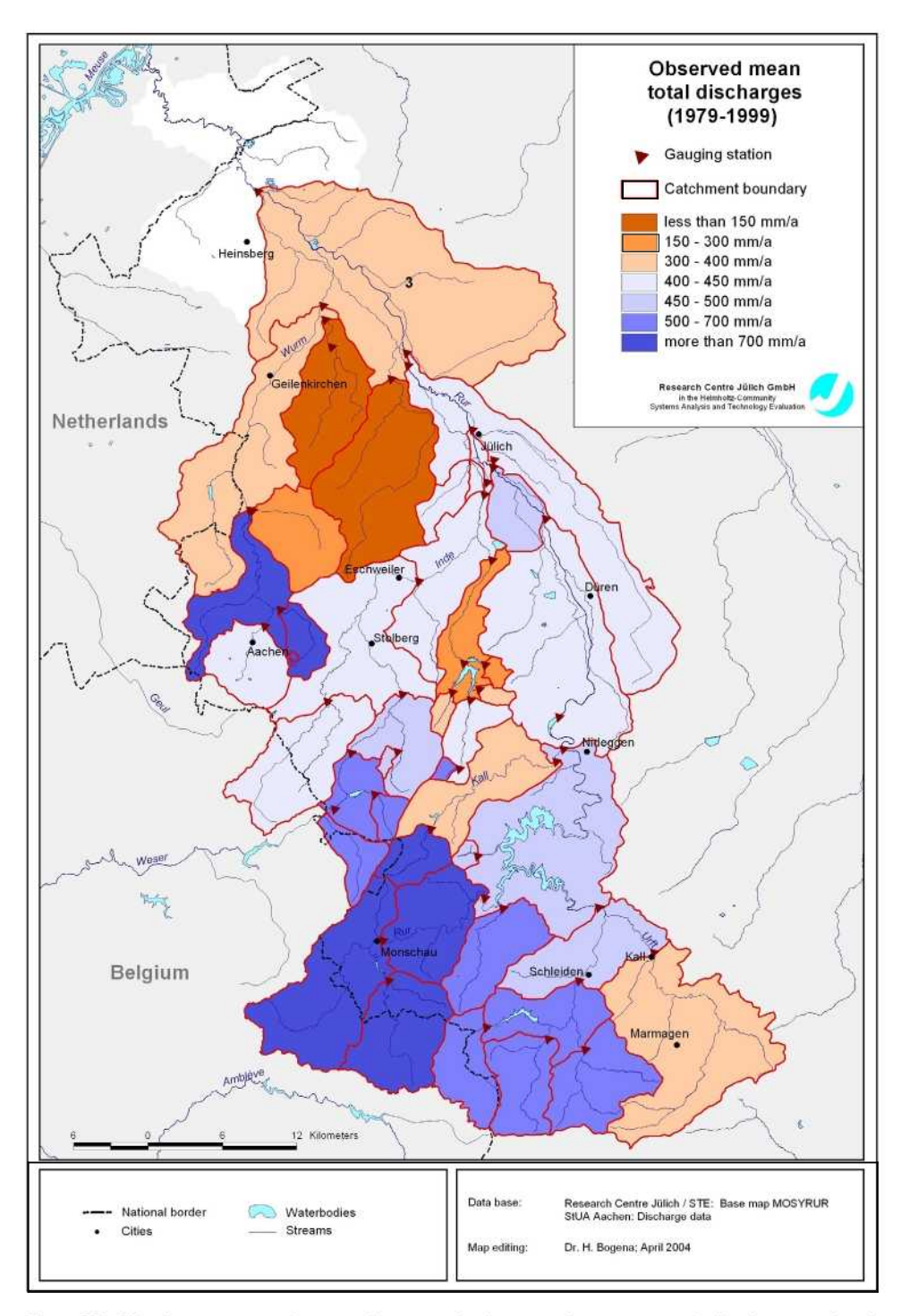


Fig. 29: Procedure for the validating the simulated water balances by the GROWA model.

First of all, a blending of the gauge-related catchment areas with the total runoff levels calculated by the GROWA model in an area-differentiated manner is performed. The individual values of the grid cells are then integrated over the respective catchment areas and compared with the measured runoff levels. Care should be taken here that the same reference period is used for both the calculation and the gauge through-flow values. If satisfactory agreement is achieved for a sufficiently large number of catchment areas, it may be assumed that representative information has been obtained with the underlying model.



Map 23: Discharge gauging stations and observed mean total discharges in the catchment of the Rur River.

The validation of the model results was performed for 40 catchment areas (see Map 23 and Tab. 22). In order to demonstrate the suitability of the model for different landscapes, the greatest possible bandwidth of different land uses and different climatic, pedological and topographic conditions was aimed at in selecting the catchment areas considered. Furthermore, the validation for interlaced catchment areas was always performed relative to the whole region of the respective gauge.

Tab. 22: The gauging stations used for the validation of the GROWA model and the observed mean total runoff.

D	Gauging station	Period	River	Operating institution	Catchment area [km²]	Percentage of area of consolidated rock	Observed mean total runoff [mm/a]	
359	Zweifall	1961-1989	Solchbach	StUA Aachen	2.15	100	486	
365	Hürtgenwald	1975-1989	Wehebach	StUA Aachen	2.39	90.1	650	
14	Rurberg	1960-2003	Weidenbach	StUA Aachen	3.51	96.06	454	
4	Rötgen Zul	1982-2003	Dreilägerbach	SIUA Aachen	8.12	100	510	
18	Rötgen	1981-2003	Weserbach	StUA Aachen	12	91.65	507	
31	Haaren	1978-2003	Haarbach	StUA Aachen	15.32	46.16	816	
5	Rollesbroich	1982-2000	Kallbach	StUA Aachen	19	94.31	733	
35	Kalkofen	1980-2003	Wurm	StUA Aachen	33.63	33.74	413	
11	Hellenthal	1970-2003	Platissbach	StUA Aachen	36.4	95.85	671	
30	Herzogenrath 2	1978-2003	Broicher Bach	StUA Aachen	41.39	0.35	269	
360	Mulartshütte	1985-2003	Vicht	StUA Aachen	45.6	94.91	581	
12	Reifferscheid	1970-2003	Reifferscheider Bach	StUA Aachen	48.95	95.44	587	
32	Honsdorf	1978-2003	Beekfließ	SIUA Aachen	56.55	0	60	
362	Luchem	1985-2003	Wehebach	StUA Aachen	62.47	87.02	168	
26	Kornelimünster	1973-2003	Inde	StUA Aachen	65.02	80.83	408	
21	Zerkali 2	1981-2003	Kall	StUA Aachen	74.53	93.99	394	
358	Platenhammer	1971-1991	Vicht	StUA Aachen	76.47	94.17	495	
23	Herzogenrath 1	1970-2003	Wurm	StUA Aachen	96.29	35.6	710	
33	Welz	1978-2003	Merzbach	StUA Aachen	98.16	1.25	127	
29	Kall Sportplatz	1975-2003	Urft	SIUA Aachen	131.11	93.61	386	
13	Monschau	1954-2003	Rur	StUA Aachen	143.63	86.04	909	
8	Schleiden	1970-2003	Olef	StUA Aachen	159.41	94.46	577	
361	Dedenborn	1971-2003	Rur	StUA Aachen	199,1	88.65	792	
19	Eschweiler	1966-2003	Inde	StUA Aachen	232.15	59.98	419	
20	Randerath	1967-2003	Wurm	StUA Aachen	310.52	11.13	389	
364	Gemünd	1952-2003	Urft	StUA Aachen	344.55	93.5	483	
367	Kirchberg	1971-2003	Inde	SIUA Aachen	358.07	67	429	
6	Zerkall 1	1951-2003	Rur	StUA Aachen	787	90.92	483	
15	Selhausen	1961-2003	Rur	StUA Aachen	934.75	82.79	448	
368	Altenburg	1971-2003	Rur	StUA Aachen	958.76	80.73	466	
27	Jülich-Stadion	1973-2003	Rur	StUA Aachen	1334.57	76.97	429	
366	Linnich 1	1951-2003	Rur	StUA Aachen	1471.75	70.64	407	
3	Stah	1961-2003	Rur	StUA Aachen	2135.15	49.83	348	
357	Höfener Mühle	1958-2003	Perlenbach	Wasserwerk Perlenbach	56.01	93.49	868	
372	Weberbach	1982-2001	Weberbach	WVER	3.63	99.08	345	
371	Thönbach	1982-2001	Thönbach	WVER	3.75	100	262	
370	Roter Wehebach	1982-2001	Roter Wehebach	WVER	5.38	99.85	336	
369	Wehebach	1982-2001	Weißer Wehebach	WVER	22.35	95.29	415	
224	Stauwurzel	1961-2001	Olef	WVER	34.3	95.7	689	
356	Einruhr	1971-1998	Erkensruhr	WVER	41.72	96.14	587	

5.2.1 Total runoff

The total runoff levels calculated for all 40 catchment areas for the period 1979-1999 were compared with the mean values of the mean daily runoffs (MQ) of the same period (see Fig. 30).

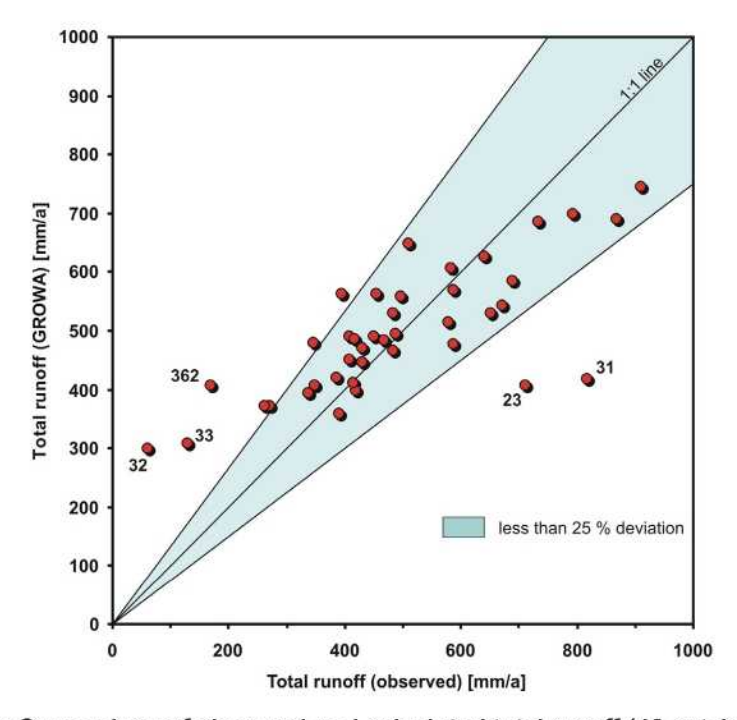


Fig. 30: Comparison of observed and calculated total runoff (40 catchments).

The mean deviation is 19.98 % and the coefficient of determination is 0.58. For 20 subcatchment areas the differences between calculated and measured values are less than 15 %. In view of the data available and the size and heterogeneity of the region investigated, this represents very satisfactory agreement considering, in particular, that the calculated total runoff levels were not calibrated. For the catchment areas for which major deviations between calculated and measured runoff values are observed, it must be examined in detailed studies whether the reasons for this are attributable to specific catchment-area-related features or to water management interventions not covered by the model.

For example, the rivers Beekfließ (gauging station Honsdorf, ID 32) and Merzbach (gauging station Welz, ID 33) have completely lost the contact to the local groundwater aquifers, because of the impact of the brown coal mining

leading to a lowering of the local groundwater table of 50 m and more. Hence, the discharge of these rivers is mainly controlled by the sewage disposal of the local sewage plants (Schröter, 2004). In this cases, the observed total runoff is much lower than the calculated total runoff. This occurs also in the case of rivers influenced by water reservoirs, e.g. the Wehebach River (gauging station Luchem, ID 362).

In the case, that local sewage plants have to dispose the sewage water of high industrialised and densely populated regions, the river discharge can be significantly increased. For example, the rivers Wurm (gauging station Herzogenrath 1, ID 23) and Haarbach (gauging station Haaren, ID 31) receive the main portion of the sewage water of the city of Aachen in the Middle West of the Rur catchment leading to an almost duplication of the discharge rate in these catchments. These examples the difficulty of validating hydrological models in highly influenced catchments by using runoff discharge data.

If the ten most artificially influenced catchments are excluded in this validation, the mean deviation is lowered to a value of 0.48 % and the coefficient of determination is 0.82. This finding indicates that the GROWA model is able to calculated the inartificial long-term annual total runoff very well.

5.2.2 Groundwater recharge and direct runoff

In validating the calculated groundwater recharge levels, it should be noted that the groundwater recharge only corresponds in the ideal case to the groundwater runoff, i.e. to the amount of water that feeds the recipients as spring discharge or base flow in a river basin. This is not always the case since, as shown in Fig. 31, a variety of natural and anthropogenic factors of influence may cause the groundwater recharge and the resultant groundwater runoff to deviate from each other.

An important natural factor influencing the groundwater runoff is the hydrodynamic situation in the catchment area. Glugla & Müller (1993), for example, report on a region northeast of Berlin, in which about 40 % of the groundwater recharge is transported with the groundwater outflow from a catchment area. Groundwater withdrawal for public and industrial water supply, for agricultural irrigation and for mining represents an important anthropogenic factor of influence. In this connection, groundwater recycling e.g. by irrigation measures also plays a role, since part of the groundwater withdrawn is passed back into the groundwater body. Often, however, withdrawn groundwater is exported to other regions, so that it is exempted from balancing.

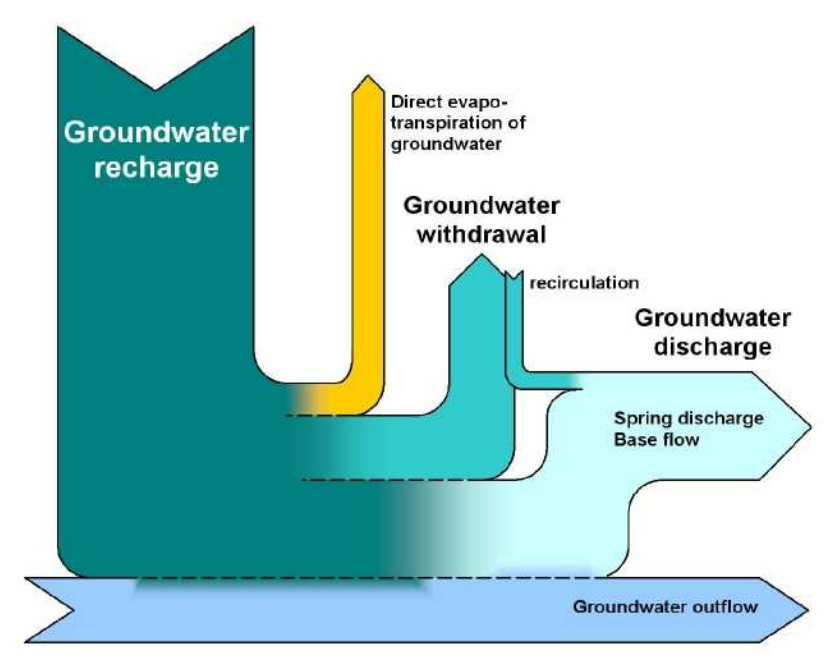


Fig. 31: Relation between Groundwater recharge, groundwater withdrawal and groundwater discharge (according to Struckmeier, 1990). The width of the bars approximately corresponds to the portions of volume of the related components.

A large portion of the groundwater withdrawn for public water supply is indirectly recycled into the flowing waters by discharge from sewage plants. In this way, the flow of a recipient is increased by a permanent contribution and the low-water runoff no longer corresponds to the natural groundwater runoff or only to a limited extent.

The groundwater recharge can only be indirectly derived from the runoff values observed (see Chapter 2.2.5). In unconsolidated rock and in solid rock this was done on the basis of different procedures. In solid rock areas, the MoMNQ value after Kille (1970) was used in order to largely eliminate the influence of the interflow. For unconsolidated rock regions, the MoMNQ value after Wundt (1958) was taken as a basis, since this value has proved to be a good measure of the groundwater recharge for the unconsolidated rock regions of the Elbe catchment area (Kunkel & Wendland, 1998) and the federal state of Lower Saxony (Dörhöfer et al., 2001).

Fig. 32 and Fig. 33 show the comparison of the measured and calculated arearelated direct runoff and groundwater recharge levels for 30 considered subbasins.

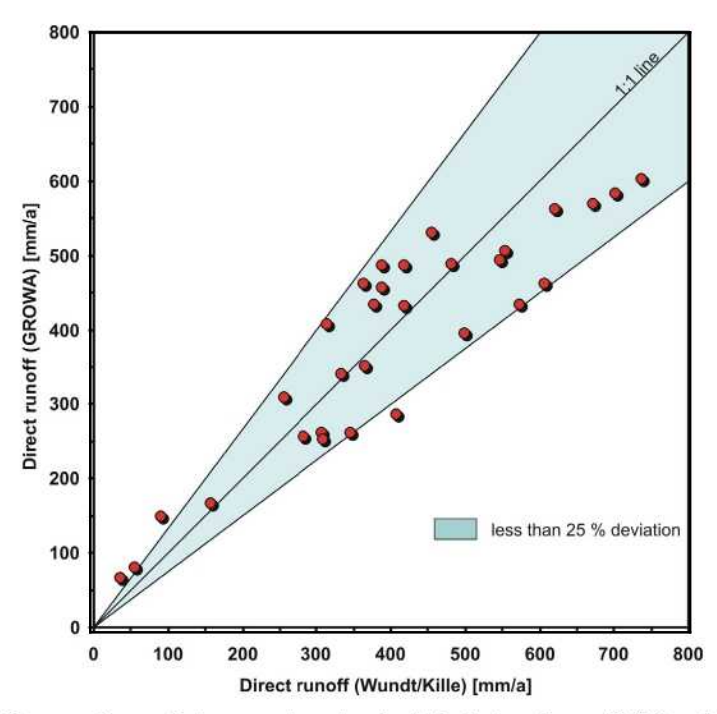


Fig. 32: Comparison of observed and calculated direct runoff (30 catchments).

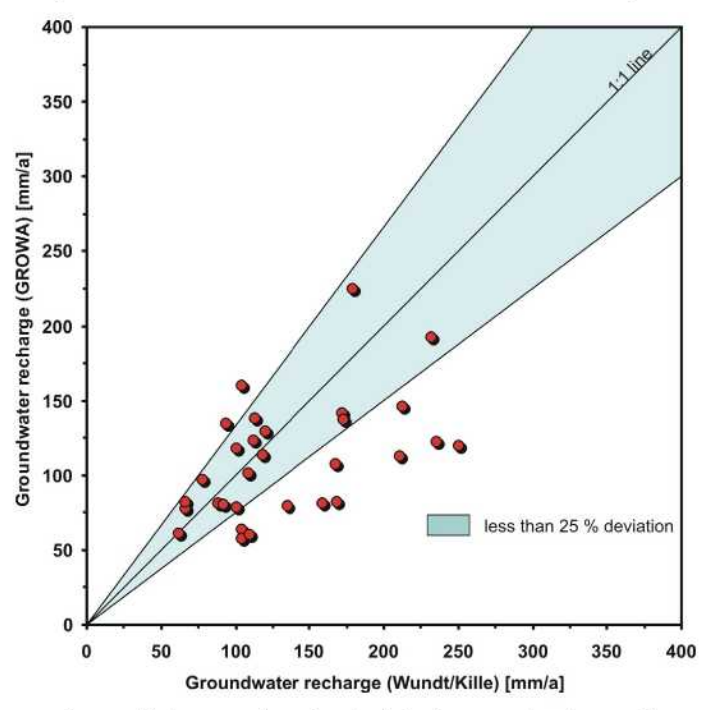


Fig. 33: Comparison of observed and calculated groundwater recharge (30 catchments).

In most cases, satisfactory agreement is found between calculated and measured values, as was already the case for the total runoffs. The deviations encountered are, however, increased in comparison to those of the total runoff, because the scattering contributions of two submodels (total runoff modelling, separation of the runoff components) are superimposed for the direct runoff and groundwater recharge levels. Consequently, the mean deviations across all the gauges used are 4.75 % for the direct runoff and 11.19 % for the groundwater recharge levels.

5.3 Analysis of scale effects

The processes determining the water balance exhibit very different spatial and temporal scales (Blöschl & Sivapalan, 1995). In considering the different aspects of the water balance in a catchment area it is therefore often meaningful to use different hydrological models. For the purpose of a consistent calculation of the water balance parameters across scales it is necessary to investigate the scaling effects resulting from differently scaled data bases and model assumptions.

In this Chapter the investigations of scaling effects within the framework of the research project MOSYRUR are presented. On the basis of this analysis it is possible to evaluate to which degree input data and process representation influence the model results. Firstly the procedure developed for this analysis is described. Secondly the results of the comparison of different data bases and the different models used in this study are presented.

5.3.1 Procedure

In this investigation, in principle, a difference is made between scaling effects resulting from differently scaled input data and those caused by different modelling approaches. For this reason, a two-stage analysis was performed. First of all, the actual evapotranspiration levels calculated with the GROWA model on the macroscale are compared with those obtained with the same model on the microscale.

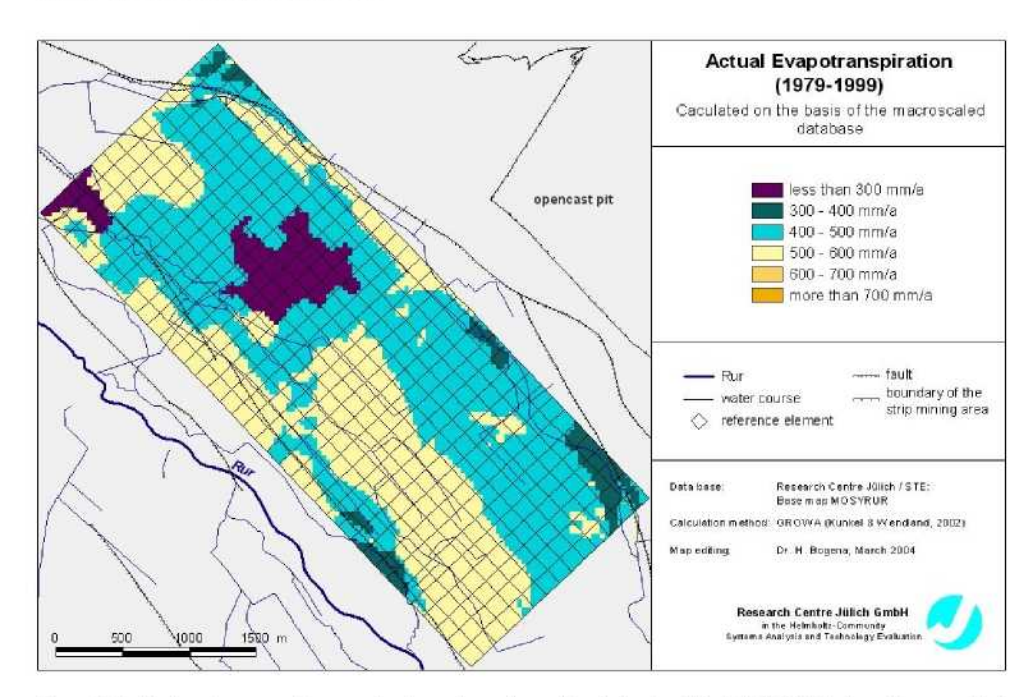
The comparison is made for the microscale test region using a reference grid with an edge length of 200 m for the correlation calculation. This reference grid was chosen, since it corresponds to the spatial resolution of the TRACE model. Furthermore, the macroscale dataset is replaced step by step by microscale data to obtain data-specific information. The second part of the analysis contains the comparison of the different modelling approaches of

GROWA and TRACE. For this purpose, the input data of the two models were unified in order to prevent data-specific influences. To this end, the microscale datasets for the GROWA model (resolution: 5m) were transformed to the spatial discretization of the TRACE model (resolution: 200 m).

5.3.2 Results

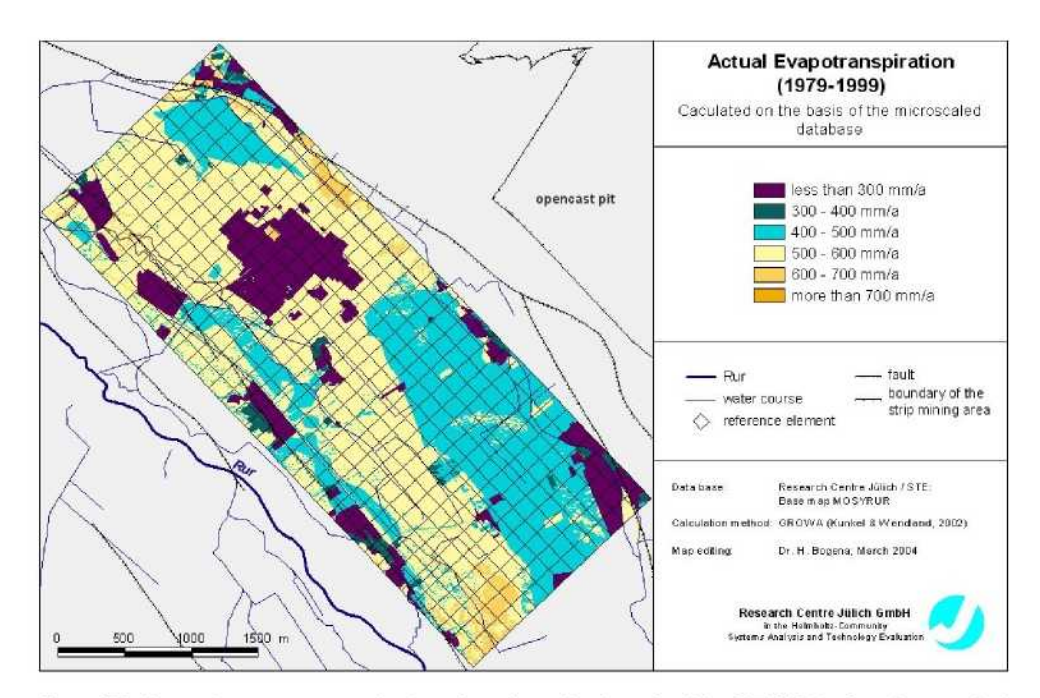
Comparison of different data bases

Maps 24 and 25 show the evapotranspiration levels calculated with the GROWA model using the macroscale dataset in the first case and the microscale dataset in the second.



Map 24: Actual evapotranspiration levels calculated with GROWA for the period 1979-1999 using the macroscale dataset (case a, resolution: 50 m).

Due to the different datasets, great spatial differences in the calculated evapotranspiration levels arise in case a) with deviations of more than 400 mm/a in the reference elements. Consequently, the coefficient of determination is relatively low in case a), amounting to 0.48. However, these deviations are cancelled out again in spatial averaging (difference 4 mm/a).



Map 25: Actual evapotranspiration levels calculated with GROWA for the period 1979-1999 using the microscale dataset (case b, resolution: 5 m).

In Fig. 34 the correlations of different simulation runs a, b and c are shown:

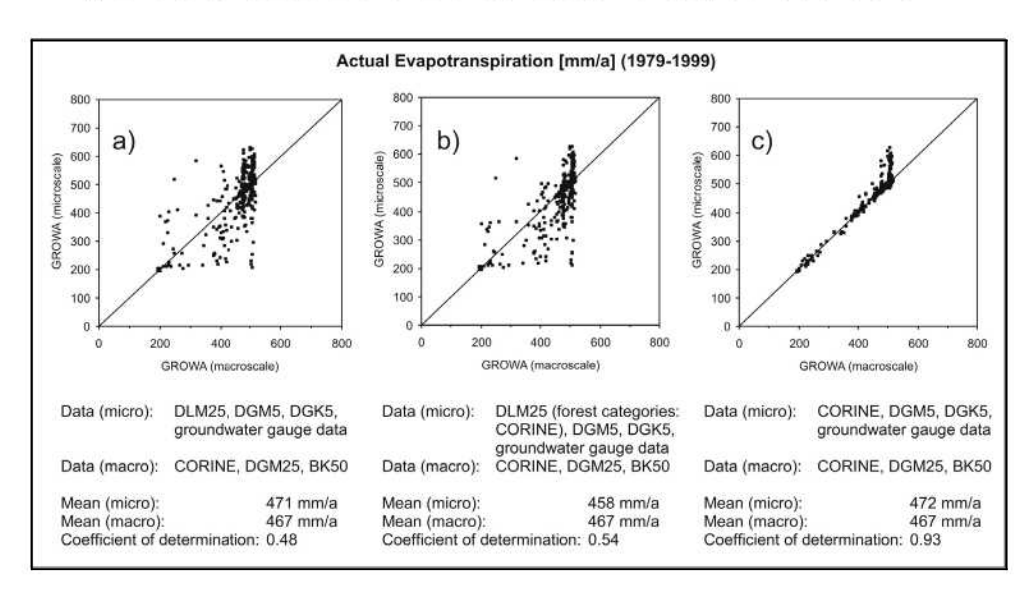


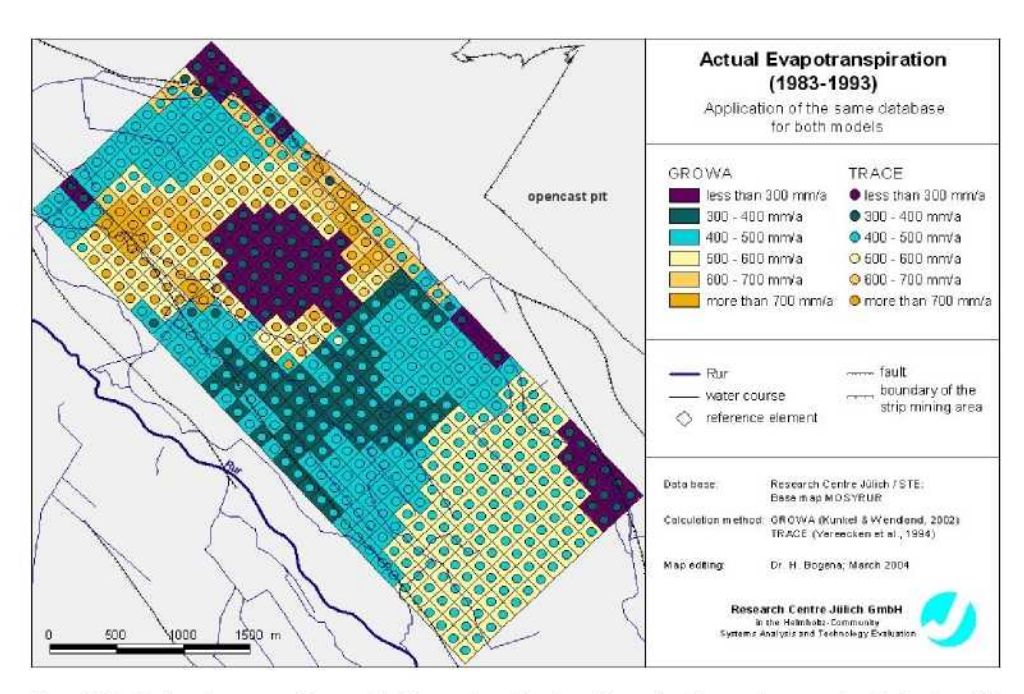
Fig. 34: Correlation diagrams of the actual evapotranspiration levels determined with the macroscale and microscale datasets (calculation method: GROWA).

A slight improvement of the coefficient of determination was achieved by integrating land use information (forest categories) from CORINE into the DLM25 (case b), r²: 0.54). Taking the CORINE dataset as a basis for microscale modelling increased the coefficient of determination significantly (case c, r²: 0.93). This confirms the special influence of land use on the spatial distribution of the model results. The remaining deviations result primarily from the different depths to the groundwater. According to BK50 there are no groundwater-affected soils, whereas on the basis of the groundwater measuring points depths to the groundwater of less than 1 m were widely determined. This led in part to calculations of markedly higher actual evapotranspiration levels on the microscale.

Model comparison

The TRACE model was used to simulate the water flows in the soil and groundwater for the period from 1983 to 1993. The model result was validated with the aid of groundwater measuring point data (see Chapter 5.1). In the model comparison, the actual evapotranspiration levels calculated with the TRACE and GROWA models for the subarea of the middle Rur are compared (Map 26).

The evapotranspiration levels simulated with the TRACE model were first compared (case a, Fig. 35) with the evapotranspiration levels obtained on the basis of the microscale dataset and the GROWA model. As already in Chapter 5.2.1, great spatial deviations result from the differently scaled data bases on land use, here due to the different resolution (5 m and 200 m). The coefficient of determination of 0.18 is very low in case a), but the spatially averaged values only differ slightly from each other (17 mm/a or 3.5 %). If the calculation of evapotranspiration with the GROWA model is based on the same land use, the coefficient of determination increases to 0.40. If the entire dataset for the GROWA calculation is adjusted, the coefficient of determination increases further to 0.47. Only in this case is it possible to speak of a real model comparison, since no spatial scaling effects on the basis of the data should occur. For the same land use TRACE simulates a higher variability of evapotranspiration. This is due to the TRACE dynamic calculation of groundwater flow in contrast to the static approach of the GROWA model. The comparison shows, however, that comparable results are attainable despite clearly different modelling concepts.



Map 26: Actual evapotranspiration levels in the test region calculated with GROWA and TRACE for the period 1983-1993 using the same dataset (resolution: 200 m).

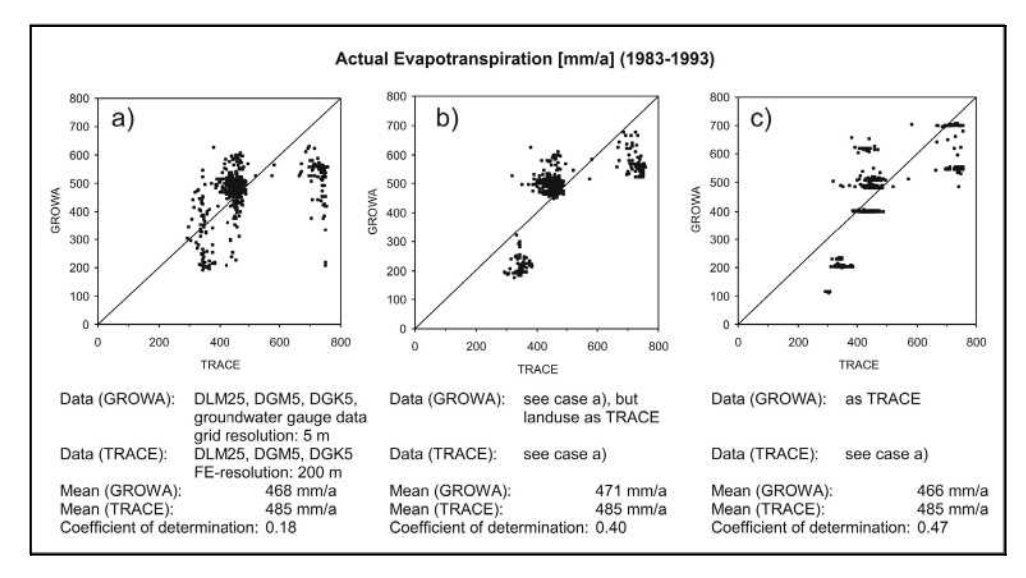


Fig. 35: Correlation diagrams of the actual evapotranspiration levels determined with the GROWA and TRACE models.

The results of these investigations indicate that under comparable boundary conditions the GROWA model is also capable of realistically calculating the spatial distribution of actual evapotranspiration on the macroscale. For a macroscale application of the model it should be noted, however, that the possibility of obtaining small-area information depends, in particular, on the land use data employed. Therefore, an application of the GROWA model using land use classifications by remote sensing is planed in the next MOSYRUR period. An application of remote sensing using LANDSAT 7 ETM+ data was already preformed in the first MOSYRUR period as it is shown in the next Chapter.

Disaggregation of nutrient balances

6.1 Introduction and Objectives

In this section the use of modern technologies of remote sensing and digital image processing for disaggregation of nitrogen balance surpluses at the district level is evaluated. In this way, agricultural production areas with a certain hazard potential for water pollution can be identified more exactly. Furthermore the accuracy of nutrient transport modelling can be increased.

In this analysis different classification algorithms are applied to the heterogeneous study area of the River Rur in order to determine the most appropriate methodological approaches. The analysis of remote sensing data by classification enables to efficiently process large data volumes by means of automation. Once the land use in the Rur catchment area is available in a plot-accurate form, nitrogen balances can be disaggregated from district to plot level (Montzka, 2003).

6.2 Database

In order to identify the land use in the hydrological catchment area of the River Rur, in particular, ASTER (Advanced Spaceborne Thermal Emission and Reflection Radiometer) and LANDSAT lend themselves as remote sensors. Above all, ASTER scenes from the period of vegetation growth (April - June) are suitable for identifying the agricultural structure. However, cloud-free scenes from the period April - June of the years 1999 - 2003 are not available for this study area; only the period September - March is sufficiently imaged, when a lot of crop areas lie fallow or harvesting in the fertile plain landscape has made a differentiation of land uses impossible. The most recent scenes of the growth phase are provided by LANDSAT 7 ETM+. LANDSAT data are also excellently suited for the identification of land use, but they provide a coarser spatial resolution than ASTER. It is being attempted to compensate this deficiency by a wavelet fusion.

The basis for this work is therefore three scenes of LANDSAT 7 ETM+. They all date back to the year 2001 and were imaged on 25 May, 26 June and 29 August. Since these are satellite data from 2001, it is not possible to determine soil reference data at the time of imaging. However, a data collection in the study area is absolutely necessary for the analysis and subsequent interpretation of remote sensing data. For this reason, a survey was made among farm-

ers to obtain information about areas under agricultural use and the crops cultivated in 2001. The exact documentation in a field book made it possible to determine the crop species cultivated at the time of satellite imagery for numerous plots.

Settlement and open-cast mining areas are taken from ATKIS data and masked out for the German territory. For the Dutch and Belgian regions, a supervised classification was made for extracting the paved areas. The masks generated were overlaid to obtain one mask for the entire scene, so that the satellite images can be classified in each case in a single run.

The crops of relevance for this work are sugar beets, wheat, potatoes, barley, vegetables, maize, fruit and grassland. Grassland must be divided into two subunits to allow for the internal heterogeneity, since reaped meadows for hay production are differentiated from vegetated areas. In addition, there are fallow areas, coniferous forest, deciduous forest and waters. The training regions are spitted in two parts: One part is used as a reference for a supervised classification and the second part for the subsequent evaluation of the classification quality.

Nutrient balance surpluses made available by the Research Association for Agricultural Policy and Rural Sociology (FAA) in Bonn are currently available disaggregated to district level. For the districts and autonomous towns in Germany, the nitrogen balance is specified in kg/ha for each crop species.

6.3 Image Processing

6.3.1 Preprocessing

In order to perform a classification, the LANDSAT raw data must be preprocessed. Since LANDSAT ETM+ provides images with 15 m edge length of the pixels in addition to the multispectral channels with 30 m spatial resolution in the panchromatic spectral region, their integration into the multispectral image is meaningful to increase the spatial information. This is to be achieved by an image fusion for the multispectral region.

A suitable method with respect to the following analyses is wavelet fusion. The ARSIS model (Ranchin & Wald, 2000) used in this study improves the spatial information of a multispectral image by means of the panchromatic channel, whereas the spectral properties are only slightly changed. The method, which works with compression, substitution and subsequent expansion, provides loss-free results.

All the six nonthermal channels of the LANDSAT ETM+ sensor are artificially sharpened in this way, as is shown in Fig. 36 for the area of the Research Centre Jülich. For comparison, the same scale was chosen for the three images, and the uncorrected multispectral image (centre) was thus enlarged by a factor of two. Traffic infrastructure and land use boundaries as well as structures in forest and building areas are not as pronounced here as in the result (on the right) of wavelet transformation. The spectral information of the false colour representations of channels 7-5-4, in contrast, does not in the least deviate from the original.

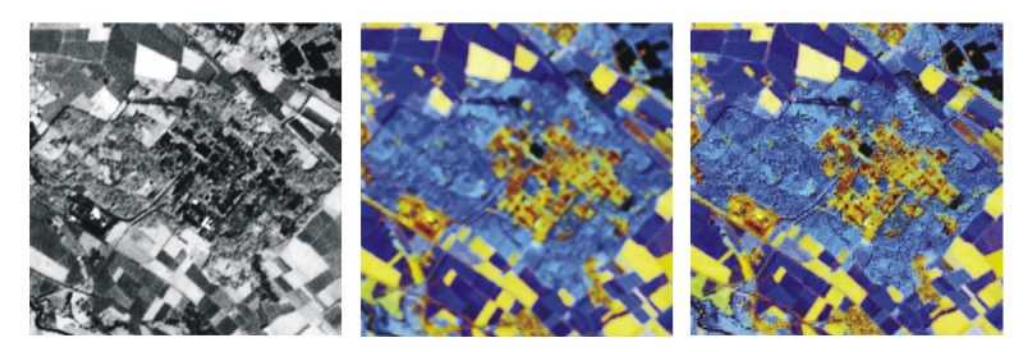


Fig. 36: Result (on the right, channels 7-5-4) of wavelet fusion using the example of Research Centre Jülich. The panchromatic image (on the left) is used to increase the spatial information of the multispectral image (centre, channels 7-5-4).

The collection of data by satellites contains errors in geometry, which must be corrected or largely minimized especially for comparison purposes and for combining two or more satellite images. The position accuracy is impaired by the rotation and curvature of the Earth or by the topography. In spite of these geometrical aberrations, a pixel-accurate comparability of the image data to be analysed must be ensured. The data are therefore georeferenced to a vector dataset.

Finally, the spectral information from six channels is to be combined in three channels by a *Principal Component Transformation*. This will reduce the data complexity and only produce minor information loss. Due to the calculation of synthetic channels, the maximum variance of the grey values is represented in the first principal component, the second largest perpendicular to this in the second principal component etc. The existing system of coordinates is thus rotated linearly, so that the new coordinate axis will lie in the maximum variance. In addition, the coordinate origin is shifted to the mean value. A principal

component thus serves as a coordinate axis. The highly correlated multispectral channels of LANDSAT ETM+ are transformed in a way that they lose their correlation.

One advantage is that the background noise is filtered out with a minimum variance and shifted to the last principal components. As a rule, the first three thus already contain more than 95 % and the first four more than 99 % of the total variance. For a further analysis, therefore, only the first three principal components are used. This provides an advantage not only for the observer, but this data reduction from six to three channels is also meaningful for the following complex transformations.

6.3.2 Classification

With a classification it is intended to group each pixel of a satellite image into categories which, depending on the intention, represent different spectral classes. Spectral signatures extracted from satellite data are related to features of objects of the Earth's surface in order to be able to specify the land-cover for the later disaggregation of the nutrient balance surpluses. Special attention is paid here to the differentiation of crops on agriculturally used land. For pixel-based methods there are two fundamentally different approaches. Cluster analysis or unsupervised classification calculates the class membership of a pixel in a point cloud from a purely statistical set of rules without including any background information of the user. This method is used here prior to a supervised classification in order to test the separability of the classes.

The channels of the satellite image span a feature space as the coordinate axes. Each pixel is given a fixed position in this space due to its feature vector. Pixels with similar spectral properties are located close to each other and can thus be grouped in a cluster. The classification of the data in subsets is generally performed calculating the Euclidean distance in an iterative process (Richards, 1995). On the one hand, a homogeneity within and, on the other hand, a heterogeneity between the clusters can be ensured. Assuming that the pixels of a group provide similar information about the landcover, it will be later possible to differentiate land use types with the aid of ground truth data. However, it is possible that the clusters are overlapping or that the point cloud can be distributed in such a way that no unique cluster centres can be defined, leading to erroneous results. Various methods have been developed to cope with this problem. In contrast to conventional crisp clustering, i.e. the hard

grouping of a pixel in either one or the other class, in a *fuzzy approach* an object can be a component of several clusters with different degrees of membership. Fuzzy means working with unsharp, blurred cluster boundaries (Bezdek & Pal, 1992). This opens up a diversified application field, in which models are capable of representing uncertainties. The LANDSAT data were clustered by *fuzzy k-means* and *fuzzy maximum likelihood*.

A supervised classification by the conventional *maximum likelihood* method or by *neural networks*, in contrast, presupposes a-priori terrain knowledge. The user selects training regions about which he has information. Statistical methods will then search for pixels with similar spectral properties, which are combined in one class. It is thus assumed that these pixels represent an identical landcover in nature. Additional information is thus only needed for a fraction of a satellite image in order to obtain knowledge about the entire space under investigation.

An important assumption in using maximum likelihood is the approximating Gaussian distribution of the spectral information around the mean value of the land use class in the feature space. Each pixel can thus be allocated to that class to which it belongs with the highest statistical probability or to which it has the greatest similarity. The algorithm calculates the probability density function per class from the spectral values of the test regions. If the unknown pixels are then classified, the probability that it belongs to a certain class is determined for each pixel with the aid of its grey values.

A great advantage of the classification by neural networks is that no assumptions concerning the probability density of the grey values must be formulated, e.g. a normal distribution in the maximum likelihood method. A classification is merely performed on the basis of the properties of training data. A neural network handles noise background in the data very tolerantly. In the feature space of the channels (or principal components) a discriminant function is searched for, which enables point clouds to be separated into different groups (Canty, 1999). Neural networks consist of artificial *neurons*, which calculate these discriminant functions.

The grey values of a satellite image are emitted to the distributor units 1, ..., N as input signals x_1 , ..., x_N . These forward the information as a function of threshold values to the neurons 1, ..., L which, however, are multiplied before by *synaptic weights*. Neuron j calculates as the result the output signal n_j using the discriminant function and this input. A special case in Fig. 37 is the upper subsystem, which is independent of the satellite image and causes the sepa-

rating function not necessarily having to pass through the coordinate origin. It is termed bias weight.

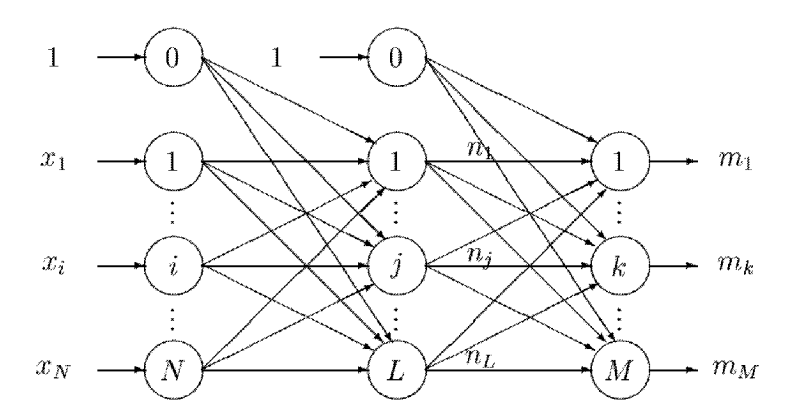


Fig. 37: Feed-forward network. A two-layer perceptron without feedbacks (Canty, 1999).

A unit consisting of distributors, weights and a single neuron is called *perceptron*. If the input is a linear function, the result of this calculation, n_j, will also be a straight line. A nonlinear function, also called *activation function*, is more successful for common applications. In the case of a logistic function, which is very suitable for classification, a logistic result is also expected. The output of such a sigmoidal function represents the a-posteriori probabilities of the classes to be categorized (Bishop, 1997). The number of neurons in the input layer corresponds here to the dimensionality of the signals to be classified, that of the output layer to the number of classes to be identified.

The advantage of using neural networks is their "learning capability". Learning capability in this context means the capability of a learning algorithm to correctly have the weights and threshold values determined by the algorithm. The neurons can thus be trained in a way that they generate a desired output signal for a given input signal. At the beginning, the output signal will not correspond to the desired result. The *least mean square method* is used to calculate a cost function of the deviation, which must be minimized by changing the weights. If the distance in fact becomes smaller in an iteration, then the system has learned.

The process thus takes place according to the following scheme: The synaptic weights are randomly initialized. From the training regions, a pixel is selected again randomly (stochastic learning), for which the desired target value, the

land use class, is known. For this pixel, the actual output value is calculated using the weights and the discriminant function. The weight vector is now shifted by the learning rate in the direction of the negative gradient. If the cost function across all weights, i.e. the difference between desired and actual output, is small enough, the process is stopped. Otherwise, the gradient is further shifted and thus the weights fitted.

The structure of a neural network does not merely consist of one neuron, but – as shown in Fig. 37 – of an array in which several neurons are connected in parallel and additionally perform calculations consecutively in several layers. Equivalently to biological neurons, the nodal points interact by processing the weighted results of neighbouring neurons and passing them on to others. Without the specification of a further layer, certain results cannot be reproduced by fitting the weights (Rumelhart, McClelland & PDP Research Group, 1989).

Since this array contains three types of layers, i.e. distributor, intermediate and output layer, it is termed a *multi-layer perceptron* (Atkinson & Tatnall, 1997). Since there is no backward computation loop, i.e. the information is forwarded from the input through the (hidden) processing to the output layer, a feed-forward network is obtained. However, feed forward only relates to the signals processed and not to the error, which is normally carried back through the network from the output layer towards the input layer for fitting the synaptic weights. This is called *error back propagation*. In this way, the network is trained with the aid of ground truth data in order to subsequently classify the other satellite data.

If a thematic map is to be obtained as the result, as in this case the land use of a study region, then an excessively heterogeneous, fissured structure may possibly be recognized. The interpretation of such information is thus not easy. In the agricultural structure of Central Europe, a pixel which spectrally belongs to another class can be allocated with high probability to that class for which the entire plot is classified. A misclassification of individual pixels can thus be corrected.

The ENVI/IDL 3.5 software produces a rule image in addition to the desired classification result in the case of maximum likelihood and neural networks, which maps the membership probabilities of each pixel in each land use class. This is exploited by a *probabilistic label relaxation*, a method applied after a classification to obtain improved information, where direct neighbourhoods are

included in an analysis as spatial filters in order to generate internally homogeneous land use areas (Canty, 1999).

A kind of kernel is moved across the satellite image from upper left to bottom right in such a way that only every 10th, 100th or 1000th pixel is examined. This ensures that all important probability distributions are recorded and the processing time does not increase immensely. Another possibility is an iterative application to a dataset until no significant alterations are performed any more. If, for example, a pixel is considered which represents forest, then it is examined what class is arranged above, below, to the right and to the left of this pixel. Since forest generally comprises a self-contained region and has a large area, the probability that the neighbours are also forest pixels is very high. Consequently, if for some reason a single pixel within a forest area exhibits a different class, such as water, then a misclassification may be assumed. If this pixel was only identified with a probability of 60 % as water and 40 % as forest, then a probabilistic label relaxation can be used to correct this. In this way, inhomogeneities in a plot or patch are filtered out for generalization.

A modern approach for the analysis of satellite data is the region-based image analysis system *eCognition*. In the case of large-area study regions, an analysis of the topological regularities and geometrical shapes may be useful to support multispectral classification. eCognition is capable of representing complex facts in semantic networks whose concept presupposes that important semantic information cannot be found in individual pixels, but in image objects with mutual relations.

For analysis, input formats such as satellite images are used in different spatial resolutions, vector files and also digital terrain models. In addition, the texture and shape of an object may be used for classification. This software forms a bridge between remote sensing and Geographic Information Systems (Baatz & Schaepe, 1999). A segment, i.e. the spatially correlated amount of pixels, is generated on the basis of neighbourhood relations. Neighbouring image regions are thus combined whose degree of fitting is below a given threshold value (scale parameter). This method, called *multiresolution segmentation*, which is above all based on the region growing approach, starts with one-pixel objects, two of which are always combined depending on the specifications such as minimum size of the objects, colour homogeneity and shape parameter.

6.3.3 Accuracy assessment and classification results

In order to be able to assess the informative value of a classification and determine the method for classification suited best, a quality control must be performed. For this purpose, some pixels of the classified satellite image are compared with ground truth data. In this way, it is not only possible to specify the percentage of correctly classified pixels, but also the class in which wrongly classified pixels are contained.

The classification of each supervised method is now examined for its confusion or error matrix. This is a square matrix whose lines and columns reproduce the individual classes. In this array, either the absolute numbers of the pixels are entered or their percentage distribution. In the main diagonal, those values are specified which have been correctly classified. The sum of these values divided by the total number of pixels gives the overall accuracy of the classification. Quality criteria derived from the error matrix are the producer's accuracy and the user's accuracy. They specify an individual quality criterion for each class. The producer's accuracy is calculated column by column through the number of correctly defined pixels in a class k divided by the total number of pixels classified as k of the reference data.

The user's accuracy, in contrast, is subjected to a line-by-line consideration of the confusion matrix in order to divide the pixels correctly identified as k by the total number of pixels classified as k per classification algorithm. This may lead to considerable differences (Congalton & Green, 1999). The difference is to be found in the commission and omission errors. Commission means that a pixel has been classified into a class to which it actually does not belong, whereas omission excludes the pixel from the class to which it actually belongs. In order to significantly compare several confusion matrices directly with only a single criterion, the kappa index is calculated. The approximately normally distributed index explains the quality of each classification with respect to the reference data used:

$$\kappa = \frac{N\sum_{i=1}^{k} x_{kk} - \sum_{i=1}^{k} x_{k+} x_{+k}}{N^2 - \sum_{i=1}^{k} x_{k+} x_{+k}}$$
(44)

N is the total number of pixels, x_{kk} the correctly classified pixels in class k. If the confusion matrix is considered line by line for class k, then x_{k+} is the user's accuracy, whereas a column-by-column analysis specifies the producer's accuracy as x_{+k} .

Tab. 23: Classification quality according to method and database.

Classification algorithm	Dataset	Kappa- Coefficient	Overall Accuracy Percent (Pixel)
	2001/5/25	0.8735	90.0525 (26407/29324)
Maximum Likelihood	2001/6/26	0.9623	97.0502 (28459/29324)
	bitemporal	0.9443	95.6350 (28044/29324)
	2001/5/25	0.8790	90.4924 (26536/29324)
ML Relaxation	2001/6/26	0.9714	97.7629 (28668/29324)
	bitemporal	0.9591	96.7944 (28384/29324)
	2001/5/25	0.7765	82.4035 (24164/29324)
Neural Net	2001/6/26	0.8610	89.0908 (26125/29324)
	bitemporal	0.8496	88.2042 (25865/29324)
	2001/5/25	0.7881	83.3379 (24438/29324)
NN Relaxation	2001/6/26	0.8710	89.8752 (26355/29324)
	bitemporal	0.8622	89.2136 (26161/29324)
Objectoriented	multitemporal	0.9415	94.7598 (-)

On this basis, a decision is to be made concerning the classification to be used for disaggregating the nutrient balance surpluses. The results whose basis is the training regions not used for classification can be compared in Tab. 23.

Frizzelle & Moody (2001) expect a better classification result for neural networks than for maximum likelihood. However, this is not confirmed when considering the kappa value. The kappa value and the overall accuracy are always higher in the maximum likelihood classification than in the classification by neural networks. The difference is approx. 7 to 10 percent. The object-oriented classification with eCognition also provides a very good result ranging between the neural networks and maximum likelihood.

A comparison within the algorithms used is of interest here. Thus, for example, the LANDSAT scene of the entire Rur catchment area provides the best results on 26 June 2001, whereas the image of 25 May is considerably poorer in classification quality. The bitemporal principal component transformation of the two scenes falls behind expectations and the overall accuracy rather seems to be a weighted arithmetic mean of the quality of the two individual images. Filtering by probabilistic label relaxation proved to be meaningful. It was possible to improve the quality by a few percentage points by smoothing the results.

The methods used are in general statistically good to very good, since accuracies of 85 % to 90 % are almost normal today. Nevertheless, the hit rates in species recognition must not be overestimated. The result is strongly weighted, since above all forest regions and waters were specified as training areas, which can be separated very well from the others. Furthermore, a pos-

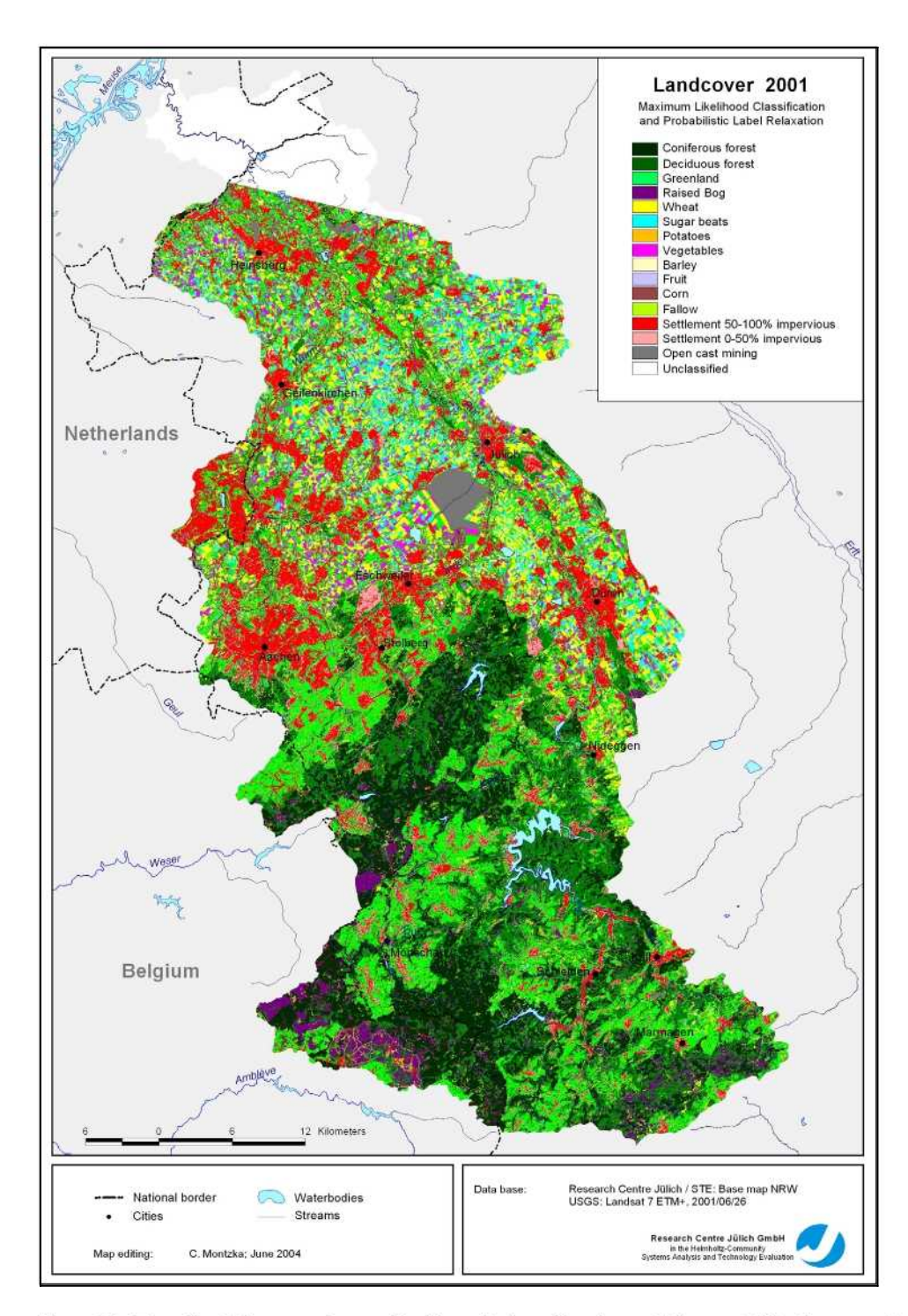
sible error in differentiating them from settlement and open-cast mining areas was precluded from the very beginning. The differences within one crop species pose problems. On the one hand, different varieties are cultivated whose spectral signatures differ from each other. On the other hand, natural variations are identified in the development process of the plant, which are characterized by different field capacities in sandy or gravely subsoils. The maximum likelihood classification of the satellite image of June 2001, as shown in Map 27, is now examined in more detail after filtering by probabilistic label relaxation. In considering the classification quality, the large span is striking to note, which ranges from very well classified landcovers such as coniferous forest (100 %) up to less well determined covers such as fruit (61.52 %) (see Tab. 24).

Tab. 24: Producer's accuracy (percent) in the confusion matrix of the maximum likelihood classification of 26 June 2001 after filtering by probabilistic label relaxation.

	DF	CF	GL I	GL II	WA	RB	PT	SB	WH	VE	MZ	BR	FL	FR	Total
UC	0	0	0	0	0	0.07	0.39	0	0	0.18	0	0	0	0	0.04
DF	95.75	0	1.38	1.04	0	1.8	0	0	0.15	0	0	0	0	0	6.81
CF	0	100	0	0	0	0.01	0	0	0	0	0	0	0	0	7.44
GL I	3.66	0	95.06	0	0	0	4.27	0	0	0	0	1.27	0	0	4.4
GL II	0	0	0.16	92.45	0	0.12	0	0	0.07	0.55	0.99	0	0	38.48	3.84
WA	0	0	0	0	100	0	0	0	0	0	0	0	0	0	32.38
RB	0.58	0	0	0	0	97.69	0	0	0	0	0	0	0	0	30.35
PT	0	0	3.32	0	0	0	94.37	0	0	0	0	0	0	0	3.45
SB	0	0	0	0	0	0	0	99.64	0	0	0	24.05	0	0	2.89
WH	0	0	0	0	0	0	0	0.12	99.78	0	0	0	0	0	4.67
VE	0	0	0	6.51	0	0	0	0	0	98.9	0	0	0	0	2.08
MZ	0	0	0	0	0	0	0	0	0	0.37	98.02	0	7.23	0	0.36
BR	0	0	0.08	0	0	0	0.97	0.24	0	0	0	74.68	0	0	0.25
FL	0	0	0	0	0	0.31	0	0	0	0	0.99	0	92.77	0	0.36
FR	0	0	0	0	0	0	0	0	0	0	0	0	0	61.52	0.69
Total	100	100	100	100	100	100	100	100	100	100	100	100	100	100	100

The classes of coniferous forest (CF) and waters (WA) could be perfectly separated from the others (100 % each). Water surfaces can be separated well from other land uses due to their low reflectance and thus very low grey values in the individual channels. Coniferous forest has also a low reflectance due to its finely structured surface. For the above reasons, the accuracy of classification is optimal for these categories.

Wheat (WH, 99.78 %), sugar beets (SB, 99.64 %), vegetables (VE, 98.90 %) and maize (MZ, 98.02 %) could also be allocated without any major errors. Its is extremely important that the first two crops are well identified, since they are the main crop species in the Lower Rhine Embayment.



Map 27: Result of the maximum likelihood classification of the satellite image of June 2001.

In comparison to wheat, sugar beets do not reach such a striking increase in the plant mass above ground. This is why they can be separated so well (Kuehbauch, 1990).

For the latter two land uses it is of advantage that settlement areas and opencast mining areas were masked out, since they would otherwise spectrally compete with each other. The producer's accuracy of raised bog (RB, 97.69 %), deciduous forest (DF, 95.75 %) and grassland I (GL I, 95.06 %) also still provides very good results, but a few pixels are already assigned to other classes here. Few of the pixels actually belonging to the category of potatoes (PT) are classified as grassland I, which results in an accuracy of 94.37 %.

Fallow land (FL, 92.77 %) mainly overlaps with maize, grassland II (GL II, 92.45 %) mostly with vegetables. Nevertheless, the results are still to be denoted as good. The producer's accuracy is no longer sufficient for barley (BR) with 74.68 % and insufficient for fruit (FR) with 61.52 %. 24 % of the reference plots on which barley is grown are identified as sugar beets. 38 % of the fruit growing areas are identified as grassland. The omission error is thus much too high.

Although the individual channels of LANDSAT ETM+ cover a relatively broad wavelength range, species recognition can be performed well after the transformations described. Problems are posed by the heterogeneity within the intensively cultivated areas of the loess regions, which, however, was adequately identified. Furthermore, the cultivation in narrow plots poses some difficulties. Narrow strips, for example, cannot or can only be wrongly identified due to the mixed pixel problem.

6.3.4 Disaggregation

On the basis of the supervised classification of the LANDSAT ETM+ scene of 26 June 2001, the disaggregation of the nutrient balances is now performed using the example of nitrogen and the maximum likelihood classifier after filtering by probabilistic label relaxation. Since not all crop species listed in the data of FAA Bonn can be separated, several species must be combined. For example, the land use classes of meadow and pasture, which cannot be differentiated by remote sensing data, are averaged in a weighted manner and allocated to the grassland category on the basis of an agricultural structure survey by the State Agency for Data Processing and Statistics NRW (Landesamt für Datenverarbeitung und Statistik NRW, 2001) of the year 1999.

On the assumption that each process unit produces the same nitrogen balance surpluses in the years 1999 and 2001 it is possible to transfer these to the classified satellite images. This transfer is performed in ArcGIS taking the district boundaries into account. The regions not on German territory, for which no data are available, cannot be modelled. The result is shown in Map 27.

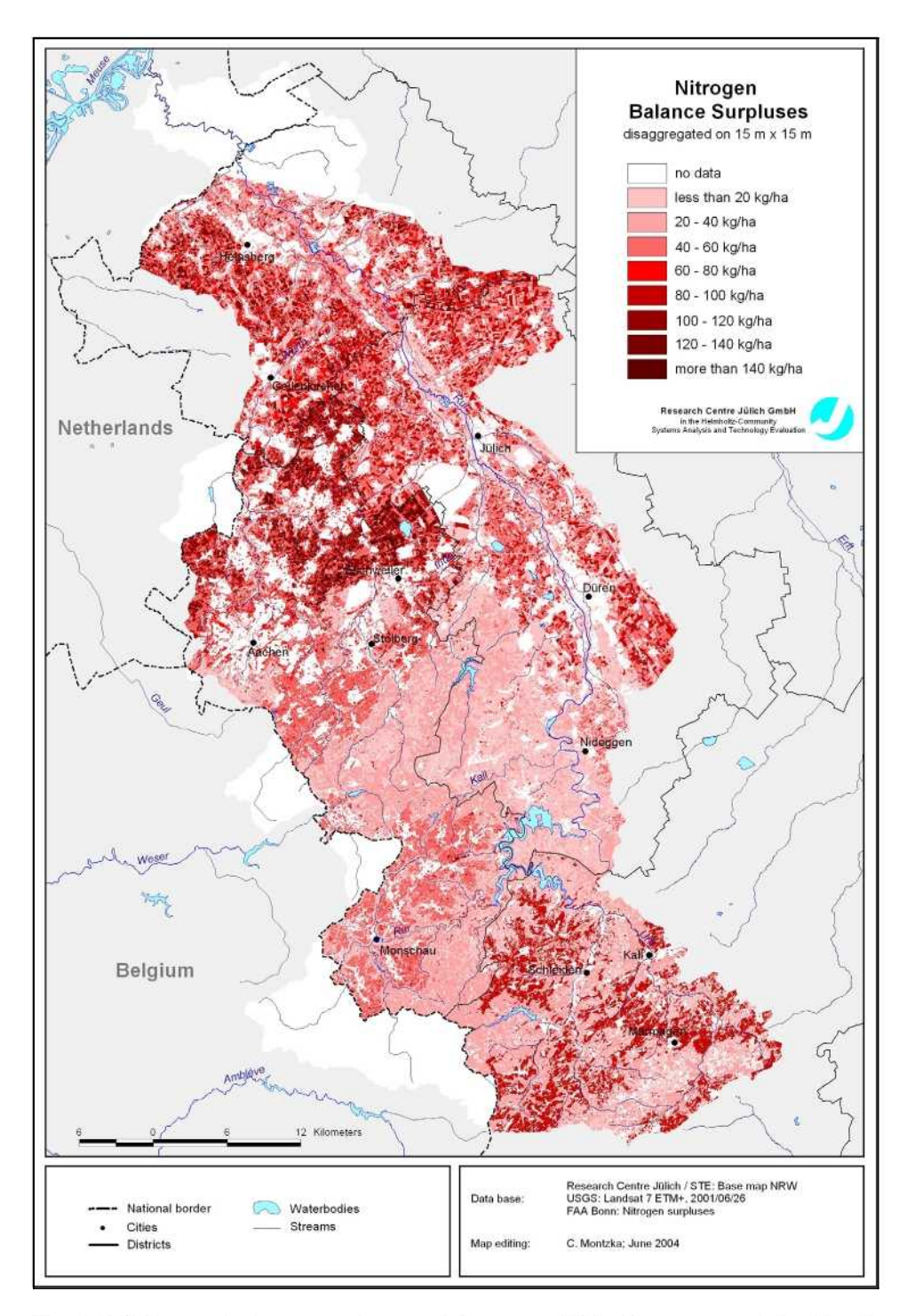
The differences in nitrogen surplus between the diverse land use types are clearly visible. For example, on lots with crops like vegetables or fruit the possible leaching of nitrogen is generally higher than on lots with wheat or barley. Generally, the northern part of the Rur catchment with an intensive agricultural economics structure displays a larger potential to pollute the groundwater with nitrogen compounds. Furthermore, differences at the district level can be recognized. For example, in the district Aachen except for grassland the level of nitrogen surpluses is much higher than in the others, many lots over 120 kg/ha.

For meadow and pasture the district Euskirchen including the cities Schleiden, Kall and Marmagen in the southeast of the catchment shows higher nitrogen surpluses than Aachen (area around Monschau) and Düren (Nideggen).

Forests, which are predominantly to be found in the southern part of the Rur catchment, have small nitrogen surpluses because only atmospheric N-deposition is considered. For settlement, mining areas and raised bog no nitrogen surplus data were available.

In order to verify the results, however, the nitrogen balance surpluses available in the 15 m x 15 m grid can be calculated back to district level. This is followed by a comparison of the total data determined and available for the districts. The nitrogen balance surpluses determined by classification do not reach those summed up from data of farmers by FAA Bonn. A comparison is shown in Fig. 38. Possible causes of the systematic discrepancy in the values are:

- Nitrogen balances recorded in 1999 were transferred to a classification based on the LANDSAT ETM+ scene of 26 June 2001.
- Errors in the statistical division of the satellite image into classes cannot be excluded.
- Not all the land use types for which nitrogen balance surpluses were available could be identified and had therefore to be combined.
- The districts of Euskirchen and Heinsberg could not be completely mapped.



Map 28: Nitrogen balance surpluses of the year 1999 disaggregated for the Rur catchment area in 2001 in kg/ha.

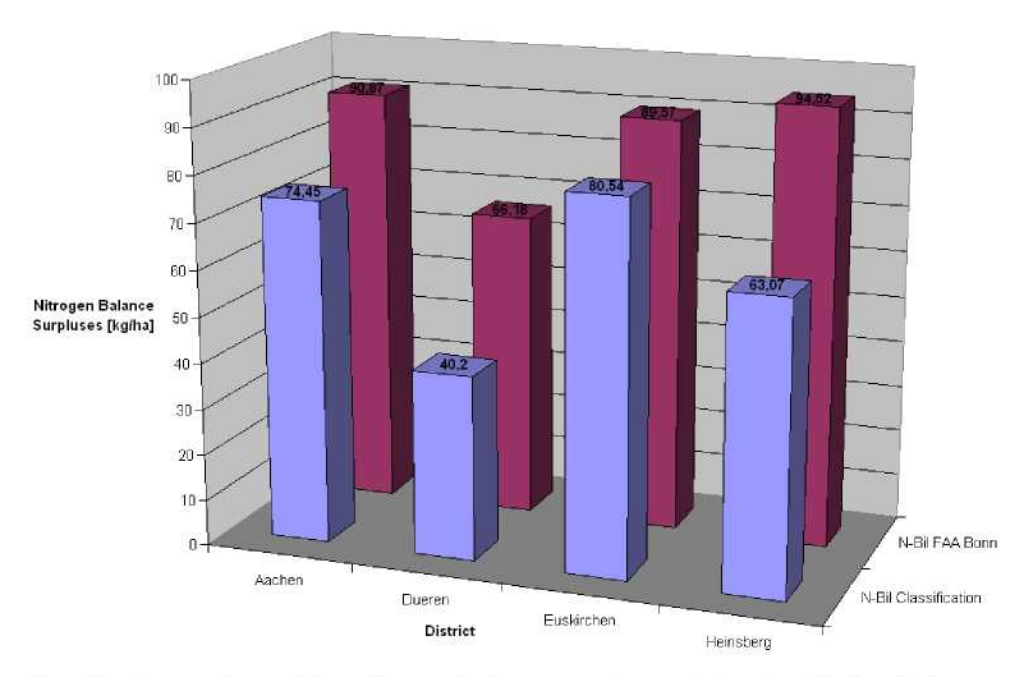


Fig. 38: Comparison of the nitrogen balance surpluses determined in the diploma thesis with those specified by FAA Bonn.

However, the most important restriction is the fact that process units providing potentially high surpluses are underrated in the land use classification.

6.4 Conclusion

Supervised classifications with maximum likelihood and neural networks have shown that the former is better suited to differentiate in detail the most important land uses in the versatile landscape of the Rur catchment area. Filtering by probabilistic label relaxation slightly improved this result.

Neural networks, in contrast, only provide comparably good results in the case of a small number of training pixels and few classes. eCognition also achieves good results and has, moreover, an additional potential for including supplementary information in the classification.

The determination of the crop species was performed as a basis for the disaggregation of nutrient balance surpluses using the example of nitrogen. The nitrate surpluses could be made available in a plot-accurate form and thus a considerable improvement of the scale level gain is gained. The use of satellite data proved to have advantages over conventional methods for data collection, which are time- and labour-intensive.

Remote sensing can also be used to cover the data demand of hydrological models. If several cloud-free satellite scenes are available for the important phenological phases and for further consecutive years, it is possible to record agricultural rotation and obtain more precise information on the condition of the Earth's surface. The use of several images of a year in the important phenological phases would be very helpful here (Herrmann & Kuhn, 1995).

Especially the technical progress to be expected in the field of spectral and spatial resolution will make the analysis of agricultural structures much more effective. In this study, an indirect approach was chosen, which does not exclusively use remote sensing data, but links statistical information with these data so as to obtain useful results. A method has been presented, which is not confined to the Rur catchment area and the element nitrogen, but is also applicable to other domains.

Other nutrients such as phosphate can be disaggregated according to the same procedure. A transfer to the Erft catchment area or to the whole of North Rhine-Westphalia would also be possible. Future analyses will be undertaken to determine in which way hydrological models like GROWA and WEKU can benefit from the transfer of such detailed information.

Summary

In this report the current results of the research activities in the MOSYRUR project are summarized. The targets of the first project phase (2002-2004) were the analysis of the quantitative status of the water resources in the catchment of the Rur (~2350 km²) and the indication of the water balance at different scales. Process orientated investigations and simulations were performed at the small meso-scale test area "Zwischenscholle" (20 km²) using the TRACE model. For the model application the potential evapotranspiration was calculated, Pedotransfer functions were utilized in order to derive the soil hydraulic properties and borehole measurements of groundwater levels were spatially and temporally interpolated in order to define the vertical boundary conditions. A one-dimensional and a three-dimensional TRACE application were performed for the period 1.12.1983 to 31.11.1993.

The one-dimensional TRACE application was validated using a lysimeter experiment dataset spanning the period from 25.11.1988 to 13.8.1990. The actual evapotranspiration is slightly underestimated, while the amount of drainage is slightly overestimated. Nevertheless the calculated model performance measures indicate that all relevant processes and state variables (evapotranspiration, drainage and soil moisture) are well described. The measured actual evapotranspiration for the whole modelling period is 990 mm, whereas TRACE calculates an amount of 977 mm. The deviation between the measured drainage amount of 158 mm and the amount predicted with TRACE (163 mm) is equal to an error of 3.4 %. A decrease in soil moisture during the first spring at 85 cm depth is not that well reproduced, which might be attributed to a plant compensation mechanism. Probably the plant adapts to the low soil moisture near the surface by taking out more water at deeper soil layers. The validation of the three-dimensional TRACE application showed that the

groundwater levels measured at the field scale are, basically, well reproduced. Wells were selected, which are located rather in the middle of the test area than close to the boundary, since the model results and measured heads are supposed to be very similar near the boundary, where the measurements are used for the imposed boundary condition. The RMSE of these wells ranges between 0.33 and 0.68, which is adequate since no calibration of the model was carried out.

The large-scaled GIS-supported **GROWA model** was applied for balancing water components at the catchment scale. For the model application datasets were used that were mainly provided by the geological survey of NRW and the state environmental agency Aachen. This are in particular the digital soil map

BK50, the digital hydro-geological map HK100, a high resolution digital elevation model and the datasets of several discharge gauging stations, which were used for the model validation. Furthermore, precipitation and a potential evapotranspiration dataset of the German weather service for the period 1979-1999 as well as the CORINE Landcover dataset of the federal office of statistic were used.

For the modelling the datasets were transformed to a consistent grid resolution of 50 m, which was seen as adequate for the scale of the chosen datasets. The validation of the model results was accomplished using the discharge data of 40 gauging stations located in the catchment of the Rur River. For most of the subbasins a very satisfying agreement between modelled and observed total runoff, direct runoff and groundwater recharge values were determined. The majority of the subbasins showed a deviation less than 15 %. Very large differences from the modelling results could only be observed for subbasins being highly influenced by water management activities, e.g. water reservoirs, sewage treatments and groundwater sumping in the lignite mining areas.

In the lowland region in the northern part of the Rur catchment **total runoff** levels of less than 350 mm/a are dominating. Values of less than 250 mm/a are to be found in the region around Heinsberg. In contrast to this, total runoff levels above 450 mm/a are predominating in the upland regions and in elevated upland regions (e.g. Hohes Venn), values of even more than 650 mm/a can be reached.

The **groundwater recharge** is primarily determined by the hydrogeological properties of the outcropping rock strata in the Rur catchment. Thus, the groundwater recharge levels in the impervious Lower and Upper Devonian solid rocks of the Rhenish Massif are mostly in the range below 100 mm/a. Only the Middle to Upper Devonian karstified carbonate rocks in the south of Stolberg and the partially karstified limestones in the lime troughs of the North Eifel show groundwater recharges of more than 300 mm/a. In the unconsolidated rock region, groundwater recharge levels between 200 and 300 mm/a occur to a large extend and are mainly associated with the occurrence of Loess.

In the lowland regions, direct runoff values below 50 mm/a predominantly occur, whereas the urbanized areas show values between 150 - 300 mm/a. Also the steep slopes of the open mine pits reveal high direct runoff levels (up to 300 mm/a and more). In contrast to this, direct runoff levels of more than

400 mm/a dominate in the upland regions and even peak values of more than 650 mm/a can be reached in elevated upland regions.

The analysis of predominating runoff components showed that in the consolidated rock regions of the Rur catchment a completely different discharge pattern is to be found. In most cases the GD-relation is lower than 100 %. Hence, the predominating portion of the total runoff is discharged by overland flow and interflow into the receiving streams. In regions where Palaeozoic noncarbonate rocks are present, the proportion of direct runoff is four times higher than the proportion of groundwater recharge. However, the karstified carbonate rocks are an exception. Due to the high hydraulic conductivities of these geologic formations, the proportion of direct runoff is highly increased and therefore the values of GD-relation are exceeding 200 % and, in part, even 500 %.

Furthermore, an **analysis of the scale effects** of the input data and the used models was undertaken. The results of these investigations indicate that under comparable boundary conditions the GROWA model is also capable of realistically calculating the spatial distribution of actual evapotranspiration on the macroscale. For a macroscale application of the model it should be noted, however, that the possibility of obtaining small-area information depends, in particular, on the land use data employed.

Additionally a disaggregation of nitrogen balance surpluses on the district level was successfully performed by the use of modern technologies of remote sensing and digital image processing. This is an important prerequisite for modelling spatial accurate nutrient balances. Generally, the northern part of the Rur catchment with an intensive agricultural economics structure displays a larger potential to pollute the groundwater with nitrogen compounds. Furthermore, differences at the district level can be recognized. For meadow and pasture the district Euskirchen including the cities Schleiden, Kall and Marmagen in the southeast of the catchment shows higher nitrogen surpluses than Aachen (area around Monschau) and Düren (Nideggen). Forests, which are mostly found in the southern part of the Rur catchment, have small nitrogen surpluses because only atmospheric N-deposition is considered. For settlement, mining areas and raised bog no nitrogen surplus data were available.

References

- AG Boden (1994): Bodenkundliche Kartieranleitung, 4. Auflage.- Bundesanstalt Geowissenschaften u. Rohstoffe, 392 p.; Hannover.
- Atkinson P.M. & Tatnall, A.R.L. (1997): Neural networks in remote sensing.- International Journal of Remote Sensing 18(4): 699-709.
- ATV-DVWK (2001): Verdunstung in Bezug zu Landnutzung, Bewuchs und Boden. Merkblatt ATV-DVWK M 504, 139 p.; Hennef.
- Baatz, M. & Schaepe, A. (1999): Object-Oriented and Multi-Scale Image Analysis in Semantic Networks.- Proc. of the 2nd International Symposium on Operationalization of Remote Sensing August 16th 20th 1999; Enschede.
- Bezdek, J.C. & Pal, S.K. (eds.) (1992): Fuzzy Models For Pattern Recognition Methods That Search for Structures in Data; New York.
- Blöschl, G. and Sivalapan, M., 1995. Scale issues in hydrological modelling: A review. In: J.D. Kalma & M. Sivalapan (eds.), Scale Issues in Hydrologic Modelling: 9-48; Chichester.
- Blöschl, G., Sivapalan, M. (1995): Scale issues in hydrological modelling: a review. Hydrological Processes 9: 251-290.
- Bogena, H., Kunkel, R., Schöbel, T., Schrey, H.P., Wendland, F. (2003): Die Grundwasserneubildung in Nordrhein-Westfalen.- Schr. d. FZ Jülich, Reihe Umwelt 37, p. 148; Jülich.
- Bogena H., Kunkel, R., Schöbel, T., Schrey, H.P. & Wendland, F. (2005): Distributed modelling of groundwater recharge at the macroscale.- Ecological Modelling (in print).
- Brakensiek, D.L. & Rawls, W. (1994): Soil containing rock fragments: effects on infiltration. Catena 23: 99-110.
- Bucher, B. & Denneborg, M. (1993): Infiltrationsverhalten der Rur.- Wasser & Boden 3: 173-177.
- Canty, M.J. (1999): Fernerkundung mit neuronalen Netzen Theorie, Algorithmen, Programme; Renningen Malmsheim.
- Celia, M.A., Bouloutas E.T. & Zarba, R.L. (1990): A general mass-conservative numerical solution for the unsaturated flow equation. Water Resources Research, 26(7): 1483-1496.
- Congalton, R.G. & Green, K. (1999): Assessing the Accuracy of Remotely Sensed Data: Principles and Practices; Boca Raton.
- Demuth, S. (1993): Untersuchungen zum Niedrigwasser in West-Europa.- Freiburger Schr. zur Hydrologie 1, 205 p.; Freiburg.

- Doorenbos, J & Pruitt. W.O. (1977): Crop Water Requirements.- FAO Irrigation and Drainage Paper 24; Rome.
- Dörhöfer, G., Josopait, V. (1980): Eine Methode zur flächendifferenzierten Ermittlung der Grundwasserneubildungsrate. Geol. Jb. C 27: 45-65.
- Dörhöfer, G., Kunkel, R., Tetzlaff, B. & Wendland, F. (2001): Der natürliche Grundwasserhaushalt von Niedersachsen. Arbeitshefte Wasser 1/2001: 109-167.
- Döring, U. (1997): Transport der reaktiven Stoffe Eosin, Uranin und Lithium in einem heterogenen Grundwasserleiter.- ph.D. thesis, University of Kiel, 118 p.; Kiel.
- DVWK (1996): Ermittlung der Verdunstung von Land- und Wasserflächen.-DVWK-Merkblätter zur Wasserwirtschaft 238, 135 p.; Bonn.
- Englert, A. (2003): Mesurement, estimation and modelling of groundwater flow velocity at Krauthausen test site.- ph.D. thesis, RWTH Aachen, 89 p.; Aachen.
- Feddes, R.A., Kowalik, P.J. & Zaradny H. (1978): Simulation of field water use and crop yield.- Simulation Monographs, 188 p.; Wageningen.
- Frizelle, B.G. & Moody, A. (2001): Mapping Continuous Distributions of Land Cover: A Comparison of Maximum-Likelihood Estimation and Artificial Neural Networks.- Photogrammetric Engineering and Remote Sensing 67(6): 693-705.
- Gabriel, B. & Ziegler, G. (1989): Lithofazieseinheiten ein neues Konzept zur Berechnung der Grundwasserneubildung im Festgesteinsbereich.- Wasserwirtschaft-Wassertechnik, 39 (7): 163-165. Beyer, W. (1964): Zur Bestimmung der Wasserdurchlässigkeit von Kiesen und Sanden aus der Kornverteilungskurve.- Wasserwirtschaft-Wassertechnik 14(6): 165-168.
- Gardner. W.R. (1958): Some steady state solutions of the unsaturated moisture flow equation with application to evaporation from a water table.- Soil Science 85: 228-232.
- Glugla, G. & Müller, E. (1993): Grundwasserneubildung als Komponente der Abflussbildung.- Freiberger Schriften zur Hydrologie 1, 205 p.; Freiburg i. Breisgau.
- Glugla, G., Jankiewicz, P., Rachimow, C., Lojek, K., Richter, K. Fürtig, G. & Krahe, P. (2002): Wasserhaushaltsverfahren BAGLUVA zur Berechnung vieljähriger Mittelwerte der tatsächlichen Verdunstung und des Gesamtabfluss.-BfG-Bericht 1342, Bundesanstalt f. Gewässerkunde; Berlin/Koblenz.

- Glugla, G., Müller, E., Jankiewicz, P., Rachimow, C. & Lojek, K. (1999): Entwicklung von Verfahren zur Berechnung langjähriger Mittelwerte der flächendifferenzierten Abflussbildung. Abschlussbericht zum DFG-Projekt GI 242/1-2 "Wasserhaushalts-verfahren", BfG-Außenstelle; Berlin.
- Goemann, H. et al. (2003): Koppelung agrarökonomischer und hydrologischer Modelle Ein Meilenstein in der modellgestützten Agrar- und Agrarumweltpolitikberatung.- Agrarwirtschaft 53(4): 195-203.
- Golf, W. (1981): Ermittlung der Wasserressource im Mittelgebirge.- Wasserwirtschaft-Wassertechnik 31: 93-95.
- Gutknecht, D., Blaschke, A.P., Sengschmitt, D. & Steiner, K.-H. (1997): Kolmationsvorgänge in Flussstauräumen Konzeptionen und Beobachtungen.-Österreichische Ingenieur- und Architekten-Zeitschrift (ÖIAZ) 143(1/1998): 21-32; Vienna.
- HAD, Hydrologischer Atlas Deutschland (1998): Bundesministerium für Umweltschutz, Naturschutz und Reaktorsicherheit (Hrsg.): Hydrologischer Atlas von Deutschland.
- Hamon, W. R. (1961): Estimating potential evapotranspiration. Journal of the Hydraulics Division.- Proceedings of the American Society of Civil Engineers 87(No. HY 3): 2817-2822.
- HAUDE, W. (1954): Zur praktischen Bestimmung der aktuellen und potentiellen Evapotranspiration.- Mitt. dt. Wetterdienst 8: 1-24.
- Hennings, V. (Ed.) (2000): Methodendokumentation Bodenkunde Auswertemethoden zur Beurteilung der Empfindlichkeit und Belastbarkeit von Böden.-Geologisches Jahrbuch, Reihe F, 232 p.; Hannover.
- Herbst, M., Ciocanaru, M., Hardelauf, H., Harms, R. & Vereecken, H. (2003):
 Modelling the regional scale transport of pesticides.- Tagungsbeiträge zum
 6. Workshop zur hydrologischen Modellierung: 167-176, Kassel University Press; Magdeburg.
- Herrmann, S. & Kuhn, W. (1995): Flächenscharfe Erfassung von Fruchtfolgen aus Satellitenbildern.- Zeitschrift f. Kulturtechnik u. Landentwicklung 36: 69-74.
- Hoyningen-Huene, J.V.F (1983): Die Interzeption des Niederschlages in landwirtschaftlichen Pflanzenbeständen.- Schr. D. Deutschen Verbandes f. Wasserwirtschaft und Kulturbau e.V. 57: 1-53.
- Huang, K., Mohanty, B.P & van Genuchten M.Th. (1996): A new convergence criterion for the modified Picard iteration method to solve the variably saturated flow equation. Journal of Hydrology 178: 69-91.

- Jahn, R (2002): Erstellung eines hydrogeologischen Modells für die Jülicher Zwischenscholle.- ph.D. thesis, RWTH Aachen, 79 p.; Aachen
- Kille, K. (1970): Das Verfahren MoMNQ, ein Beitrag zur Berechnung der Grundwasser-neubildung mit Hilfe der monatlichen Niedrigwasserflüsse.- Z. dt. geol. Ges., Sonderh. Hydrogeol. Hydrogeochem.: 89-95.
- Klosterman J. (1992): Das Quartär der Niederrheinischen Bucht. Geologische Landesamt Nordrhein-Westfalen, 200p.; Krefeld.
- Kuebauch, W. et al. (1990): Fernerkundung in der Landwirtschaft.- Luft- und Raumfahrt 4: 36-45.
- Kunkel, R. & Wendland, F. (1998): Der Landschaftswasserhaushalt im Flußeinzugsgebiet der Elbe Verfahren, Datengrundlagen und Bilanzgrößen.- Schr. d. FZJ, Reihe Umwelt 12, 107 p.; Jülich
- Kunkel, R. & Wendland, F. (2002): The GROWA98 model for water balance analysis in large river basins - the river Elbe case study.- Journal of Hydrology 259: 152-162.
- Landesamt für Datenverarbeitung und Statistik NRW (2001): Landwirtschaftszählung/ Agrarstrukturerhebung 1999 Gemeinde und Kreisstatistik der landwirtschaftlichen Betriebe Betriebsgrößen, Bodennutzung und Viehhaltung; sozialökonomische Betriebstypen und Betriebssystematik; Arbeitskräfte, Hofnachfolge und Besitzverhältnisse.- Statistische Berichte; Düsseldorf.
- LAWA (2001): Arbeitshilfe zur Umsetzung der EG-Wasserrahmenrichtlinie.- Länderarbeits-gemeinschaft Wasser, 67 p.; Berlin.
- Makkink, G. F. (1957): Testing the penman formula by means of lysimeters.- Journal of the Institute of Water Engineers 11: 277-288.
- Monteith, J.L. (1975): Vegetation and the atmosphere.- Academic Press, 439 p.; London.
- Montzka, C. (2003): Cluster Analyse und überwachte Klassifikation von LAND-SAT Daten für die Disaggregierung von Nährstoffbilanzüberschüssen im Flusseinzugsgebiet der Rur.- diploma thesis, University of Bonn, 161 p.;
- Müller, U. (1997): Dokumentation zur Methodenbank des Fachinformationssystem Bodenkunde (FIS BODEN).- Technische Berichte zum NIBIS, 2. Aufl. unter Mitarbeit von Malessa, V., Bergmann, A.: Nieders. Landesamt f. Bodenforschung. E.; Stuttgart.
- Nash, J.E & Sutcliffe J.V. (1970): River flow forecasting through conceptual models: Part I A discussion of principles.- J. of Hydrology 10: 282-290.

- Neuendorf, O. (1996): Numerische 3-D Simulation des Stofftransports in einem heterogenen Aquifer.- ph.D. thesis, RWTH Aachen, 305 p.; Aachen.
- Peschke, G. (1997): Der komplexe Prozess der Grundwasserneubildung und Methoden zu ihrer Bestimmung. In: Leibundgut, C. & Demuth, S. (eds.): Freiburger Schriften zur Hydrologie 5: 1-13, Freiberg.
- Proksch, W. (1990): Lysimeterauswertungen zur flächendifferenzierten Ermittlung mittlerer Grundwasserneubildungsraten.- Bes. Mitt. dt. gewässerkdl. Jb. 55, 74 p.; Koblenz.
- Pütz, T. (1993): Lysimeterversuche zum Verlagerungsverhalten von Methabenzthiazuron und gelöstem organischen Kohlenstoff in einer Parabraunerde, Aufbau von zwei Klimameßstationen und Untersuchungen zur Validierung des Lysimetersystems.- ph.D. thesis, University of Bonn, 223 p.; Bonn.
- Ranchin, T. & Wald, L. (2000): Fusion of High Spatial and Spectral Resolution Images: The ARSIS Concept and Its Implementation.- Photogrammetric Engineering and Remote Sensing 66(1): 49-61.
- Rawls, W. & Brakensiek, D.L. (1985): Prediction of soil water properties for hydrologic modelling.- Proceedings of the American Society of Civil Engineers Watershed Management in the Eighties Symposium, American Society of Civil Engineers, New York: 293-299.
- Renger, M. & Strebel, O. (1980): Jährliche Grundwasserneubildung in Abhängigkeit von Bodennutzung und Bodeneigenschaften.- Wasser u. Boden 32(8): 362-366.
- Renger, M. & Wessolek, G. (1996): Berechnung der Verdunstungsjahresnummern einzelner Jahre.- DVWK-Merkblätter zur Wasserwirtschaft 238, 47 p.; Bonn.
- Renger, M., Strebel, O., Münnich, K.O. & Sonntag, C. (1977): Methoden zur Bestimmung der Grundwasserneubildungsrate.- Geol. Jb. C19; Hannover.
- Richards, J.A. (1995): Remote Sensing Digital Image Analysis An Introduction. 2nd Edition; Berlin.
- Rijtema, P. E. (1968). On the relation between transpiration, soil physical properties and crop production as a basis for supply plants.- Techn. Bull. Inst., Land and Water Management Research 58; Wageningen.
- Rumelhart, D.E., McClelland, J.L. & PDP Research Group (1989): Parallel Distributed Processing Explorations in the Microstructure of Cognition. Vol. 1: Foundations. Cambridge.
- Rutter, A.J., Kershaw, K.A., Robins, P.C. & Morton A.J. (1971): A predictive model of rainfall interception in forests 1. Derivation of the model from observations in a plantation of corcican pine.- Agri. Meteorology 9: 367-384.

- RWE Power (2004): http://www.rwepower.com
- Schrey, H. P. (1994): Die großmaßstäbige Bodenkartierung in Nordrhein-Westfalen als Weg vom Bohrpunkt zur Fläche; 2. Teil: Die quantifizierende Codierung als Grundlage EDV-gestützter Auswertungen.- Mitt. Dtsch. Bodenkundl. Ges. 74: 225-228.
- Schrey, H. P. (1996): Schätzrahmen für die effektive Durchwurzelungstiefe mehrschichtiger Böden.- Z. Pflanzenernähr. Bodenk. 159: 453-457.
- Schwarze, H, Jaeckel, U. & Vereecken, H. (2001): Estimation of macrodispersion by different approximation methods for flow and transport in randomly generated heterogenous media, Transport in Porous Media 43: 265-287.
- Smith, M., Allen, R. & Pereira, L. (1996): Revised FAO Methodology for crop water requirements.- FAO-Report, 10 p.; Rome.
- Spitters, C.J.T.,van Keulen H. & van Kraalingen H. (1988): A simple but universal crop growth simulation model, SUCROS87. In: R. Rabbinge, H. Van Laar & Ward, S.E. (eds.), Simulation and system management in crop protection.-Simulation Monographs 32. PUDOC; Wageningen.
- Statistisches Bundesamt (1997): Informationsblatt zur CD-ROM "Daten zur Bodenbedeckung für die Bundesrepublik Deutschland"; Wiesbaden.
- Struckmeier, W. (1990): Wasserhaushalt und Hydrologische Systemanalyse des Münsterländer Beckens.- LWA Schriftenreihe des Landesamtes für Wasser und Abfall NRW, Bd. 45, 72 p.; Düsseldorf.
- Van Genuchten, M.Th. (1980): A closed form equation for predicting the hydraulic conductivity of unsaturated soils.- Soil Sci. Soc. of Am. J. 44: 892-898.
- Van Heemst, H.D.J. (1988): Plant data values required for simple crop growth simulation models: review and bibliography,- Simulation Rep. CABO-TT 17, Wageningen, 107 p.
- Vereecken, H & Kaiser R. (1999): Analysis of multi-step outflow data and pedotransfer functions to characterise soil water and solute transport at different scales. In: M. Th. van Genuchten, F.J. Leij & Wu L. (eds.): Characterization and measurement of the hydraulic properties of unsaturated porous media, part 2, 1089-1102; Riverside, California.
- Vereecken, H., J. Feyen, J. Maes & Darius P. (1989): Estimating the soil moisture retention characteristic from texture, bulk density and carbon content.- Soil Science 148: 389-403.
- Vereecken, H., J. Maes & Feyen J. (1990): Estimating unsaturated hydraulic conductivity from easily measured soil properties. Soil Science 149: 1-12.

- Vereecken, H., Lindenmayr, G., Neuendorf, O., Döring, U. & Seidemann, R. (1994): TRACE A mathematical model for reactive transport in 3D variably saturated porous media.- Internal Report KFA-ICG-4-501494, 67 p.; Jülich.
- Wendland, F., Kunkel, R., Grimvall, A., Kronvang, B. & Müller-Wohlfeil, D.I. (2001): Model system for the management of nitrogen leaching at the scale of river basins and regions.- Water Science and Technology 43(7): 215-222.
- Wendling, U. (1995): Berechnung der Gras-Referenzverdunstung mit der FAO Penman-Monteith-Beziehung.- Wasserwirtschaft 85(12): 602-604.
- Wessolek, G. & Facklam, M. (1997): Standorteigenschaften und Wasserhaushalt von versiegelten Flächen.- Z. Pflanzenernähr. Bodenk. 160: 41-46.
- Willmott, C.J. (1981): On the validation of models, *Physical Geography* 2: 184-194.
- Wundt, W. (1958): Die Kleinstwasserführung der Flüsse als Maß für die verfügbaren Grundwassermengen. In: Grahmann, R. (ed.): Die Grundwässer in der Bundesrepublik Deutschland und ihre Nutzung.- Forsch. Dtsch. Landeskunde 104: 47-54; Remagen.
- Yeh, G. (1987): 3DFEMWATER, a three dimensional finite element model of water flow through saturated-unsaturated media.- Report ORNL-6386; Oak Ridge.

1. Energiemodelle in der Bundesrepublik Deutschland. Stand der Entwicklung

IKARUS-Workshop vom 24. bis 25. Januar 1996 herausgegeben von S. Molt, U. Fahl (1997), 292 Seiten

ISBN: 3-89336-205-3

2. Ausbau erneuerbarer Energiequellen in der Stromwirtschaft

Ein Beitrag zum Klimaschutz

Workshop am 19. Februar 1997, veranstaltet von der Forschungszentrum Jülich GmbH und der Deutschen Physikalischen Gesellschaft herausgegeben von J.-Fr. Hake, K. Schultze (1997), 138 Seiten

ISBN: 3-89336-206-1

3. Modellinstrumente für CO₂-Minderungsstrategien

IKARUS-Workshop vom 14. bis 15. April 1997 herausgegeben von J.-Fr. Hake, P. Markewitz (1997), 284 Seiten ISBN: 3-89336-207-X

IKARUS-Datenbank - Ein Informationssystem zur technischen, wirtschaftlichen und umweltrelevanten Bewertung von Energietechniken

IKARUS. Instrumente für Klimagas-Reduktionsstrategien Abschlußbericht Teilprojekt 2 "Datenbank" H.-J. Laue, K.-H. Weber, J. W. Tepel (1997), 90 Seiten

ISBN: 3-89336-214-2

5. Politikszenarien für den Klimaschutz

Untersuchungen im Auftrag des Umweltbundesamtes

Band 1. Szenarien und Maßnahmen zur Minderung von CO₂-Emissionen in Deutschland bis zum Jahre 2005

herausgegeben von G. Stein, B. Strobel (1997), 410 Seiten

ISBN: 3-89336-215-0

6. Politikszenarien für den Klimaschutz

Untersuchungen im Auftrag des Umweltbundesamtes

Band 2. Emissionsminderungsmaßnahmen für Treibhausgase, ausgenommen energiebedingtes CO₂

herausgegeben von G. Stein, B. Strobel (1997), 110 Seiten

ISBN: 3-89336-216-9

7. Modelle für die Analyse energiebedingter Klimagasreduktionsstrategien

IKARUS. Instrumente für Klimagas-Reduktionsstrategien

Abschlußbericht Teilprojekt 1 "Modelle"

P. Markewitz, R. Heckler, Ch. Holzapfel, W. Kuckshinrichs, D. Martinsen,

M. Walbeck, J.-Fr. Hake (1998), VI, 276 Seiten

ISBN: 3-89336-220-7

8. Politikszenarien für den Klimaschutz

Untersuchungen im Auftrag des Umweltbundesamtes

Band 3. Methodik-Leitfaden für die Wirkungsabschätzung von Maßnahmen zur Emissionsminderung

herausgegeben von G. Stein, B. Strobel (1998), VIII, 95 Seiten

ISBN: 3-89336-222-3

9. Horizonte 2000

6. Wolfgang-Ostwald-Kolloquium der Kolloid-Gesellschaft

3. Nachwuchstage der Kolloid- und Grenzflächenforschung

Kurzfassungen der Vorträge und Poster

zusammengestellt von F.-H. Haegel, H. Lewandowski, B. Krahl-Urban (1998),

150 Seiten

ISBN: 3-89336-223-1

10. Windenergieanlagen - Nutzung, Akzeptanz und Entsorgung

von M. Kleemann, F. van Erp, R. Kehrbaum (1998), 59 Seiten

ISBN: 3-89336-224-X

11. Policy Scenarios for Climate Protection

Study on Behalf of the Federal Environmental Agency

Volume 4. Methodological Guideline for Assessing the Impact of Measures for Emission Mitigation

edited by G. Stein, B. Strobel (1998), 103 pages

ISBN: 3-89336-232-0

12. Der Landschaftswasserhaushalt im Flußeinzugsgebiet der Elbe

Verfahren, Datengrundlagen und Bilanzgrößen

Analyse von Wasserhaushalt, Verweilzeiten und Grundwassermilieu im Flußeinzugsgebiet der Elbe (Deutscher Teil). Abschlußbericht Teil 1.

von R. Kunkel, F. Wendland (1998), 110 Seiten

ISBN: 3-89336-233-9

13. Das Nitratabbauvermögen im Grundwasser des Elbeeinzugsgebietes

Analyse von Wasserhaushalt, Verweilzeiten und Grundwassermilieu im Flußeinzugsgebiet der Elbe (Deutscher Teil). Abschlußbericht Teil 2. von F. Wendland, R. Kunkel (1999), 166 Seiten

ISBN: 3-89336-236-3

14. Treibhausgasminderung in Deutschland zwischen nationalen Zielen und internationalen Verpflichtungen

IKARUS-Workshop am 27.05.1998, Wissenschaftszentrum Bonn-Bad Godesberg. Proceedings

herausgegeben von E. Läge, P. Schaumann, U. Fahl (1999), ii, VI, 146 Seiten

ISBN: 3-89336-237-1

15. Satellitenbildauswertung mit künstlichen Neuronalen Netzen zur Umweltüberwachung

Vergleichende Bewertung konventioneller und Neuronaler Netzwerkalgorithmen und Entwicklung eines integrierten Verfahrens

von D. Klaus, M. J. Canty, A. Poth, M. Voß, I. Niemeyer und G. Stein (1999),

VI, 160 Seiten

ISBN: 3-89336-242-8

16. Volatile Organic Compounds in the Troposphere

Proceedings of the Workshop on Volatile Organic Compounds in the Troposphere held in Jülich (Germany) from 27 - 31 October 1997 edited by R. Koppmann, D. H. Ehhalt (1999), 208 pages

ISBN: 3-89336-243-6

17. CO₂-Reduktion und Beschäftigungseffekte im Wohnungssektor durch das CO₂-Minderungsprogramm der KfW

Eine modellgestützte Wirkungsanalyse

von M. Kleemann, W. Kuckshinrichs, R. Heckler (1999), 29 Seiten

ISBN: 3-89336-244-4

18. Symposium über die Nutzung der erneuerbaren Energiequellen Sonne und Wind auf Fischereischiffen und in Aquakulturbetrieben

Symposium und Podiumsdiskussion, Izmir, Türkiye, 28.-30.05.1998.

Konferenzbericht

herausgegeben von A. Özdamar, H.-G. Groehn, K. Ülgen (1999), IX, 245 Seiten

ISBN: 3-89336-247-9

19. Das Weg-, Zeitverhalten des grundwasserbürtigen Abflusses im Elbeeinzugsgebiet

Analyse von Wasserhaushalt, Verweilzeiten und Grundwassermilieu im Flußeinzugsgebiet der Elbe (Deutscher Teil). Abschlußbericht Teil 3. von R. Kunkel, F. Wendland (1999), 122 Seiten

ISBN: 3-89336-249-5

20. Politikszenarien für den Klimaschutz

Untersuchungen im Auftrag des Umweltbundesamtes

Band 5. Szenarien und Maßnahmen zur Minderung von ${\rm CO_2}\text{-Emissionen}$ in Deutschland bis 2020

herausgegeben von G. Stein, B. Strobel (1999), XII, 201 Seiten

ISBN: 3-89336-251-7

21. Klimaschutz durch energetische Sanierung von Gebäuden. Band 1

von J.-F. Hake, M. Kleemann, G. Kolb (1999), 216 Seiten

ISBN: 3-89336-252-2

22. Electroanalysis

Abstracts of the 8th International Conference held from 11 to 15 June 2000 at the University of Bonn, Germany

edited by H. Emons, P. Ostapczuk (2000), ca. 300 pages

ISBN: 3-89336-261-4

23. Die Entwicklung des Wärmemarktes für den Gebäudesektor bis 2050

von M. Kleemann, R. Heckler, G. Kolb, M. Hille (2000), II, 94 Seiten

ISBN: 3-89336-262-2

24. Grundlegende Entwicklungstendenzen im weltweiten Stoffstrom des Primäraluminiums

von H.-G. Schwarz (2000), XIV, 127 Seiten

ISBN: 3-89336-264-9

25. Klimawirkungsforschung auf dem Prüfstand

Beiträge zur Formulierung eines Förderprogramms des BMBF Tagungsband des Workshop "Klimaforschung", Jülich, vom 02. bis 03.12.1999 von J.-Fr. Hake, W. Fischer (2000), 150 Seiten

ISBN: 3-89336-270-3

26. Energiezukunft 2030

Schlüsseltechnologien und Techniklinien Beiträge zum IKARUS-Workshop 2000 am 2./3. Mai 2000 herausgegeben von U. Wagner, G. Stein (2000), 201 Seiten

ISBN: 3-89336-271-1

27. Der globale Wasserkreislauf und seine Beeinflussung durch den Menschen

Möglichkeiten zur Fernerkundungs-Detektion und -Verifikation von D. Klaus und G. Stein (2000), 183 Seiten

ISBN: 3-89336-274-6

28. Satelliten und nukleare Kontrolle

Änderungsdetektion und objektorientierte, wissensbasierte Klassifikation von Multispektralaufnahmen zur Unterstützung der nuklearen Verifikation von I. Niemeyer (2001), XIV, 206 Seiten

ISBN: 3-89336-281-9

29. Das hydrologische Modellsystem J2000

Beschreibung und Anwendung in großen Flußgebieten von P. Krause (2001), XIV, 247 Seiten

ISBN: 3-89336-283-5

30. Aufwands- und ergebnisrelevante Probleme der Sachbilanzierung

von G. Fleischer, J.-Fr. Hake (2002), IV, 64 Blatt

ISBN: 3-89336-293-2

31. Nachhaltiges Management metallischer Stoffströme

Indikatoren und deren Anwendung Workshop, 27.-28.06.2001 im Congresscentrum Rolduc, Kerkrade (NL) herausgegeben von W. Kuckshinrichs, K.-L. Hüttner (2001), 216 Seiten ISBN: 3-89336-296-7

32. Ansätze zur Kopplung von Energie- und Wirtschaftsmodellen zur Bewertung zukünftiger Strategien

IKARUS-Workshop am 28. Februar 2002, BMWi, Bonn. Proceedings herausgegeben von S. Briem, U. Fahl (2003), IV, 184 Seiten

ISBN: 3-89336-321-1

33. TRACE. Tree Rings in Archaeology, Climatology and Ecology

Volume 1: Proceedings of the Dendrosymposium 2002, April 11th – 13th 2002, Bonn/Jülich, Germany edited by G. Schleser, M. Winiger, A. Bräuning et al., (2003), 135 pages, many partly coloured illustrations ISBN: 3-89336-323-8

34. Klimaschutz und Beschäftigung durch das KfW-Programm zur CO₂-Minderung und das KfW-CO₂-Gebäudesanierungsprogramm

von M. Kleemann, R. Heckler, A. Kraft u. a., (2003), 53 Seiten ISBN: 3-89336-326-2

35. Klimaschutz und Klimapolitik: Herausforderungen und Chancen

Beiträge aus der Forschung herausgegeben von J.-Fr. Hake, K. L. Hüttner (2003), III, 231 Seiten ISBN: 3-89336-327-0

36. Umweltschutz und Arbeitsplätze, angestoßen durch die Tätigkeiten des Schornsteinfegerhandwerks

Auswertung von Schornsteinfeger-Daten von M. Kleemann, R. Heckler, B. Krüger (2003), VII, 66 Seiten ISBN: 3-89336-328-9

37. Die Grundwasserneubildung in Nordrhein-Westfalen

von H. Bogena, R. Kunkel, T. Schöbel, H. P. Schrey, F. Wendland (2003), 148 Seiten

ISBN: 3-89336-329-7

38. Dendro-Isotope und Jahrringbreiten als Klimaproxis der letzten 1200 Jahre im Karakorumgebirge/Pakistan

von K. S. Treydte (2003), XII, 167 Seiten ISBN: 3-89336-330-0

39. Das IKARUS-Projekt: Energietechnische Perspektiven für Deutschland

herausgegeben von P. Markewitz, G. Stein (2003), IV, 274 Seiten ISBN: 3-89336-333-5

40. Umweltverhalten von MTBE nach Grundwasserkontamination

von V. Linnemann (2003), XIV, 179 Seiten

ISBN: 3-89336-339-4

41. Climate Change Mitigation and Adaptation: Identifying Options for Developing Countries

Proceedings of the Summer School on Climate Change, 7-17 September 2003, Bad Münstereifel, Germany

edited by K. L. Hüttner, J.-Fr. Hake, W. Fischer (2003), XVI, 341 pages ISBN: 3-89336-341-6

42. Mobilfunk und Gesundheit: Risikobewertung im wissenschaftlichen Dialog

von P. M. Wiedemann, H. Schütz, A. T. Thalmann (2003), 111 Seiten ISBN: 3-89336-343-2

43. Chemical Ozone Loss in the Arctic Polar Stratosphere: An Analysis of Twelve Years of Satellite Observations

by S. Tilmes (2004), V, 162 pages

ISBN: 3-89336-347-5

44. TRACE. Tree Rings in Archaeology, Climatology and Ecology

Volume 2: Proceedings of the Dendrosymposium 2003, May 1st – 3rd 2003, Utrecht, The Netherlands edited by E. Jansma, A. Bräuning, H. Gärtner, G. Schleser (2004), 174 pages ISBN: 3-89336-349-1

45. Vergleichende Risikobewertung: Konzepte, Probleme und Anwendungsmöglichkeiten

von H. Schütz, P. M. Wiedemann, W. Hennings et al. (2004), 231 Seiten ISBN: 3-89336-350-5

46. Grundlagen für eine nachhaltige Bewirtschaftung von Grundwasserressourcen in der Metropolregion Hamburg

von B. Tetzlaff, R. Kunkel, R. Taugs, F. Wendland (2004), 87 Seiten ISBN: 3-89336-352-1

47. Die natürliche, ubiquitär überprägte Grundwasserbeschaffenheit in Deutschland

von R. Kunkel, H.-J. Voigt, F. Wendland, S. Hannappel (2004), 207 Seiten ISBN: 3-89336-353-X

48. Water and Sustainable Development

edited by H. Bogena, J.-Fr. Hake, H. Vereecken (2004), 199 pages

ISBN: 3-89336-357-2

49. Geo- and Biodynamic Evolution during Late Silurian / Early Devonian Time (Hazro Area, SE Turkey)

by O. Kranendonck (2004), XV, 268 pages

ISBN: 3-89336-359-9

50. Politikszenarien für den Umweltschutz

Untersuchungen im Auftrag des Umweltbundesamtes Langfristszenarien und Handlungsempfehlungen ab 2012 (Politikszenarien III)

herausgegeben von P. Markewitz u. H.-J. Ziesing (2004), XVIII, 502 Seiten

ISBN: 3-89336-370-X

51. Die Sauerstoffisotopenverhältnisse des biogenen Opals lakustriner Sedimente als mögliches Paläothermometer

von R. Moschen (2004), XV, 130 Seiten

ISBN: 3-89336-371-8

52. MOSYRUR: Water balance analysis in the Rur basin

von Heye Bogena, Michael Herbst, Jürgen-Friedrich Hake, Ralf Kunkel, Carsten Montzka, Thomas Pütz, Harry Vereecken, Frank Wendland (2005), 155 Seiten

ISBN: 3-89336-385-8

Despite the fact that a clear water resources surplus is available in the Rur basin, local availability of water for industrial and ecological purposes, however, is problematic. Additionally, the groundwater and the surface waters are affected by agrochemicals (e.g. plant nutrients, pesticides) and point source emissions. In the near future the water recourses may also be effect by Global Change (e.g. decrease of water availability, increase of flooding probability, etc.).

For this reasons the MOSYRUR research project was initiated by the Institute of Chemistry and Dynamics of the Geosphere, Agrosphere Institute (ICG-IV) and the Program Group Systems Analysis and Technology Evaluation (STE) of the Research Centre Jülich. The aim of the project was to develop an integrated modelling system to facilitate a sustainable management of the water resources in the Rur basin. This is in accordance with the EU Water Framework Directive "integrated river basin management for Europe" that requires the establishment of management scenarios to ensure the good status for all waters in all European river basins.

This report summarizes the results of the research activities of the period 2002–2004, which has been focused on the analysis of the quantitative status of the water resources in Rur basin and the water balance at different scales. The research activities included process-oriented studies and modelling in small representative test areas and GIS-based water balance estimations at the catchment scale.



Band/Volume 52 ISBN 3-89336-385-8 Umwelt Environment